

University of Windsor

Scholarship at UWindor

Electronic Theses and Dissertations

Theses, Dissertations, and Major Papers

2017

Studies of Branched Dialkyldithiophosphinic Acids on Gold and Stretchable Gold Films Using Silica Nanoparticles

Jincheng Xu
University of Windsor

Follow this and additional works at: <https://scholar.uwindsor.ca/etd>

Recommended Citation

Xu, Jincheng, "Studies of Branched Dialkyldithiophosphinic Acids on Gold and Stretchable Gold Films Using Silica Nanoparticles" (2017). *Electronic Theses and Dissertations*. 5920.
<https://scholar.uwindsor.ca/etd/5920>

This online database contains the full-text of PhD dissertations and Masters' theses of University of Windsor students from 1954 forward. These documents are made available for personal study and research purposes only, in accordance with the Canadian Copyright Act and the Creative Commons license—CC BY-NC-ND (Attribution, Non-Commercial, No Derivative Works). Under this license, works must always be attributed to the copyright holder (original author), cannot be used for any commercial purposes, and may not be altered. Any other use would require the permission of the copyright holder. Students may inquire about withdrawing their dissertation and/or thesis from this database. For additional inquiries, please contact the repository administrator via email (scholarship@uwindsor.ca) or by telephone at 519-253-3000ext. 3208.

**Studies of Branched Dialkyldithiophosphinic Acids on
Gold and Stretchable Gold Films Using Silica
Nanoparticles**

By

Jincheng Xu

A Thesis

Submitted to the Faculty of Graduate Studies
through the Department of **Chemistry and Biochemistry**
in Partial Fulfillment of the Requirements for
the Degree of **Master of Science**
at the University of Windsor

Windsor, Ontario, Canada

2016

© 2016 Jincheng Xu

**Studies of Branched Dialkyldithiophosphinic Acids on Gold
and Stretchable Gold Films Using Silica Nanoparticles**

by

Jincheng Xu

APPROVED BY:

I. Samson

Department of Earth and Environmental Sciences

C. Macdonald

Department of Chemistry and Biochemistry

T. Carmichael, Advisor

Department of Chemistry and Biochemistry

October 13, 2016

Declaration of Originality

I hereby certify that I am the sole author of this thesis and that no part of this thesis has been published or submitted for publication.

I certify that, to the best of my knowledge, my thesis does not infringe upon anyone's copyright nor violate any proprietary rights and that any ideas, techniques, quotations, or any other material from the work of other people included in my thesis, published or otherwise, are fully acknowledged in accordance with the standard referencing practices. Furthermore, to the extent that I have included copyrighted material that surpasses the bounds of fair dealing within the meaning of the Canada Copyright Act, I certify that I have obtained a written permission from the copyright owner(s) to include such material(s) in my thesis and have included copies of such copyright clearances to my appendix.

I declare that this is a true copy of my thesis, including any final revisions, as approved by my thesis committee and the Graduate Studies office, and that this thesis has not been submitted for a higher degree to any other University or Institution.

Abstract

This first half of the thesis reports the synthesis of new branched symmetric dithiophosphinic acids (DTPAs), and the formation and characterization of DTPA SAMs on As-Dep and TS gold. Chapter 1 introduces the definition of self-assembled monolayers (SAMs) and SAMs with multidentate adsorbates. The binding of DTPA SAMs on gold depends on the roughness of gold: on as-deposited (As-Dep) gold, DTPA adsorbates bind in a mixture of bidentate (60%) and monodentate (40%), while on templated-stripped (TS) gold, the SAMs chelated to the gold surface. Chapter 3 investigates packing density, organization of alkyl chain and chain crystallinity of $(C_6C_2)_2DTPA$ and $(C_5C_1)_2DTPA$ SAMs on As-Dep and TS gold.

The second half of the thesis focused on the research area of stretchable electronics. Chapter 2 presents the background and application of stretchable electronics and different ways that have been used to increase the stretchability and conductivity of stretchable electronics, such as conductive materials, soft substrates and topographies of substrates. Chapter 4 reports the using of E-Beam evaporation to deposit Au thin film onto polydimethyl siloxane (PDMS) elastomeric substrates, by inducing micro-structured modified fumed silica interlayer to enhance the stretchability and conductivity of the thin metal films. Also, by simply altering the weight ratio of modified silica:PDMS interlayer, the resistance change can be tuned, which leads to different functional samples.

Dedication

This thesis is dedicated to my parents abroad, who always cheer me up and give me motivation every time I feel stressful. They provide me the chance to study and live in Canada with endless support for these many years.

Acknowledgements

I really appreciate my supervisor, Dr. Tricia B. Carmichael who supervised me for the last two years at University of Windsor. I thank you for making me believe in myself, and know the meaning of responsibility. Also, I would like to thank Steve Carmichael for cooking delicious food, great BBQ, sharing wines and everything in our group parties.

I should thank all my colleagues in my lab for providing help and support, especially Michael-Anthony who supervised me when I firstly worked in the lab, and Akhil who always makes me spend money and talks about gossip after hard working in the lab. I would also thank for all the friends in the departments for motivating me in a “different” way, and also Beini who are always by my side wherever I go and whatever I do.

I would like to give special thanks to my committee members, Dr. Iain M. Samson, Dr. Charles L. B. Macdonald, for their productive and critical comments on my thesis.

Table of Contents

| | |
|---|------|
| Declaration of Originality | iii |
| Abstract | iv |
| Dedication | v |
| Acknowledgements | vi |
| List of Figures | x |
| List of Supporting Figures | xi |
| List of Schemes | xii |
| List of Tables | xiii |
| List of Abbreviations | xiv |
| Chapter 1 | 1 |
| Introduction of Self-Assembled Monolayers (SAMs) | 1 |
| 1.1 Background | 2 |
| 1.2. Structure of alkanethiolate SAMs | 3 |
| 1.3. Chelating SAMs with multidentate adsorbates | 4 |
| 1.4. Dithiophosphinic Acids..... | 7 |
| 1.5. Roughness of gold | 8 |
| 1.6. Scope of thesis | 10 |
| 1.7. References | 10 |
| Chapter 2 | 17 |
| Introduction of Stretchable Electronics | 17 |
| 2.1. Background | 18 |
| 2.2. Applications of Stretchable Electronics | 18 |
| 2.3. Conductive materials on stretchable substrates | 21 |
| 2.4. Metal films on stretchable substrates | 22 |

| | |
|---|----|
| 2.5. Scope of thesis | 26 |
| 2.6. References | 26 |
| Chapter 3 | 33 |
| Branched Dialkyldithiophosphinic Acid Self-Assembled Monolayers on Gold | 33 |
| 3.1. Introduction | 34 |
| 3.2. Experimental Section | 37 |
| 3.2.1. Synthesis of Branched DTPAs | 37 |
| 3.2.2. Gold Substrate Preparation and SAM Formation | 39 |
| 3.2.3. Characterization | 39 |
| 3.3. Results and Discussion | 40 |
| 3.3.1. Synthesis of Branched Alkyl DTPAs | 40 |
| 3.3.2. SAM Formation | 41 |
| 3.3.3. Binding of the DTPAs Head Group to the Gold Surface | 42 |
| 3.3.4. Organization of the Alkyl Chains | 45 |
| 3.4. Conclusions | 49 |
| 3.6. References | 50 |
| 3.7. Supporting Information | 53 |
| Chapter 4 | 59 |
| Stretchable Gold Film on Modified Silica Nanoparticles | 59 |
| 4.1. Introduction | 60 |
| 4.2. Experimental Methods | 62 |
| 4.3. Results and Discussion | 65 |
| 4.4. Conclusion | 80 |
| 4.5. References | 80 |
| 4.6. Supporting Information | 84 |
| Chapter 5 | 87 |
| Outlook | 87 |
| 5.1. Branched DTPAs with Other Terminal Groups or Chain Length | 88 |
| 5.2. Ways to Increase Stretchability of PDMS _x Si/Au Samples | 89 |
| 5.3. References | 90 |

| | |
|---------------------------|-----|
| Appendices..... | 91 |
| Copyright Permission..... | 91 |
| Vita Auctoris..... | 105 |

List of Figures

| | |
|---|----|
| Figure 1.1. Schematic diagram of an ideal n-alkanethiol SAM on gold with the anatomy and characteristics. ¹ | 3 |
| Figure 1.2. Illustration of components of SAMs monodentate, bidentate, and tridentate bonding modes between adsorbate and substrate. ³⁵ | 5 |
| Figure 1.3. Structures of chelating adsorbates for SAM formation. | 5 |
| Figure 1.4. Mesomeric forms of the DTC headgroup chelates on gold. | 6 |
| Figure 1.5. Dialkyldithiophosphinic Acid bond to gold surface: a) monodentate and b) bidentate binding..... | 7 |
| Figure 1.6. Contact mode AFM topographic images of (a) As-Dep and (b) TS gold films. ⁴⁴ | 9 |
| Figure 2.1. Applications of flexible electronics: (a) paper-like flexible screen, (b) flexible solar cell panel. ⁶ | 19 |
| Figure 2.2. Applications of stretchable electronics: (a) a hemispherical electronic eye camera, ¹⁰ (b) an intrinsically stretchable polymer light-emitting device, ¹² (c) a stretchable sensor on an expandable catheter, ¹³ (d) smart artificial skin covering a prosthetic hand. ⁴ | 20 |
| Figure 2.3. a) buckled gold surface structure after release from 15% pre-stretch, ⁴¹ b) serpentine structured metal embedded in PDMS. ³³ | 24 |
| Figure 3.1. HR-XPS spectra of the S 2p region of (C ₆ C ₂) ₂ DTPA (a,b) and C ₆ C ₂ SH (c,d) SAM on As-Dep gold (a,c) and TS gold (b,d). | 44 |
| Figure 3.2. RAIRS spectra (2990-2820 cm ⁻¹) of (C ₆ C ₂) ₂ DTPA, (C ₅ C ₁) ₂ DTPA and C ₆ C ₂ SH SAMs on As-Dep and TS gold. Dashed vertical lines indicate the positions of crystalline $\nu_{as}(\text{CH}_2)$ and $\nu_s(\text{CH}_2)$ of C ₁₆ SH SAMs on gold (2918 and 2850 cm ⁻¹ , respectively). | 47 |
| Figure 4.1. Dark-field optical micrographs of PDMS _{10Si} (a), PDMS _{15Si} (b), PDMS _{20Si} (c), PDMS _{25Si} (d) and PDMS _{30Si} (e) samples before Au deposition. Scale bar –20 μm | 66 |
| Figure 4.2. AFM images (a-e) and cross section (f-j) of PDMS _{10Si} (a, f), PDMS _{15Si} (b, g), PDMS _{20Si} (c, h), PDMS _{25Si} (d, i) and PDMS _{30Si} (e, j) samples before Au deposition. | 68 |
| Figure 4.3. Optical images of PDMS _{xSi} /Au samples captured without stretch PDMS _{10Si} /Au (a), PDMS _{15Si} /Au (b), PDMS _{20Si} /Au (c), PDMS _{25Si} /Au (d) and PDMS _{30Si} /Au (e). Scale bar – 200 μm | 72 |
| Figure 4.4. PDMS _{xSi} /Au sample images. | 72 |
| Figure 4.5. Evolution of cracks on PDMS _{xSi} /Au samples with stretching. Optical images captured at 5% (top), 50 % (middle) and 70% (bottom) strain for PDMS _{10Si} /Au (a-c), PDMS _{15Si} /Au (d-f), PDMS _{20Si} /Au (g-i) and PDMS _{25Si} /Au (j-l) samples. In all images, the samples were stretched in the horizontal direction. Scale bar – 200 μm | 74 |
| Figure 4.6. Plot of normalized resistance as a linear strain for 0% (Au/PDMS sample) and PDMS _{10Si} /Au (a) and PDMS _{15Si} /Au, PDMS _{20Si} /Au, and PDMS _{25Si} /Au (b) samples. | 76 |
| Figure 4.7. Evolution of cracks on PDMS _{xSi} /Au films with stretching. Optical images captured at 5% (top), 50% (middle) and 70% (bottom) strain for PDMS _{15Si} /Au (a-c), PDMS _{20Si} /Au (d-f) and PDMS _{25Si} /Au (g-i) samples. In all images, the samples were stretched in the horizontal direction. Scale bar – 800 μm | 79 |

List of Supporting Figures

| | |
|---|----|
| Figure S 3.1. ^{31}P , ^1H and ^{13}C NMR of $(\text{C}_6\text{C}_2)_2\text{DTPAs}$ | 54 |
| Figure S 3.2. ^{31}P , ^1H and ^{13}C NMR of $(\text{C}_5\text{C}_1)_2\text{DTPAs}$ | 56 |
| Figure S 3.3. XPS survey spectra of $(\text{C}_6\text{C}_2)_2\text{DTPAs}$ on TS (top) and As-Dep (bottom) gold. | 57 |
| Figure S 3.4. XPS survey spectra of $\text{C}_6\text{C}_2\text{SH}$ on TS (top) and As-Dep (bottom) gold. | 58 |
| Figure S 4.1. AFM images (a-e) and cross section (f-j) of 10% (a, f), 15% (b, g), 20% (c, h), 25% (d, i) and 30% (e, j) PDMS_{xSi} samples after 250 Å Au deposition..... | 84 |
| Figure S 4.2. SEM images of 15% (a), 20% (b) and 25% (c) $\text{PDMS}_{\text{xSi}}/\text{Au}$ samples under 40% strain. In all images, the samples were stretched in vertical direction..... | 85 |
| Figure S 4.3. Evolution of cracks on PDMS/gold structures with stretching. Optical images captured at (a) 5% strain and (b) 25% strain. In all images, the samples were stretched in vertical direction..... | 86 |

List of Schemes

| | |
|--|----|
| Scheme 3.1. Dialkyldithiophosphinic Acid bond to gold surface: a) monodentate and b) bidentate binding..... | 35 |
| Scheme 3.2. Synthetic Procedure to prepare dialkyldithiophosphinic acids. | 41 |

List of Tables

| | |
|---|----|
| Table 3.1. S 2p _{3/2} Binding Energy and the ratio of Chemisorbed : Non-interacting S species of (C ₆ C ₂) ₂ DTPA and C ₆ C ₂ SH SAM on As-Dep and TS gold. | 44 |
| Table 3.2. $\nu_{as}(\text{CH}_2)$ and $\nu_s(\text{CH}_2)$ peak positions of (C ₆ C ₂) ₂ DTPA, (C ₅ C ₁) ₂ DTPA and C ₆ C ₂ SH on TS and As-Dep gold..... | 48 |
| Table 3.3. Contact angles of water and hexadecane for (C ₅ C ₁) ₂ DTPA, (C ₆ C ₂) ₂ DTPA and C ₆ C ₂ SH SAMs on TS and As-Dep gold. | 48 |
| Table 4.1. RMS roughness S _{dr} value of PDMS _{xSi} samples with and without Au deposition. | 69 |
| Table 4.2. Sheet resistance (R _s) of 250-Å-thick-gold PDMS _{xSi} samples..... | 73 |

List of Abbreviations

| | |
|-----------|-----------------------------------|
| AFM | Atomic force microscopy |
| As-Dep Au | As-deposited gold |
| BEs | Binding energies |
| CNTs | Carbon nanotubes |
| °C | Degree Celcius |
| cm | Centimeter |
| DTCs | Dithiocarbamates |
| DIBAL | Diisobutylaluminium hydride |
| DTPA | Dithiophosphinic acid |
| EDTA | Ethylene diamine tetraacetic acid |
| EGaIn | Gallium-indium eutectic |
| hrs | Hours |
| HR-XPS | High-resolution XPS |
| Hz | Hertz |
| kcal | Kilocalorie |
| MCT | Mercury cadmium telluride |
| MPTMS | 3-Mercaptopropyl trimethoxysilane |
| mM | Millimolar concentration |
| mL | Milliliter |
| mm | Millimeter |
| nm | Nanometer |
| NMR | Nuclear magnetic resonance |
| PDMS | Polydimethylsiloxane |
| PU | Polyurethane |

| | |
|-----------------|---|
| PVAc | Polyvinyl acetate |
| RAIRS | Reflection-adsorption infrared spectroscopy |
| R | Alkyl chains |
| RSHs | n-alkanethiols |
| RS-SRs | Dialkyldisulfides |
| RSRs | Dialkylsulfides |
| RMS | Root-mean-square |
| R _s | Sheet resistance |
| SAM | Self-assembled monolayer |
| SEM | Scanning electron microscope |
| S _{dr} | Surface area ratio |
| THF | Tetrahydrofuran |
| TPDTC | Terphenyldithiocarbamate |
| TGA | Thermogravimetric analysis |
| TS Au | Template-stripped gold |
| UV | Ultraviolet |
| XPS | X-ray photoelectron spectroscopy |
| μm | Micrometer |
| ν _{as} | Asymmetric stretch |
| ν _s | Symmetric stretch |

Chapter 1

Introduction of Self-Assembled Monolayers (SAMs)

1.1 Background

Self-assembled monolayers (SAMs) are highly ordered, single layer molecular films formed from the adsorption of organic molecules, with three specific features, onto a solid or liquid surface as shown in Figure 1.1. The head group has a highly affinity to the metal substrate, the adsorption between the molecule and the metal surface happens with the formation of a covalent bond. This exothermic process is called chemisorption.¹ In the middle of the molecule, alkane chains are most common, facilitating ordering during assembling process through van der Waals interactions. Longer alkyl chains have more van der Waals interactions, producing more ordered SAMs than those formed from shorter alkyl chains.^{2,3} Although the self-assembly process is driven by the chemisorption of the head group and van der Waals interactions between neighbouring molecules, the interfacial properties (wettability by water, which can affect its adhesion, friction and lubrication⁴) of the SAM are dictated by the terminal group that is present at the surface of the monolayer. Self-assembled monolayers can be formed on a wide range of substrate including metal oxides, and coinage metals (Au, Ag, Cu, Pt, Pd).⁵⁻⁸ SAMs with a siloxane headgroup have been shown to form on glass, however, this class of molecular adsorbates require more difficult conditions during assembling, including synthesize, purify, soak and anneal steps.⁹ Another type of SAMs are phosphonic acids on metal oxides and silicon. To produce ordered SAMs, high-temperature annealing and substrate pre-treating might be used, which is too complicated to prepare.¹⁰

The most well-studied SAMs are thiol-functionalized molecules on coinage metals. Of all the metals, gold has been most studied because chemisorption of the organosulfur compound to gold is highly favourable (~ 30 kcal/mol^{11,12,13}). Additionally, gold is inert; it

does not oxidize in ambient conditions like copper or silver¹⁴ and does not react with most chemicals.

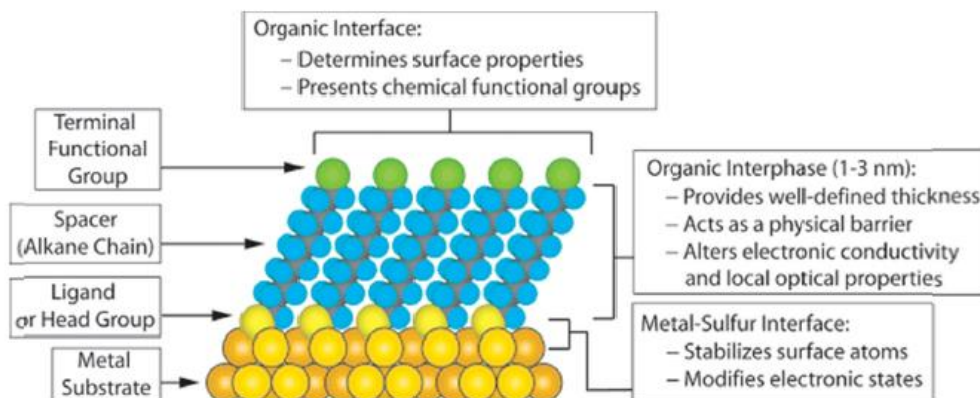


Figure 1.1. Schematic diagram of an ideal n-alkanethiol SAM on gold with the anatomy and characteristics.¹

1.2. Structure of alkanethiolate SAMs

The organosulfur adsorbates are widely used in SAM formation, includes organic alkanethiols, aromatic thiols, sulfides, disulfide, thiocarbamates and dithiolcarbinates.^{15,16} The organosulfur compounds are known to coordinate to surfaces of gold, which can be achieved from solution immersion. The simplest structure organosulfur compound (alkanethiols, RSHs) can produce robust and well-defined SAMs, when the alkanethiol, in solution, is brought in contact with a clean gold surface, a highly favorable Au-S bond will form.^{17,18,19} Besides, alkanethiols have a superior solubility, which enables the formation of alkanethiolate SAMs on gold of varying chain lengths.^{1,20}

The preparation of SAMs by adsorption of alkanethiols on gold is very easy, by immersing a clean gold substrate, into a dilute solution of the adsorbate (~1 mM). The typical immersion time ranges from 12-18 hours at room temperature (25°C). During the process, the alkanethiols adsorb on the gold and lose the hydrogen, which is not been proved.^{16,21,22} The most common surface structure of SAMs of on an Au (111) surface is generally believed to be trans-extended and tilted approximately 30° from normal, and the spacing of sulfur atoms on the surface is 4.99 Å, $n > 11$ (for $n < 10$, the SAMs are less ordered);^{23,24} alkanethiolates has a similar structure with dialkyldisulfides, the S-S bond is cleaved at the gold surface.^{25,26} Chain orientation in alkanethiol SAMs have a tilt angle on the linear backbone away from the surface normal (α), and the angle of rotation about the long axis of the molecule (β).^{1,8,16} These two angles change (depending strongly on the substrate) to maximize both the packing density and the number of van der Waals interactions between neighboring molecules.

1.3. Chelating SAMs with multidentate adsorbates

Alkanethiolate SAMs provide a simple, ordered system for many applications, such as molecular junctions and etch resists.²⁷⁻³³ However, the low energy barrier to molecular diffusion and desorption causes poor thermal or electrical stability and packing density of the SAM, which may limit the life time of a real device and prevent their use in real electronic devices.³⁴ A paper by Chinwangso *et al.* describes a variety of multidentate (bidentates and tridentates) adsorbate structures that have been used to generate well-defined SAMs with multiple attachment points to the underlying substrate. This bonding arrangement allows the formation of SAMs with enhanced stability through the entropy-driven “chelate effect” (Figure 1.2).³⁵

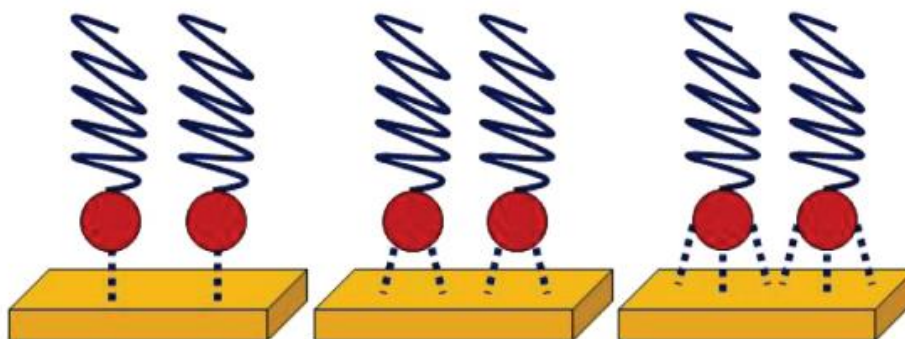


Figure 1.2. Illustration of components of SAMs monodentate, bidentate, and tridentate bonding modes between adsorbate and substrate.³⁵

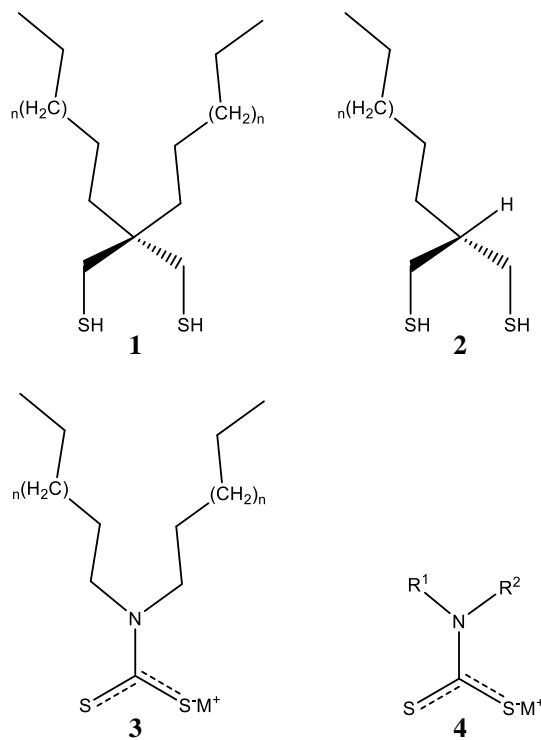


Figure 1.3. Structures of chelating adsorbates for SAM formation.

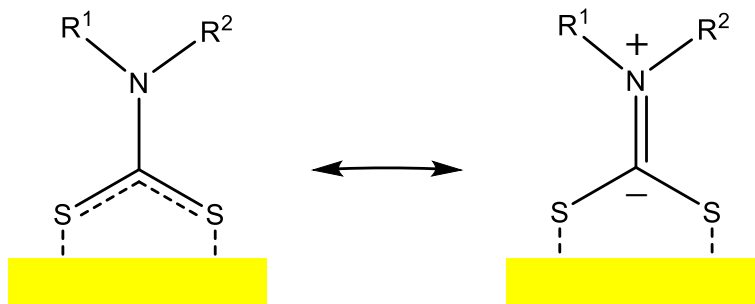


Figure 1.4. Mesomeric forms of the DTC headgroup chelates on gold.

Spiroalkanedithiols (**1**, **2**) and dithiocarbamates (DTC, **3**, **4**) (Figure 1.3) are two well studied SAMs where the headgroups can chelate to the gold surface leading to stronger metal-molecule coupling and improve thermal stability compared to the thiol analogue. The structure of spiroalkanedithiols are dominant to the alkyl chain packing density and also influence the frictional properties of the formed SAMs.^{36,37} SAMs generated from long chain dialkanedithiols **1** are highly oriented and well packed, while the SAMs formed from monoalkanedithiols **2** are less crystalline than those of analogous from dialkanedithiol.³⁸ The DTC head group chelates to the gold surface so that even short chain DTC SAMs are stable up to 12 hrs at 85 °C (Figure 1.4).³⁹ Incorporating aromatic groups in the DTC structures allows for the formation of SAMs that are robust with high thermal stability and conductivity, which is good for the DTC-based molecular junctions. von Wrochem *et al.* studied forming terphenyldithiocarbamate (TPDTC) SAMs on gold, which has a conductance that is two orders of magnitude higher than the SAM of analogous terphenylthiol.⁴⁰

1.4. Dithiophosphinic Acids

One potentially interesting molecule that can chelate to the substrate is the dithiophosphinic acid (DTPA), which consists of a tetrahedral phosphorus center that binds to two sulfur atoms to give a P(S)SH headgroup and also attaches to two pendant groups (Figure 1.5), similar to spiroalkanedithiols. Dialkyl-DTPA molecules have previously been used in industrial applications such as selective separation of precious metals from sulfide ores.^{41,42}

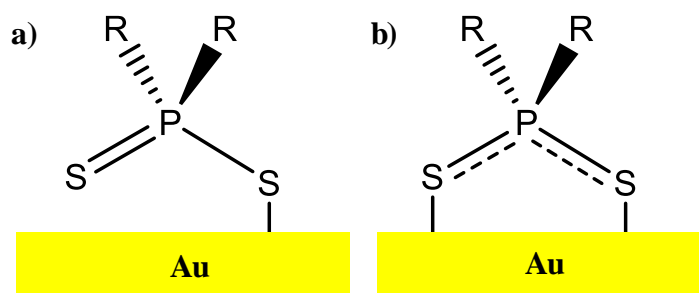


Figure 1.5. Dialkyldithiophosphinic Acid bond to gold surface: a) monodentate and b) bidentate binding.

In recent years, our research group studied more on the self-assembly of phosphorus-containing adsorbates on coinage metals (mostly gold), the potential to investigate the nature of chelating between two sulfur atoms makes DTPA molecules interesting. San Juan and Miller *et al.* examined the nature of binding of the P(S)SH headgroup, the alkyl chain organization and packing density, and the electrochemical properties as a function of varying the R groups. They investigated the van der Waals interactions between the

symmetric and asymmetric, short and long alkyl chains, the resulting packing density and organization in comparison to those of analogous RSH SAMs. They also introduce a phenyl moiety as a pendant group in the DTPAs and form SAMs from a series of PhRDTPAs while varying the alkyl chain length.⁴³⁻³⁷ From the studies that we know, DTPA SAMs formed from adsorbates with short alkyl chain (n=5) are disordered and liquid-like, and the alkyl groups become more crystalline and ordered as the alkyl chain length is increased. While on ultrasmooth gold, an opposite trend can be exhibited in which the alkyl layer becomes more disordered and liquid-like as the methylene units is increased.⁴⁸

1.5. Roughness of gold

From Figure 1.5a, monodentate DTPAs have one bounded sulfur to the underlying gold substrate, while the other sulfur does not interact with gold and retains the double bond to phosphorus. Bidentate DTPAs have both sulfur atoms bounded to the gold and have resonance associated with chelation (Figure 1.5b). The chelating structure of the adsorbates depends on the morphology and roughness of the gold substrates. There are two types of gold substrates with different roughness, As-Dep and TS gold, and the way these DTPA SAMs bind to surface depends on the gold substrates. Gold films deposited by electron-beam evaporation (As-Dep gold) are composed of a layer of small grains of ~50 nm, separated by deep grain boundaries of ~10 nm (Figure 1.6), lead to a large root-mean-square (RMS) roughness value of 3 - 5 nm^{44,50,51,52} which inhibit the DTPA adsorbates to chelate, provide a mixture of bidentate (60%) and monodentate (40%) in the SAM. The monodentate DTPA molecules have the freedom of rotation about the Au-S bond, resulting in flexible Au-S-P bond angles, which allows dense packing of the

chain. As the van der Waals interactions between alkyl groups increase with increasing chain length, SAMs that formed are more crystalline.^{43,44} In contrast, gold substrates produced by a process known as template-stripped (TS)⁴⁹ provide an ultrasmooth surface, which consists of large but flat grains of $\sim 200\text{-}500$ nm, separated by shallow grain boundaries of ~ 1.5 nm, lead to a RMS roughness value of $\sim 5\text{\AA}$.^{44,50,51,52} In the SAMs that formed on TS gold, all the adsorbates chelate to the gold surface, the bidentate DTPA molecules prevent rotation about the Au-S bond and fix the Au-S-P bond angles. As the length of alkyl chains increases, steric demands of the chains limit the van der Waals interactions, making the alkyl layer disordered and loosely packed.^{44,48}

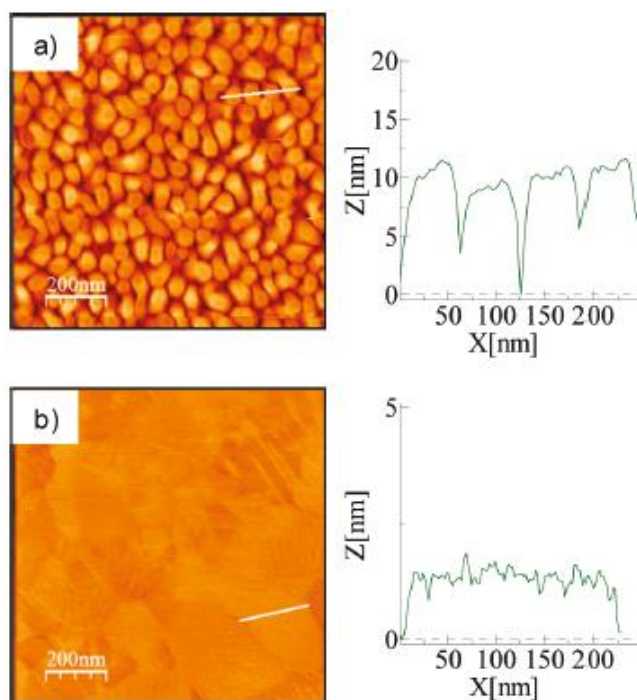


Figure 1.6. Contact mode AFM topographic images of (a) As-Dep and (b) TS gold films.⁴⁴

1.6. Scope of thesis

The focus of first half of this thesis is to use a new R₂DTPA to form SAMs on both As-Dep and TS gold films. We use branched symmetric short chain DTPA adsorbates, (C₆C₂)₂DTPA and (C₅C₁)₂DTPA, which have a similar molecular structure to (C₆)₂DTPA, and exam the packing density, organization of the alkyl chains and chain crystallinity of the SAMs on gold. This work is presented in Chapter 3.

1.7. References

1. Love, J. C.; Estroff, L. A.; Kriebel, J. K.; Nuzzo, R. G.; Whitesides, G. M. Self-Assembled Monolayers of Thiolates on Metals as a Form of Nanotechnology. *Chem. Rev.* **2005**, 105, 1103-1169.
2. Schlecht, C. A.; Maurer, J. A., Functionalization of glass substrates: Mechanistic insights into the surface reaction of trialkoxysilanes. *RSC Advances* **2011**, 1, 1446-1448.
3. Varatharajan, S.; Berchmans, S.; Yegnaraman, V., Tailoring self-assembled monolayers at the electrochemical interface. *J. Chem. Sci.* **2009**, 121, 665-674.
4. Whitesides, G. M. Self-Assembling Materials. *Sci. Am.* **1995**, 273, 146-149.
5. Chang, S.-C.; Chao, I.; Tao, Y.-T., Structure of Self-Assembled Monolayers of Aromatic-Derivatized Thiols on Evaporated Gold and Silver Surfaces: Implication on Packing Mechanism. *J. Am. Chem. Soc* **1994**, 116, 6792-6805.
6. Quiñones, R.; Gawalt, E. S., Study of the formation of self-assembled monolayers on nitinol. *Langmuir* **2007**, 23, 10123-10130.
7. Raman, A.; Dubey, M.; Gouzman, I.; Gawalt, E. S., Formation of self-assembled

- monolayers of alkylphosphonic acid on the native oxide surface of SS316L. *Langmuir* **2006**, *22*, 6469-6472.
8. Gao, W.; Dickinson, L.; Grozinger, C.; Morin, F. G.; Reven, L., Self-assembled monolayers of alkylphosphonic acids on metal oxides. *Langmuir* **1996**, *12*, 6429-6435.
 9. Yanker, D.; Maurer, J., Direct printing of trichlorosilanes on glass for selective protein adsorption and cell growth. *Mol. BioSyst* **2008**, *4*, 502-504.
 10. Dubey, M.; Weidner, T.; Gamble, L.; Castner, D., Structure and Order of Phosphonic Acid-Based Self-Assembled Monolayers on Si (100). *Langmuir* **2010**, *26*, 14747-14754.
 11. Nuzzo, R. G.; Zegarski, B. R.; Dubois, L. H. Fundamental Studies of the Chemisorption of Organosulfur Compound on Au (111). Implication for Molecular Self-Assembly on Gold Surfaces. *J. Am. Chem. Soc.* **1987**, *109*, 733-740.
 12. Lavrich, D. J.; Wetterer, S. M.; Bernasek, S. L; Scoles, G. Physisorption and Chemisorption of Alkanethiols and Alkyl Sulfides on Au (111). *J. Phys. Chem. B.* **1998**, *102*, 3456-3465.
 13. Fischer, D.; Curioni, A.; Andreoni, W. Decanethiols on Gold: The Structure of Self-Assembled Monolayers Unraveled with Computer Simulations. *Langmuir* **2003**, *19*, 3567-3571.
 14. Laibinis, P. E.; Whitesides, G. M.; Allara, D. L.; Tao, Y. T.; Parikh, A. N.; Nuzzo, R. G. Comparison of the Structures and Wetting Properties of Self-Assembled Monolayers of *n*-Alkanethiols on the Coinage Metal Structures, Cu, Ag, Au. *J. Am. Chem. Soc.* **1991**, *113*, 7152-7167.

15. Ulman, A. Formation and Structure of Self-Assembled Monolayers. *Chem. Rev.* **1996**, 96, 1533-1554.
16. Schreiber, F. Structure and Growth of Self-Assembling Monolayers. *Prog. Surf. Sci.* **2000**, 65, 151-256.
17. Jung, C.; Dannenberger, O.; Xu, Y.; Buck, M.; Grunze, M. Self-Assembled Monolayers from Organosulfur Compounds: A comparison Between sulfides, Disulfides, and Thiols. *Langmuir* **1998**, 14, 1103-1107.
18. Strong, L.; Whitesides, G. M. Structures of Self-Assembled Monolayer Films of Organosulfur Compounds Adsorbed on Gold Single Crystals: Electron Diffraction Studies. *Langmuir* **1988**, 4, 546-558.
19. Brain, C. D.; Biebuyck, H. A.; Whitesides, G. M. Comparison of Self-Assembled Monolayers on Gold: Coadsorption of Thiols and Disulfides. *Langmuir* **1989**, 5, 723-727.
20. Love, J. C.; Wolfe, D. B.; Haasch, R.; Chabinyc, M. L.; Paul, K. E.; Whitesides, G. M.; Nuzzo, R. G. Formation and Structure of Self-Assembled Monolayers of Alkanethiolates on Palladium. *J. Am. Chem. Soc.* **2003**, 125, 2597-2609.
21. Dubois, L.H.; Nuzzo, R.G. Synthesis, Structure, and Properties of Model Organic Surfaces. *Annu. Rev. Phys. Chem.* **1992**, 43, 437-463.
22. Dubois, L.H.; Zegarski, B.R.; Nuzzo, R.G. Molecular Ordering of Organosulfur Compounds on Au(111) and Au(100): Adsorption from Solution and in Ultrahigh Vacuum. *J. Chem. Phys.* **1993**, 98, 678-688.
23. Poirier, G.E. Characterization of Organosulfur Molecular Monolayers on Au(111) Using Scanning Tunneling Microscopy. *Chem. Rev.* **1997**, 97, 1117-1127.

24. Porter, M.D.; Bright, T.B.; Allara, D.L.; Chidsey, C.E.D. Spontaneously Organized Molecular Assemblies. 4. Structural Characterization of n-Alkyl Thiol Monolayers on Gold by Optical Ellipsometry, Infrared Spectroscopy, and Electrochemistry. *J. Am. Chem. Soc.*, **1987**, 109, 3559-3568.
25. Chon, S.; Paik, W. -K. Adsorption of Self-Assembling Sulfur Compounds Through Electrochemical Reactions: Effects of Potential, Acid and Oxidizing Agents. *Phys. Chem. Chem. Phys.* **2001**, 3, 3405-3410.
26. Biebuyck, H. A.; Bain, C. D.; Whitesides, G. M. Comparison of Organic Monolayers on Polycrystalline Gold Spontaneously Assembled from Solutions Containing Dialkyl Disulfides or Alkanethiols. *Langmuir* **1994**, 10, 1825-1831.
27. Tarlov, M.J.; Burgess, D.R.F. Jr.; Gillen, G. UV Photopatterning of Alkanethiolate Monolayers Self-Assembled on Gold and Silver. *J. Am. Chem. Soc.* **1993**, 115, 5305-5306.
28. Behm, J.M.; Lykke, K.R.; Pellin, M.J.; Hemminger, J.C. Projection Photolithography Utilizing a Schwarzschild Microscope and Self-Assembled Alkanethiol Monolayers as Simple Photoresists. *Langmuir* **1996**, 12, 2121-2124.
29. Reed, M.A. Molecular Electronics Under Control. *Nat. Mater.* **2004**, 3, 286-287.
30. Kim, T.-W.; Wang, G.; Lee, H.; Lee, T. Statistical Analysis of Electronic Properties of Alkanethiols in Metal-Molecule-Metal Junctions. *Nanotechnology* **2007**, 18, 315204-315215.
31. Haick, H.; Cahen, D. Contacting Organic Molecules by Soft Methods: Towards Molecule-Based Electronic Devices. *Acc. Chem. Res.* **2008**, 41, 359-366.
32. Thuo, M.M.; Reus, W.F.; Nijhuis, C.A.; Barber, J.R.; Kim, C.; Shulz, M.D.;

- Whitesides, G.M. Odd–Even Effects in Charge Transport Across Self-Assembled Monolayers. *J. Am. Chem. Soc.* **2011**, 133, 2962-2975.
33. Reus, W.F.; Nijhuis, C.A.; Barber, J.; Thuo, M.N.; Tricard, S.; Whitesides, G.M. Statistical Tools for Analyzing Measurements of Charge Transport. *J. Phys. Chem. C* **2012**, 116, 6714-6733.
34. Schreiber, F.; Eberhardt, A.; Leung, T. Y. B.; Schwartz, P.; Wetterer, S. M.; Lavrich, D. J.; Berman, L.; Fenter, P.; Eisenberger, P.; Scoles, G. Adsorption Mechanisms, Structures and Growth Regimes of an Archetypal Self-Assembling System: Decanethiol on Au (111). *Phys. Rev. B* **1998**, 57, 12476-12481.
35. Chinwangso, P.; Jamison, A.C.; Lee, T.R. Multidentate Adsorbates for Self-Assembled Monolayer Films. *Acc. Chem. Res.* **2011**, 44, 511-519.
36. Shon, Y.-S.; Lee, T.R. Desorption and Exchange of Self-Assembled Monolayers (SAMs) on Gold Generated from Chelating Alkanedithiols. *J. Phys. Chem. B* **2000**, 104, 8192-8200.
37. Lee, S.; Shon, Y.-S.; Colorado, R., Jr.; Guenard, R.L.; Lee, T.R.; Perry, S.S. The Influence of Packing Densities and Surface Order on the Frictional Properties of Alkanethiol Self-Assembled Monolayers (SAMs) on Gold: A Comparison of SAMs Derived from Normal and Spiroalkanedithiols. *Langmuir* **2000**, 16, 2220-2224.
38. Shon, Y.-S.; Colorado, R., Jr.; Williams, C.T.; Bain, C.D. Lee, T.R., Low-Density Self-Assembled Monolayers on Gold Derived from Chelating 2-Monoalkylpropane-1,3-dithiols. *Langmuir* **2000**, 16, 541-548.
39. Zhao, Y.; Pérez-Segarra, W.; Shi, Q.; Wei, A. Dithiocarbamate Assembly on Gold. *J. Am. Chem. Soc.* **2005**, 127, 7328-7329.

40. von Wrochem, F.; Gao, D.; Scholz, f.; Nothofer, H. -G.; Nelles, G.; Wessels, J. M. Efficient Electronic Coupling and Improved Stability with Dithiocarbamate-Based Molecular Junctions. *Nat. Nanotechnol.* **2010**, *5*, 618-624.
41. Hope, G.A.; Woods, R.; Boyd, S.; Watling, K. A Spectrochemical Investigation of the Interaction of Diisobutyldithiophosphate with Copper, Silver and Gold Surfaces: I. Raman and NMR Spectra of Diisobutyldithiophosphate Compounds. *Colloids Surf. A Physicochem. Eng. Aspects* **2003**, *214*, 77-85.
42. Hope, G.A.; Woods, R.; Watling, K. A Spectrochemical Investigation of the Interaction of Diisobutyldithiophosphate with Copper, Silver and Gold Surfaces: II. Electrochemistry and Raman Spectroscopy. *Colloids Surf. A Physicochem. Eng. Aspects* **2003**, *214*, 87-97.
43. San Juan, R. R.; Miller, M. S.; Ferrato, M, -A.; Carmichael, T. B.; Influence of Alkyl Chain Length on the Structure of Dialkyldithiophosphinic Acid Self-Assembled Monolayers on Gold. *Langmuir* **2012**, *28*, 13253-13260.
44. Miller, M. S.; San Juan, R. R.; Ferrato, M. -A.; Carmichael, T. B. New Dialkyldithiophosphinic Acid Self-Assembled Monolayers (SAMs): Influence of Gold Substrate Morphology on Adsorbate Binding and SAM Structure. *Langmuir* **2011**, *16*, 10019-10026.
45. San Juan, R. R.; Allan, C. J.; Iqbal, M.; Eichhorn, S. H.; Macdonald, C. L. B.; Carmichael, T. B. New Dihexadecyldithiophosphate SAMs on Gold Provide Insight into the Unusual Dependence of Adsorbate Chelation on Substrate Morphology in SAMs of Dialkyldithiophosphinic Acids. *J. Am. Chem. Soc.* **2013**, *42*, 15784-15793.
46. San Juan, R. R.; Carmichael, T. B.; Formation of Self-Assembled Monolayers with

- Homogeneously Mixed, Loosely Packed Alkyl Groups Using Unsymmetrical Dialkyldithiophosphinic Acids. *Langmuir* **2012**, 28, 17701-17708.
47. San Juan, R. R. PhD Dissertation “Self-Assembled Monolayers of Dithiophosphinic Acids on Gold.” *Chapter 5: Self-Assembled Monolayers of Unsymmetrical Dithiophosphinic Acids Bearing Phenyl and Alkyl Groups.*
48. Miller, M. S.; San Juan, R. R.; Ferrato, M. -A.; Carmichael, T. B. The Unusual Self-Organization of Dialkyldithiophosphinic Acid Self-Assembled Monolayers on Ultrasoother Gold. *J. Am. Chem. Soc.* **2014**, 136, 4212-4222.
49. Weiss, E. A.; Kaufman, G. K.; Kriebel, J. K.; Li, Z.; Schalek, R.; Whitesides, G. M. Si/SiO₂-Templated Formation of Ultraflat Metal Surface on Glass, Polymer, and Solder Supports: Their Used as Substrates for Self-Assembled Monolayers. *Langmuir* **2007**, 23, 9686-9694.
50. Naumann, R.; Schiller, S. M.; Giess, F.; Grohe, B.; Hartman, K. B.; Karcher, I.; Koper, I.; Lubben, J.; Vasilev, K.; Knoll, W. Tethered Lipid Bilayers on Ultraflat Gold Surfaces. *Langmuir* **2003**, 19, 5435–5443.
51. Hegner, M.; Wagner, P.; Semenza, G. Ultralarge Atomically Flat Template-stripped Au Surface for Scanning Probe Microscopy. *Surf. Sci.* **1993**, 291, 39–46.
52. Wagner, P.; Zaugg, F.; Kernen, P.; Hegner, M.; Semenza, G. J. ω -Functionalized Self-Assembled Monolayers Chemisorbed on Ultraflat Au (111) Surfaces for Biological Scanning Probe Microscopy in Aqueous Buffers. *Vac. Sci. Technol. B* **1996**, 14, 1466–1471.

Chapter 2

Introduction of Stretchable Electronics

2.1. Background

During the past decade, electronic devices are becoming more and more important in our daily life. These devices are rigid because the electronic components are made of brittle and stiff conductive materials. As the development the material science, it is a trend to enable the transistors or circuitries in the electronic devices to be stretchable and flexible to provide convenience for us. So flexible and stretchable electronics have the potential to outperform the traditional rigid devices in terms of flexibility, stretchability and weight.

2.2. Applications of Stretchable Electronics

Electronics have the potential to enrich our daily lives with soft, bendable and even wearable devices that can monitor body conditions, sensors that can accommodate the human body's curvilinear shape, rollable and foldable paper-like displays, wearable smart surgical gloves, and skin-like prosthesis.¹⁻⁵ A paper-like display/screen is so thin and flexible that it can be rolled into small volumes, it is expected to be used for various applications from big screen TVs, to car displays which can bend around the contours inside of the vehicle (Figure 2.1 a). Similar to paper-like screen, flexible solar panel can also be rolled into a tube and conform to various shapes (Figure 2.1 b).⁶

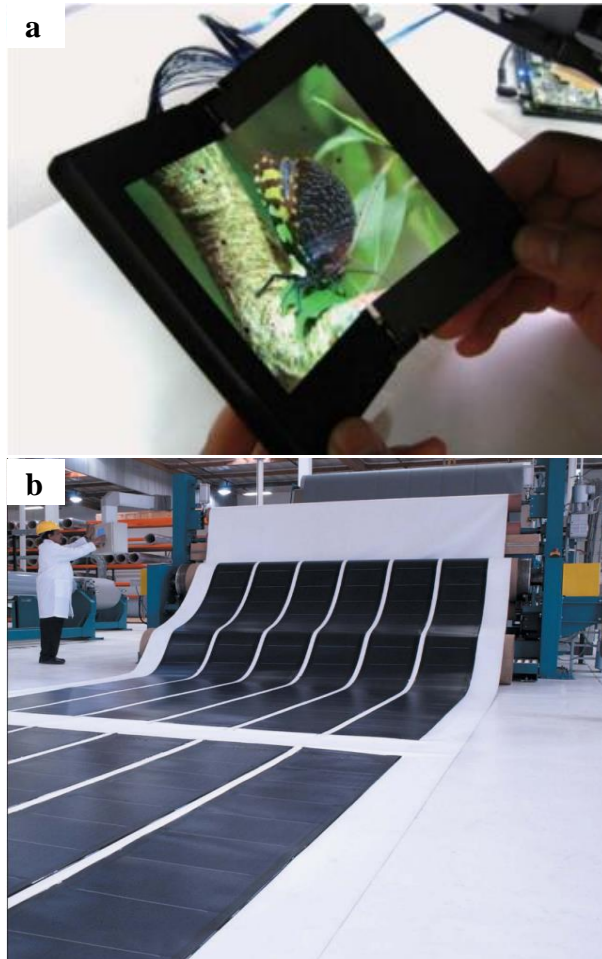


Figure 2.1. Applications of flexible electronics: (a) paper-like flexible screen,⁷ (b) flexible solar cell panel.⁶

However, ability to be bent and flex is not enough to satisfy every daily need, to overcome the restriction, stretchable electronics is extended. It is now well studied in materials science, which can maintain the functionality and conductivity when a large strain is applied and restore back. Stretchable electronics represent a much more challenging class of research for applications where circuits must be wrapped conformally around complex curvilinear shaped surfaces, or integrated with soft biological tissues that are impossible using devices that offer only flexibility.⁸ Rogers'

group introduced an electronic eye by using stretchable electronics (Figure 2.2 a).^{9,10} Intrinsically stretchable polymer light-emitting devices were created as shown in Figure 2.2 b.¹¹ The stretchable sensors can be made on very thin elastic substrates that fabricated on a catheter has also delivered into the other human organs, such as blood vessel (Figure 2.2 c).¹² Figure 2.2 d shows prosthetic skin which can bend and stretch like normal skin and allow the wearer to feel pressure, temperature and moisture.⁴

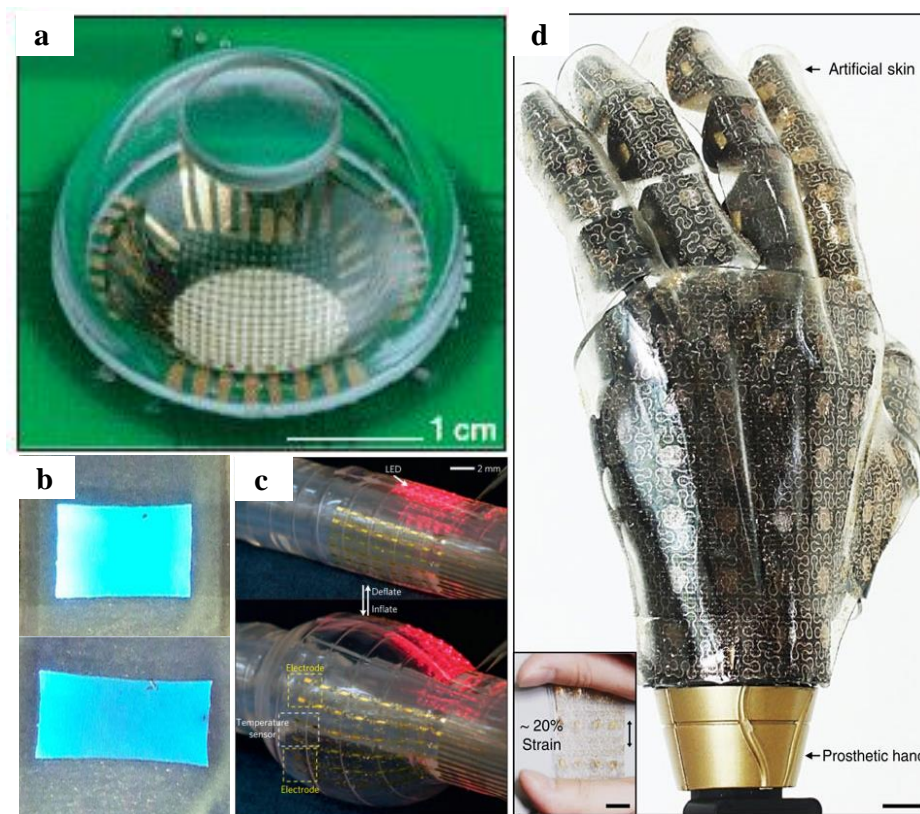


Figure 2.2. Applications of stretchable electronics: (a) a hemispherical electronic eye camera,¹⁰ (b) an intrinsically stretchable polymer light-emitting device,¹² (c) a stretchable sensor on an expandable catheter,¹³ (d) smart artificial skin covering a prosthetic hand.⁴

Stretchable electronics is a modern technology to fabricate stretchable electronic devices by depositing electronic onto soft substrates. The key to make functional, stretchable electronics is good electrical performance and mechanical robustness. Organic semiconductors and conducting polymers were appealing materials for stretchable electronics attributing to their intrinsic stretchability, light weight, and low cost.^{13,14} These stretchable electronics prototypes have the potential to enrich our lives.

2.3. Conductive materials on stretchable substrates

Soft materials, such as polydimethyl siloxane (PDMS), polyurethane (PU), butyl rubber and Ecoflex,^{15,16,17} show excellent mechanical deformability while having unsatisfactory electrical properties (not conductive). Among all these materials, PDMS has become the most popular soft substrate due to its high stretchability, biocompatibility, transparency, commercial availability, and its ability to be molded.¹⁸ The PDMS elastomer and cross-linker mixture are prepared and casted on the patterned Si mould or simply poured into a petri dish, then after degassing in vacuum and thermal curing, a PDMS thin film can be peeled off. The geometry and shape of the micro-features are well-controlled by the patterns on Si mould, which is made with photolithography. However, the ability to stretch is not enough to fabricate the stretchable electronic device.

Some strategies to thin film fabrication is develop materials that can withstand high strain because of their physical properties. Carbon based materials such as carbon nanotubes (CNTs) and graphene have the desirable mechanical and electrical properties. The CNT/PDMS composite films show very little variation in resistance under multiple stretching-and-releasing cycles up to a strain level of 40%.¹⁹ Lee *et al.* presented

stretchable, printable, and transparent transistors composed of monolithically patterned graphene film, which can maintain stable operation at stretching up to 5% after 1000 or more cycles.²⁰ Besides, metal nanowires, conductive polymer, and nanoparticles^{21,22} have been identified as attractive materials for stretchable devices due to excellent electrical properties, high transparency, and mechanical flexibility, stretchability and stability.^{23,24} A highly conductive and stretchable conductor with silver nanowires (AgNWs) embedded just below PDMS can achieve a large range of tensile strain (0 – 50%) after a few cycles of stretching/releasing of substrate.²⁵ Lipomi *et al.* demonstrated a transparent conducting polymer (PEDOT : PSS) with a fluorosurfactant onto stretchable PDMS substrates, where no significant cracking (~ 2 cracks mm^{-1}) occurs before 30% uniaxial strain.²⁶ Although these nano materials were developed in the past decade, metal is still the best conductor in terms of conductivity, stability, compatibility, and cost.²⁷

2.4. Metal films on stretchable substrates

Another approach to achieve stretchable electronics include the use of naturally flexible and stretchable polymeric substrates in combination with metal thin films.²⁸ Most conductive rigid materials like metals may exhibit good electrical performance and stability, but freestanding metal films fracture at tensile strains below $\sim 1\%$,²⁹ even for gold, which is the most malleable and ductile of all known metals. It has been observed that when free-standing metal films are expanded during the deformation of a substrate they fracture at strains of a few percent.^{30,31} Bulk metals are normally considered rigid materials, however, any material in sufficiently thin form is flexible and become stretchable when structured into proper shapes, which have been demonstrated by the work from the groups of Suo, Someya and Rogers.^{32,33,34} Thus, metal films which are

well-attached on elastomeric substrates must show excellent stretchability. Thin metal films attached on soft elastomeric substrates can sustain much larger tensile strain (by tens of percent) compared to free-standing metal film, because strain can be delocalized over the whole surface, the metal film only experience small strains, without suffering fatigue.^{35,36}

Layering the rigid conductive metal film with stretchable elastomers to achieve a combination of desirable properties for stretchable electronics/devices is more appealing than the other conductive materials on elastomers. As we mentioned above, even ductile metal, like freestanding gold film, fractures at tensile strains below $\sim 1\%$, despite of the film thickness.³⁰ Various technologies have emerged for depositing thin metal film on soft substrates such as sputter deposition,³⁵ physical vapor deposition,²⁹ chemical vapor deposition,³⁷ ink-jet printing,³⁸ and electroless deposition.³⁹ In this thesis, we choose electron beam evaporation, which is a physical vapor deposition technique, for the appeal of non-contact and programmable control to ensure precise metal thickness. By depositing metal film on soft substrates, such as PDMS, can suppress the strain localization, makes it stretchable on the conductors. The challenge is that as the stretchability is increasing, the conductivity of the metal film is decreasing rapidly, due to the cracks that propagate across the metal film as it is elongated and interrupt the conductive pathway.

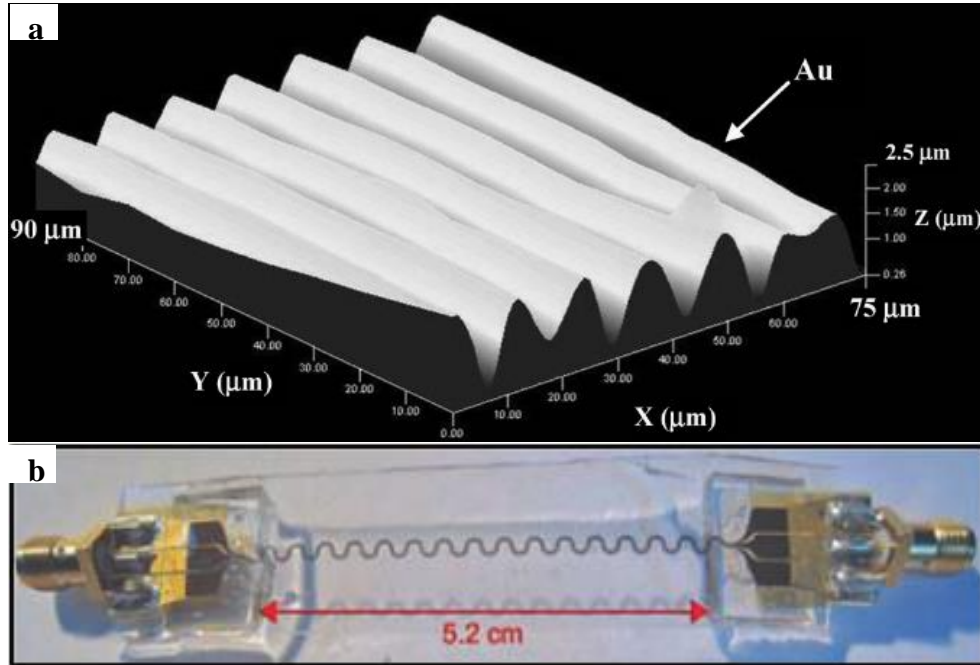


Figure 2.3. a) buckled gold surface structure after release from 15% pre-stretch,⁴¹ b) serpentine structured metal embedded in PDMS.³³

One possible way to realize stretchability is by incorporating wavy structures in thin metal films through nonlinear buckling, or wrinkling on soft substrates.⁴⁰ The design ideas of strain-relief patterns of conductive film structures also include serpentine, and interlocking (Figure 2.3).^{41,42,43} Wavy, serpentine and interlocking structures reduce the actual strain on the film by converting external tensile motion into bending motion. As the strain experienced by the metal films is reduced by the deposition pattern of the metal, the component can be successfully incorporated in stretchable electronic devices. By inducing a buckled topography PDMS surface, increased stretchability of a few tenths of percent can be obtained, by comparing to metal on flat PDMS, but the resistance increases linearly when a critical strain is reached.²⁹ The PDMS substrate with mogul-patterned surface can be multi-directionally stretchable and versatile for various thin

metal films, also the valleys and bumps structures enable the stability. The applied strain can be efficiently absorbed by the valley regions, resulting in minimal interference with motion-induced stress to remain conductive after 1000 stretching cycles at 50% strain.⁴⁴ Lacour *et al.* showed metal films on micropillar array PDMS substrate exhibit high electrical conductivity and can stretch reversibly to 20% without failing electrically. In which cracks are allowed and the cracks seem to start or stop at the closest pillar base at site of local strain maxima, the cracks widen but do not propagate at higher strain, and additional narrower cracks appear in between the pillars.⁴⁵

Our group used spin-coating to deposit an aqueous emulsion of poly(vinyl acetate) (PVAc) onto an oxidized PDMS surface to achieve a microstructured PDMS substrate surface. When coated with gold, these structure remains conductive up to 65% elongation.⁴⁶ Because the microstructured surface provides numerous defect sites that localize strain when stretching, prevents long crack propagation and preserve the conductive pathways. Au is used for the highly conductivity, and will not be oxidized which makes gold a desirable metal in the stretchable electronics field, compared to Cu and Ag.

2.5. Scope of thesis

In the second half of the thesis, we focused on using E-Beam evaporation to deposit Au thin films onto PDMS substrates, which is oxidized and spin coated with modified-silica, to induce a micro-structured PDMS substrate by using agglomerated silica nanoparticles to enhance the stretchability and conductivity. These structures can maintain a similar stretchable electrical behavior to the PVAc glue structures. By altering the weight ratio of modified-silica:PDMS interlayer, the resistance change can be tuned, which can lead to different functional stretchable devices. This work is presented in Chapter 4.

2.6. References

1. Rogers, J. A.; Bao, Z. Printed plastic electronics and paperlike displays. *J. Polym. Sci. Part A: Polym. Chem.* **2002**, 40, 3327-3334.
2. Genlinck, G. H.; Huitema, H. E. A.; Veenendaal, E. v.; Cantatore, E.; Schrijnemakers, L.; van der Putten, J. B.; Geuns, T. C.; Beenhakkers, M.; Giesbers, J. B.; Huismane, B. H.; Meijer, E. J.; Benito, E. M.; Touwslager, F. J.; Marsman, A. W.; van Rens, B. J. E.; Deleeuw, D. M. Flexible Active-Matrix Displays and Shift Registers Based on Solution-Processed Organic Transistors. *Nature Materials* **2004**, 3, 106-110.
3. Kim, S. Y.; Park, S.; Park, H. W.; Park, D. H.; Jeong, Y.; Kim, D. H. High Sensitive and Multimodal All-Carbon Skin Sensors Capable of Simultaneously Detecting Tactile and Biological Stimuli. *Adv. Mater.* **2015**, 28, 4178-4185.

4. Kim, J.; Lee, M.; Shim, H. J.; Ghaffari, R.; Cho, H. R.; Son, D.; Jung, Y. H.; Soh, M.; Choi, C.; Jung, S.; Chu, K.; Jeon, D.; Lee, S. -T.; Kim, J. H.; Choi, S. H.; Hyeon, T.; Kim, D. -H. Stretchable Silicon Nanoribbon Electronics for Skin Prosthesis. *Nature Communications* **2014**, *5*, 5747.
5. Rogers, J. A.; Bao, Z.; Baldwin, K.; Dodabalapur, A.; Crone, B.; Raju, V. R.; Kuck, V.; Katz, H.; Amundson, K.; Ewing, J.; Drzaic, P. Paper-Like Electronic Displays: Larger-Area Rubber-Stamped Plastic Sheets of Electronics and Microencapsulated Electrophoretic Inks. *PNAS*. **2001**, *98*, 4835-4840.
6. Pagliaro, M.; Ciriminna, R.; Palmisano, G. Flexible Solar Cells. *ChemSusChem* **2008**, *1*, 880-891.
7. Kim, S.; Choi, W.; Rim, W.; Chun, Y.; Shim, H.; Kwon, H.; Kim, J.; Kee, I.; Kim, S.; Lee, S.; Park, J. A Highly Sensitive Capacitive Touch Sensor Integrated on a Thin-Film-Encapsulated Active-Matrix OLED for Ultrathin Displays. *IEEE Trans. Electron Devices* **2011**, *58*, 3609-3615.
8. Kim, D. -H.; Rogers, J. A. Stretchable Electronics: Materials Strategies and Devices. *Adv. Mater.* **2008**, *20*, 4887-4892.
9. Kim, D. H.; Stoykovich, M. P.; Song, J.; Malyarchuk, V.; Choi, W. M.; Yu, C. J.; Geddes III, J. B.; Xiao, S.; Huang, Y.; Rogers, J. A. Hemispherical Electronic Eye Camera Based on Compressive Silicon Optoelectronics," *Nature* **2008**, *454*, 748-753.
10. Jung, I.; Xiao, J.; Malyarchuk, V.; Lu, C.; Li, M.; Liu, Z.; Yoon, J.; Huang, Y.; Rogers, J. A. Dynamically Tunable Hemispherical Electronic Eye Camera System

- with Adjustable Zoom Capacity. *Proc. Natl. Acad. Sci. U.S.A.* **2010**, 108, 1788-1793,
11. Yu, Z.; Niu, X.; Liu, Z.; Pei, Q. Intrinsically Stretchable Polymer Light-Emitting Devices Using Carbon Nanotube-Polymer Composite Electrodes. *Adv. Mater.* **2011**, 23, 3989-3994.
 12. Kim, D. H.; Lu, N.; Ghaffari, R.; Kim, Y. S.; Lee, S. P.; Xu, L.; Wu, J.; Kim, R. H.; Song, J.; Liu, Z.; Viventi, J.; de Graff, B.; Elolamp, B.; Mansour, M.; Slepian, M. J.; Hwang, S.; Moss, J. D.; Won, S. M.; Huang, Y.; Litt, B.; Rogers, J. A.; Materials for Multifunctional Balloon Catheters with Capabilities in Cardiac Electrophysiological Mapping and Ablation Therapy. *Nat. Mater.* **2011**, 10, 316-323.
 13. Lu, N.; Kim, D. -H. Flexible and Stretchable Electronics Paving the Way for Soft Robotics. *Soft Robotics* **2014**, 1, 53-62.
 14. Dimitrakopoulos, C. D.; Malenfant, P. R. L. Organic Thin Film Transistors for Large Area Electronics. *Adv. Mater.* **2002**, 14, 99-117.
 15. Kojio, K.; Furukawa, M.; Nonaka, Y.; Nakamura, S. Control of Mechanical Properties of Thermoplastic Polyurethane Elastomers by Restriction of Crystallization of Soft Segment. *Materials* **2010**, 3, 5097-5110.
 16. Yu, Y.; Zeng, J.; Chen, C.; Xie, Z.; Guo, R.; Liu, Z.; Zhou, X.; Yang, Y.; Zheng, Z. three-Dimensional Compressible and Stretchable Conductive composites. *Adv. Mater.* **2014**, 26, 810-815.
 17. Vohra, A.; Filiatrault, H. L.; Amyotte, S. D.; Carmichael, R. S.; Suhan, N. D.; Siegers, C.; Ferrari, L.; Davidson, G. J. E.; Carmichael, T. B. Reinventing Butyl Rubber for Stretchable Electronics. *Adv. Funct. Mater.* **2016**, 26, 5222-5229.

18. Thangawng, A. L.; Ruoff, R. S.; Swartz, M. A.; Glucksberg, M. R. An Ultra-Thin PDMS membrane as Bio/Micro-Nano Interface: Fabrication and Characterization. *Biomed Microdevices* **2007**, *9*, 587-595.
19. Zu, M.; Li, Q.; Wang, G.; Byun, J. -H.; Chou, T, -W. Carbon Nanotube Fiber Based Stretchable Conductor. *Adv. Funct. Mater.* **2013**, *23*, 789-793.
20. Lee, S. -K.; Kim, B. J.; Jang, H.; Yoon, S. C.; Lee, C.; Hong, B. H.; Rogers, J. A.; Cho, J. H.; Ahn, J. -H. Stretchable Graphene Transistors with Printed Dielectrics and Gate Electrodes. *Nano Lett.* **2011**, *11*, 4642-4646.
21. Vena, A.; Moradi, E.; Kosko, K.; Bobar, A. A.; Sydanheimo, L.; Ukkonen, L. Design and Realization of Stretchable Sewn Chipless RFID Tags and Sensors for Wearable Applications. *IEEE International Conference on* **2013**, 176-183.
22. Kim, Y.; Zhu, J.; Yeom, B.; Di Prima, M.; Su, X.; Kim, JG; Yoo, S. J.; Yher, C.; Kotov, N. A. Stretchable Nanoparticle Conductors with Self-Organized Conductive Pathways. *Nature* **2013**, *500*, 59-63.
23. Zu, M.; Li, Q.; Wang, G.; Byun, J. -H.; Chou, T, -W. Carbon nanotube Fiber Based Stretchable Conductor. *Adv. Funct. Mater.* **2013**, *23*, 789-793.
24. Jang, H.; Park, Y. J.; Chen, X.; Das, T.; Kim, M. -S.; Ahn, J. -H. Graphene-Based Flexible and Stretchable Electronics. *Adv. Mater.* **2016**, *28*, 4184-4202.
25. Xu, F.; Zhu, Y. Highly Conductive and Stretchable Silver Nanowires Conductors. *Adv. Mater.* **2012**, *24*, 5117-5122.
26. Lipomi, D. J.; Lee, J. A.; Vosgueritchian, M.; Tee. B. C. -K.; Bolander, J. A.; Bao, Z. Electronic Properties of Transparent Conductive Films of PEDOT:PSS on Stretchable Substrates. *Chem. Mater.* **2012**, *24*, 373-382.

27. Liu, X.; Zhou, X.; Li, Y.; Zheng, Z. Surface-Grafted Polymer-Assisted Electroless Deposition of Metals for Flexible and Stretchable Electronics. *Chem. Asian J.* **2012**, *7*, 862-870.
28. Bao, Z.; Chen, X. Flexible and Stretchable Devices. *Adv. Mater.* **2016**, *28*, 4177-4179.
29. Lacour, S. P.; Wagner, S.; Huang, Z.; Suo, Z. Stretchable Gold Conductors on Elastomeric Substrates. *Appl. Phys. Lett.* **2003**, *82*, 2404-2406.
30. Huang, H.; Spacpen, F. Tensile Testing of Free-Standing Cu, Ag and Al Thin films and Ag/Cu Multilayers. *Acta Mater.* **2000**, *48*, 3261-3269.
31. Hsu, P. I.; Huang, M.; Wagner, S.; Suo, Z.; Sturm, J. C. Plastic Deformation of Thin Foil Substrates with Amorphous Silicon Islands into Spherical Shapes. *Mater. Res. Soc. Symp. Proc.* **2000**, *621*, Q8.6.1-Q8.6.6.
32. Li, T.; Huang, Z. Y.; Suo, Z.; Lacour, S. P.; Wagner, S. Stretchability of Thin Metal films on Elastomer Substrates. *Appl. Phys. Lett.* **2004**, *85*, 3435-3437.
33. Rogers, J. A.; Someya, T.; Huang, Y. Materials and Mechanics for Stretchable Electronics. *Science* **2010**, *327*, 1603-1607.
34. Sekitani, T.; Someya, T. Stretchable, Large-area Organic Electronics. *Adv. Mater.* **2010**, *22*, 2228-2246.
35. Xiang, Y.; Li, T.; Suo, Z.; Vlassak, J. J. High Ductility of a Metal Film Adherent on a Polymer Substrate. *Appl. Phys. Lett.* **2005**, *87*, 161910.
36. Lacour, S. P.; Chan, D.; Wagner, S.; Li, T.; Suo, Z. Mechanisms of Reversible Stretchability of Thin Metal Films on Elastomeric Substrates. *Appl. Phys. Lett.* **2006**, *88*, 204103.

37. Jeon, N. L.; Nuzzo, R. G. Patterned Self-Assembled Monolayers Formed by Microcontact Printing Direct Selective Metalization by Chemical Vapor Deposition on Planar and Nonplanar Substrates. *Langmuir* **1995**, 11, 3024-3026.
38. Park, B. K.; Kim, D.; Jeong, S.; Moon, J.; Kim, J. S. Direct Writing of Copper Conductive Patterns by Ink-Jet Printing. *Thin Solid Films* **2007**, 515, 7706-7711.
39. Wang, X.; Hu, H.; Shen, Y.; Zhou, X.; Zheng, Z. Stretchable Conductors with Ultrahigh Tensile Strain and Stable Metallic Conductance Enabled by Prestrained Polyelectrolyte Nanoplateforms. *Adv. Mater.* **2011**, 23, 3090-3094.
40. Wang, Y.; Li, Z.; Xiao, J. Stretchable Thin Film Materials: Fabrication, Application, and Mechanics. *Journal of Electronic Packaging* **2016**, 138, 020801 - 1-22.
41. Lacour, S. P.; Jones, J.; Wagner, S.; Li, T.; Suo, Z. Stretchable Interconnects for Elastic Electronic Surfaces. *Proc. IEEE.* **2005**, 93, 1459-1467.
42. Xu, S.; Zhang, Y.; Cho, J.; Lee, J.; Huang, X.; Fan, J. A.; Su, Y.; Su, J.; Zhang, H.; Cheng, H.; Lu, B.; Yu, C.; Chung, C.; Kim, T.; Song, T.; Shigeta, K.; Kang, S.; Dagdeviren, C.; Petrov, I.; Braun, P. V.; Huang, Y.; Paik, U.; Rogers, J. A. Stretchable Batteries with Self-Similar Serpentine Interconnects and Integrated Wireless Recharging Systems. *Nat. Comm.* **2013**, 4, 1-8.
43. Ruh, D.; Reith, P.; Sherman, S.; Theodor, M.; Ruhhammer, J.; Seifert, A.; Zappe, H. Stretchable Optoelectronic Circuits Embedded in a Polymer Network. *Adv. Mater.* **2013**, 26, 1706-1710.
44. Lee, H. -B.; Bae, C. -W.; Duy, L. T.; Sohn, I.; Kim, D. -I.; Song, Y. -J.; Kim, Y. -J.; Lee, N. -E. Mogul-Patterned Elastomeric Substrates for Stretchable Electronics. *Adv. Mater.* **2016**, 28, 3069-3077.

45. Robinson, A. P.; Minev, I.; Graz, I. M.; Lacour, S. P. Microstructured Silicone Substrate for Printable and Stretchable Metallic Films. *Langmuir* **2011**, *27*, 4279-4284.
46. Filiatrault, H. L.; Carmichael, R. S.; Boutette, R. A.; Carmichael, T. B. A Self-Assembled, Low-Cost, Microstructured Layer for Extremely Stretchable Gold Films. *ACS Appl. Mater. Interfaces* **2015**, *7*, 20745-20752.

Chapter 3

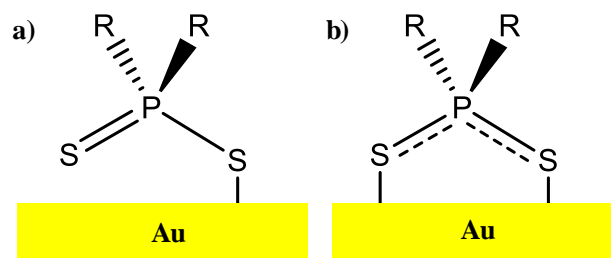
Branched Dialkyldithiophosphinic Acid Self-Assembled

Monolayers on Gold

3.1. Introduction

Forming densely-packing, well-ordered self-assembled monolayers (SAMs) on gold is one of the well-studied methods to research the surface properties, which are determined by the terminal tail group of the adsorbates. Since the introduction of SAMs, researcher have been motivated to create SAMs with a range of interfacial properties, such as wettabilities and frictional coefficient. Dialkyldithiophosphinic Acid (DTPA) molecules have two potential binding modes to gold surface: one is anchored by a single Au-S bond (monodentate), whereas the second is anchored by two Au-S bonds (bidentate) (Scheme 3.1). Srisombat *et al.* studied about the stability of mono, bis-, and trischelating alkanethiol SAMs, it showed that SAM thermal stability correlates to the degree of chelation (i.e., tridentate > bidentate > monodentate).¹

Gold films deposited by electron-beam evaporation (As-Dep gold) are composed of a layer of continuous small grains of ~25-50 nm, separated by deep grain boundaries of ~10 nm,² which inhibit the DTPA adsorbates from chelate binding, provide a mixture of bidentate (60%) and monodentate (40%) in the SAM. In contrast, gold substrates produced by a process known as template-stripping (TS) provide an ultrasmooth surface, which consists of large but flat grains of ~200-500 nm, separated by shallow grain boundaries of ~1.5 nm.³⁻⁶ In the SAMs that formed on TS gold, all the adsorbates chelate to the gold surface, the bidentate DTPA molecules prevent rotation about the Au-S bond and no changes in the Au-S-P bond angles.



Scheme 3.1. Dialkyldithiophosphinic Acid bond to gold surface: a) monodentate and b) bidentate binding.

Our group has explored the use of chelating dialkyldithiophosphinic acids (R_2 DTPA) to expand the understanding the relationship between adsorbate structure and SAM structure, as well as to access SAMs with new structures and interfacial properties.^{7,8,9} Miller *et al.* published a study of SAMs formed from $(C_{16})_2$ DTPA, which possess headgroups that are capable of either mono- or bidentate binding to a gold surface.¹⁰ As mentioned above, As-Dep gold films consist of small grains and deep grain boundaries, which causes the some of the DTPA adsorbates to adopt monodentate binding. The monodentate binding allows rotation about the Au-S bond and small changes in the Au-S-P bond angle, enables the alkyl groups to pack densely in DTPA on As-Dep gold.^{9,10} However, TS gold films consist of large and flat grains, so all the DTPA adsorbates can chelate to the surface. The resulting alkyl layer organization of DTPA SAMs on As-Dep gold DTPA is liquid-like and disordered because of a relative decrease in van der Waals interaction between the chains. As the chain length increases, the alkyl layer becomes more crystalline and ordered. While all the DTPA adsorbates chelate to the TS gold surface, which conflicts with the steric demands of the bulky DTPA headgroups, limits

the packing density as the alkyl chain length is increasing. Shortening the chain length can reduce the steric demand of the alkyl groups, and change the structure and packing density of the adsorbates in the SAM. So SAMs formed from adsorbate with short alkyl chain ($n = 5$) are ordered and crystalline, and the alkyl groups become increasingly disordered and liquid-like as the number of methylene units is increased. This trend is opposite to the behavior exhibited by DTPA SAMs on As-Dep gold substrates, in which the alkyl layer become more crystalline and ordered as the alkyl chain length is increased, in terms of flexibility of monodentate adsorbates and the increasing of van der Waals interactions between alkyl groups.

We introduce SAMs formed from branched symmetrical DTPA adsorbates, $(C_6C_2)_2DTPA$ and $(C_5C_1)_2DTPA$, which have the similar structure with $(C_6)_2DTPA$ studied in Miller's paper.¹⁷ We study whether the branch alkyl chain can fill the empty space and have a higher packing density SAM on TS gold or the steric demands of the short alkyl chain play a role to result a liquid-like SAM. Using X-ray photoelectron spectroscopy (XPS), we establish that SAMs consist of bidentate adsorbates on TS gold and a mixture of mixture of bidentate (60%) and monodentate (40%) on As-Dep gold. We compare the alkyl chain organization of the DTPA SAMs to similar main chain length without the branched chain DTPA and analogous RSH SAMs on TS and As-Dep gold using reflection-adsorption infrared spectroscopy (RAIRS), contact angle measurements.

3.2. Experimental Section

All chemicals were purchased commercially and used as received. Anhydrous tetrahydrofuran and diethyl ether were obtained from an Innovative Technologies solvent purification system. Nuclear magnetic resonance (NMR) spectroscopic data were obtained and recorded on a Bruker Avance 300 MHz or a Bruker Avance 300 MHz Ultrashield at room temperature, and shifts are reported in parts per million (ppm). $^{31}\text{P}\{^1\text{H}\}$ NMR spectra were referenced externally to 85 % H_3PO_4 ($\delta = 0$ ppm). ^1H NMR spectra were referenced to residual proton peaks of CDCl_3 ($\delta = 7.27$ ppm). $^{13}\text{C}\{^1\text{H}\}$ NMR spectra were referenced to CDCl_3 ($\delta = 77.0$ ppm).

3.2.1. Synthesis of Branched DTPAs

Synthesis of $(\text{C}_6\text{C}_2)_2\text{P}(\text{O})\text{H}$ and $(\text{C}_5\text{C}_1)_2\text{POH}$ The Grignard reagent (BrMgC_6C_2) or (BrMgC_5C_1) (generated by refluxing the appropriate alkyl halide with Mg turnings in THF) was added in excess (~4 eq.) to a solution of diethyl phosphite and refluxed in THF for 48 h, described by Müller *et al.*¹¹ Subsequent quenching, extracting and rinsing were performed according to Guoxin *et al.*¹² to give the symmetrical phosphine oxide $(\text{C}_6\text{C}_2)_2\text{P}(\text{O})\text{H}$ as a yellow oil at 20% yield and $(\text{C}_5\text{C}_1)_2\text{P}(\text{O})\text{H}$ as a grey-yellow oil at 22% yield.

$(\text{C}_6\text{C}_2)_2\text{P}(\text{O})\text{H}$: $^{31}\text{P}\{^1\text{H}\}$ NMR (CDCl_3 , 121 MHz, 298 K): δ 31.09. ^1H NMR (CDCl_3 , 300 MHz, 298 K): δ 6.97 (d, $|^1\text{J}_{\text{P-H}}| = 445$ Hz, PH), 1.78–1.30 (m, 4H, PCH_2), 1.57–1.50 (m, 2H, PCH_2CH), 1.40–1.12 (m, 16H, CH_2), 0.85–0.74 (m, 12H, CH_3).

(C₅C₁)₂P(O)H: ³¹P {¹H} NMR (CDCl₃, 121 MHz, 298 K): δ 35.39. ¹H NMR (CDCl₃, 300 MHz, 298 K): δ 6.84 (d, |¹J_{P-H}| = 445 Hz, PH), 1.85–1.60 (m, 4H, PCH₂), 1.57–1.46 (m, 2H, CH), 1.34–1.16 (m, 8H, CH₂), 0.89–0.78 (m, 12H, CH₃).

Synthesis of Nickel Complexed (C₆C₂)₂DTPA and (C₅C₁)₂DTPA The reduction of phosphine oxide precursor (C₆C₂)₂P(O)H or (C₅C₁)₂P(O)H was performed according to Klaehn *et al.*¹³ The oxidation with sulfur and the Ni complexation were performed according to Guoxin *et al.*¹² The Ni complex [(C₆C₂)₂P(S)S]₂Ni and [(C₅C₁)₂P(S)S]₂Ni were synthesized. The Ni complexes were then recrystallized in ethanol.

[(C₆C₂)₂P(S)S]₂Ni: ³¹P {¹H} NMR (CDCl₃, 121 MHz, 298 K): δ 97.8.

[(C₅C₁)₂P(S)S]₂Ni: ³¹P {¹H} NMR (CDCl₃, 121 MHz, 298 K): δ 97.7.

Synthesis of (C₆C₂)₂DTPA and (C₅C₁)₂DTPA The Ni was uncomplexed according to Guoxin *et al.*¹² by stirring with ethylenediaminetetraacetic acid (EDTA) overnight to yield the DTPA (C₆C₂)₂P(S)SH and (C₅C₁)₂P(S)SH at 6% and 4% overall yield, respectively.

(C₆C₂)₂P(S)SH: ³¹P {¹H} NMR (CDCl₃, 121 MHz, 298 K): δ 70.1. ¹H NMR (CDCl₃, 300 MHz, 298 K): δ 2.11–1.97 (m, 4H, PCH₂), 1.65–1.50 (m, 2H, PCH₂CH), 1.43–1.17 (m, 16H, CH₂), 0.90–0.82 (m, 12H, CH₃). ¹³C {¹H} NMR (CDCl₃, 75 MHz, 298 K): δ 44.3 (d, |J_{P-C}| = 37.7 Hz, 2C, PCH₂), 33.9 (d, |J_{P-C}| = 10.6 Hz, 2C, PCH₂CH), 29.3–25.9 (m, 8C, CH₂), 14.2 (s, 2C, CH₃), 10.5 (s, 2C, CH₃).

(C₅C₁)₂P(S)SH: ³¹P {¹H} NMR (CDCl₃, 121 MHz, 298 K): δ 70.8. ¹H NMR (CDCl₃, 300 MHz, 298 K): δ 2.20–1.92 (m, 4H, PCH₂), 1.70–1.40 (m, 2H, CH), 1.40–1.18 (m, 12H, CH₂), 0.93–0.86 (m, 12H, CH₃). ¹³C {¹H} NMR (CDCl₃, 75 MHz, 298 K): δ 44.2

(d, $|J_{P-C}| = 36.3$ Hz, 2C, PCH₂), 33.9 (d, $|J_{P-C}| = 9.8$ Hz, 2C, PCH₂CH₂), 29.7 (m, 2C, CH₂), 23.2 (s, 2C, CH) 14.5 (s, 2C, CH₃), 10.8 (s, 2C, CH₃).

3.2.2. Gold Substrate Preparation and SAM Formation

Template-stripped (TS) gold films were prepared according to published procedures.² 500 nm gold was deposited onto silicon wafers by e-beam evaporation, and then a small drop (10 μ L) of Norland Optical Adhesive 83H was applied to the gold surface followed by a 2 cm \times 2 cm glass substrate. After curing the adhesive using a UV lamp for 15 min, the glass slide was stripped from the silicon wafer using a scalpel. As deposited (As-Dep) gold films were produced by depositing 2 nm of titanium as an adhesion promoter onto silicon wafers, followed by 200nm of gold, using an electron-beam evaporator. Both As-Dep and TS gold films were used immediately after their fabrication for SAM formation to minimize surface contamination.

Approximately 2 cm \times 2 cm TS and As-Dep gold substrates were immersed into a 1 mM SAM solution (**1** and **2**) in anhydrous toluene for 18-24 h. Substrates were then removed from solution, rinsed with anhydrous toluene and dried under a stream of nitrogen.

3.2.3. Characterization

Infrared Spectroscopy Reflection-absorption infrared (RAIR) spectra were collected using a Bruker IFS 66/v spectrometer in single reflection mode equipped with an mercury cadmium telluride (MCT) detector and Harrick Autoseagull accessory. The p-polarized light was incident at 85° from the surface normal, and 1024 scans were collected at a resolution of 2 cm⁻¹.

Contact Angle Measurements Water and hexadecane contact angles were measured using the sessile drop method on a Ramé-Hart contact angle goniometer equipped with a microliters syringe. In each case, contact angle measurements of at least three drops from three different samples were averaged.

X-ray Photoelectron Spectroscopy (XPS) XPS spectra were collected at Surface Science Western (London, Ontario, Canada) using a Kratos Axis Nova X-ray photoelectron spectrometer with a monochromatic Al K α source. The detection limit of the instrument is 0.1-0.5 atomic percent. Both survey scan and high-resolution analyses were carried out over a 300 μm \times 700 μm scan area. Survey scan analyses were carried out with a pass energy of 160 eV, and high-resolution analyses were carried out with a pass energy of 20 eV. Samples were analyzed at a 30 $^\circ$ takeoff angle (60 $^\circ$ tilt). High-resolution sulfur line shapes were fit using one pair of spin-orbit-split components (2 p $_{3/2}$ and 2 p $_{1/2}$) assuming a Gaussian/Lorentzian (70%:30%) line shape and a fixed splitting energy of 1.18 eV with a 2:1 area ratio.

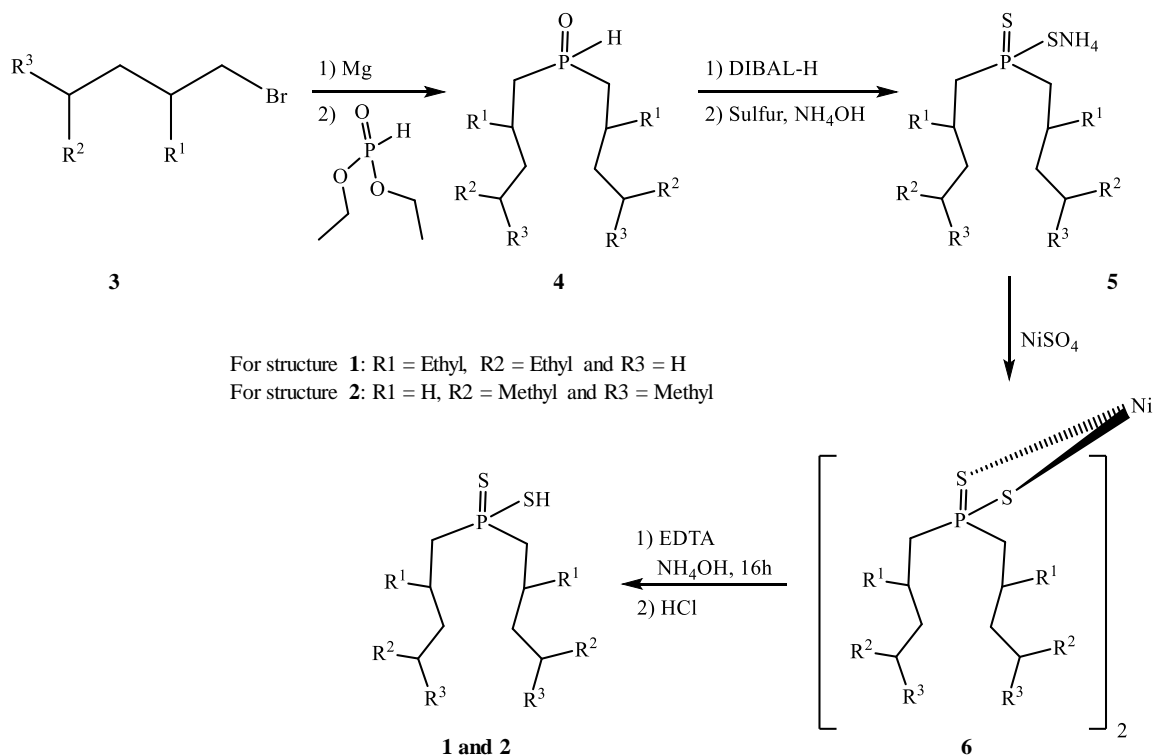
3.3. Results and Discussion

3.3.1. Synthesis of Branched Alkyl DTPAs

For synthesis of **1** (C $_6$ C $_2$) $_2$ P(S)SH and **2** (C $_5$ C $_1$) $_2$ P(S)SH, we performed a Grignard reaction using 4 equivalents **3** of the reactant with diethyl phosphite to form the phosphine oxide **4**. Reaction with diisobutylaluminium hydride (DIBAL-H) then generated the secondary phosphine, and oxidation with elemental sulfur provided the crude product **5**. We complexed the crude the product with NiSO $_4$, recrystallized the blue

oil **6** in diethyl ether and decomplexed the Ni²⁺ with EDTA in NH₄OH. The organic product was acidified with HCl to yield **1** and **2** in the 6% and 4% overall yield, respectively (Scheme 3.2).

The ³¹P, ¹H and ¹³C NMR spectra of compounds **1** and **2** are presented in supporting information (Figure S3.1 and S3.2).



Scheme 3.2. Synthetic Procedure to prepare dialkyldithiophosphinic acids.

3.3.2. SAM Formation

We prepared gold films by electron-beam evaporation on silicon wafers with Ti adhesion layer (As-Dep gold) and Template-stripped (TS) gold films,⁴ TS gold were made by evaporating 5000 Å gold on silicon wafer without an adhesion layer, a small

adhesive drop was applied to the gold surface followed by cleaned glass substrate, and cured the adhesive, stripped gold from the wafer. Then the As-Dep and TS gold films were used to prepare SAMs of these substrates by immersing the substrate into 1 mM solution of the DTPAs (**1** and **2**) in anhydrous toluene for 18-24 hrs. Substrates were then removed from solutions, rinsed with anhydrous toluene and dried under a stream of nitrogen.

3.3.3. Binding of the DTPAs Head Group to the Gold Surface

XPS survey scans of $(C_6C_2)_2DTPA$ on the TS and As-Dep gold films detected carbon, sulfur, phosphorus and gold, consistent with SAM formation (Figure S3.3 and S3.4 in the supporting information). Oxygen was also detected in the survey scan. We used high-resolution XPS (HR-XPS) of the S 2p region to determine the binding state of the DTPA adsorbates to the gold surface. The electronic environment of the sulfur atom and the nature of the interaction between sulfur and gold surface atoms influence the S 2p binding energies. HR-XPS of the S 2p region can distinguish between sulfur atoms bound to gold (S 2p_{3/2} BE ~161–162 eV), sulfur species not interacting with gold (S 2p_{3/2} BE ~163–165 eV), and oxidized sulfur species (S 2p_{3/2} BE > 166 eV).^{14,15}

HR-XPS spectra of the S 2p region of the DTPA SAMs on TS and As-Dep gold surfaces showed line shapes that we fit using one pair of S 2p_{3/2} and S 2p_{1/2} spin-orbit-split components by assuming a Gaussian/Lorentzian (70%:30%) line shape and a splitting energy fixed at 1.18 eV (Figure 3.1) and the data are summarized in Table 3.1.¹⁶ The S 2p_{3/2} binding energies of the fitted peaks, assignments of these peaks, and the ratio of chemisorbed and non-interacting sulfur species for DTPA SAMs are shown in Table

3.1. The DTPA **1** SAM on As-Dep gold shows S 2p_{3/2} peak at ~161 eV corresponding to chemisorbed to gold through a gold-sulfur bond, and a non-interacting peak at ~163 eV, indicating monodentate adsorbates presented. This mixture of binding modes is consistent with previously reported SAMs of R₂DTPA and R¹R²DTPA molecules on As-Dep gold.^{1,4,5}

For the (C₆C₂)₂DTPA SAM on As-Dep gold, the chemisorbed sulfur:noninteracting sulfur ratio is approximately 70:30, corresponding to a bidentate:monodentate DTPA ratio of 40:60 (Figure 3.1 a). It has been demonstrated that the short hexyl chain does not block oxygen from penetrating the SAM,⁹ however, it is interesting that the S 2p HR-XPS spectrum of the (C₆C₂)₂DTPA SAM on As-Dep gold does not show evidence of oxidized sulfur species, considering that oxidized sulfur species were detected in (C₆)₂DTPA.⁹ It revealed that the branched ethyl chain on the hexyl chain helped to protect the sulfur atoms from oxidation better than single alkyl chain.

(C₆C₂)₂DTPA SAM on TS gold (Figure 3.1 b) showed the presence of only one type of sulfur atoms (chemisorbed sulfur), bonded to the gold surface, which means all the adsorbates are chelated to the TS gold surface. The absence of peaks at ~167–169 eV, due to oxidized sulfur species, is consistent with previous studies of R₂DTPA SAMs on TS gold, which showed all adsorbates chelate to gold surface and protected to headgroup from oxidation even for the shortest alkyl chain lengths (from C₆ to C₁₆).¹⁷ On TS gold, chelation of the headgroup likely protect the headgroup from oxidation.

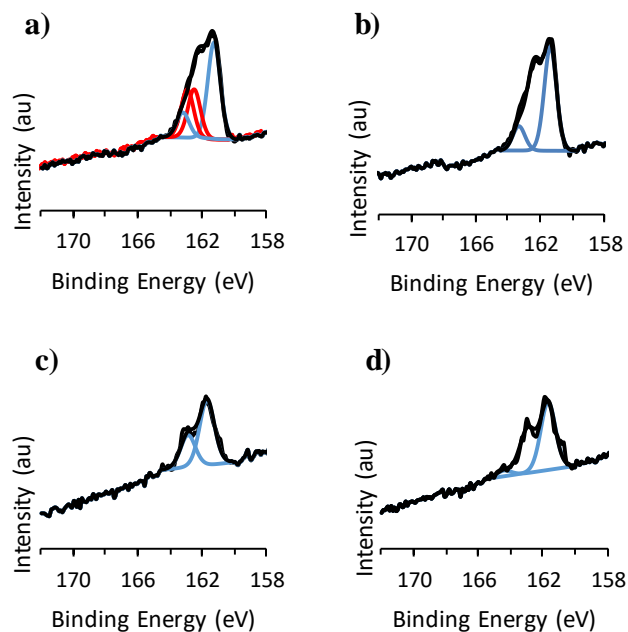


Figure 3.1. HR-XPS spectra of the S 2p region of $(C_6C_2)_2DTPA$ (a,b) and C_6C_2SH (c,d) SAM on As-Dep gold (a,c) and TS gold (b,d).

| | S $2p_{3/2}$ Binding Energies (eV) | | | |
|--|------------------------------------|------------|------------------|------------|
| | SAMs on As-Dep Gold | | SAMs on TS Gold | |
| | $(C_6C_2)_2DTPA$ | C_6C_2SH | $(C_6C_2)_2DTPA$ | C_6C_2SH |
| Chemisorbed S (blue) | 161.7 | 161.6 | 161.2 | 161.5 |
| Non-interacting S (red) | 162.4 | - | - | - |
| Ratio of chemisorbed : non-interacting S | 67:33 | 100:0 | 100:0 | 100:0 |

Table 3.1. S $2p_{3/2}$ Binding Energy and the ratio of Chemisorbed : Non-interacting S species of $(C_6C_2)_2DTPA$ and C_6C_2SH SAM on As-Dep and TS gold.

C₆C₂SH on As-Dep and TS gold shows the same results as the (C₆C₂)₂DTPA on TS gold, only chemisorbed sulfur is observed and no oxidized sulfur (Figure 3.1 c and d). Because in thiolate SAMs, only one sulfur atom is presented in the molecule, which will always form a stable S-Au bond, no matter the gold surface is flat or with deep grains.

3.3.4. Organization of the Alkyl Chains

Reflection-absorption infrared (RAIRS) of SAMs provides information about the packing density, crystallinity and conformation of alkyl groups. By examining the frequencies of the asymmetric and symmetric methylene C-H stretches, we can assess the alkyl group crystallinity,¹² while the peak intensities in spectra of the C-H stretching are determined by two factors. One is the surface selection rule, where low methylene stretching intensities indicates less molecular tilt from the surface normal in the SAM. The second factor is that low density of alkyl chains results in low stretching intensities. The RAIRS spectra of the branched DTPA SAMs **1** and **2** on TS gold are shown in Figure 3.2, along with dashed lines at 2918 cm⁻¹ and 2850 cm⁻¹ that correspond to the peak positions of the $\nu_{as}(\text{CH}_2)$ and $\nu_s(\text{CH}_2)$ stretches for the crystalline chain of C₁₆SH SAMs on gold for comparison. The organization of SAMs on TS gold shows that the short branched alkyl chain of both (C₆C₂)₂DTPA and (C₅C₁)₂DTPA SAMs are highly crystalline, which directly counters the (C₆C₂)₂DTPA and (C₅C₁)₂DTPA SAMs on As-Dep gold. The peak intensities of the SAM are low due to the presence of the few methylene groups. The methylene stretching frequencies of asymmetric and symmetric for SAMs **1** and **2** on TS and As-Dep gold are shown in Table 3.2.

The previous papers showed that on As-Dep gold, the DTPA adsorbates provide a mixture of bidentate (60%) and monodentate (40%) to underlying as the number of

methylene units in the chain increase, the crystallinity of the alkyl group increase.^{9,18,19} But on TS gold, because all the headgroups bidentate to the gold surface in the SAM, these SAMs exhibit an unusual trend in alkyl chain crystallinity; SAMs formed from adsorbates with short alkyl chains (n=5) are ordered and crystalline, and the alkyl increasingly disordered and liquid-like as the number of methylene units is increased.¹¹ It seems that the branched ethyl or methyl group in the alkyl chain does not break the ordered packing of the SAMs. So we assume the headgroups of both (C₆C₂)₂DTPA and (C₅C₁)₂DTPA adsorbates bidentate to the gold surface, and the short branched alkyl chains might fill the space in the SAM to increase the packing density of adsorbates in the SAM, with crystalline packing, comparing to (C₆)₂DTPA on TS gold.

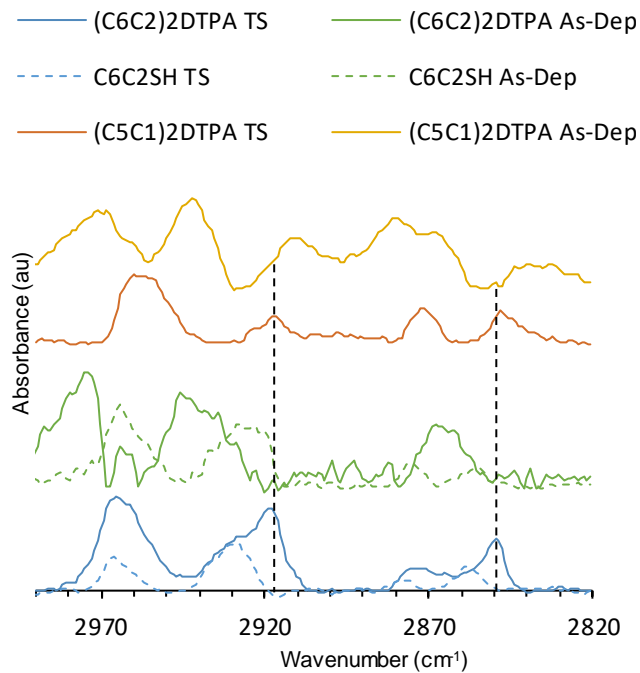


Figure 3.2. RARS spectra (2990-2820 cm^{-1}) of $(\text{C}_6\text{C}_2)_2\text{DTPA}$, $(\text{C}_5\text{C}_1)_2\text{DTPA}$ and $\text{C}_6\text{C}_2\text{SH}$ SAMs on As-Dip and TS gold. Dashed vertical lines indicate the positions of crystalline $\nu_{\text{as}}(\text{CH}_2)$ and $\nu_{\text{s}}(\text{CH}_2)$ of C_{16}SH SAMs on gold (2918 and 2850 cm^{-1} , respectively).

| SAM | Peak Position (cm ⁻¹) | |
|---|------------------------------------|-----------------------------------|
| | U _{as} (CH ₂) | U _s (CH ₂) |
| (C ₆ C ₂) ₂ DTPA on TS Au | 2918 | 2850 |
| (C ₅ C ₁) ₂ DTPA on TS Au | 2917 | 2849 |
| (C ₆ C ₂) ₂ DTPA on As-Dep Au | 2939 | 2865 |
| (C ₅ C ₁) ₂ DTPA on As-Dep Au | 2941 | 2867 |
| C ₆ C ₂ SH on TS Au | 2927 | 2857 |
| C ₆ C ₂ SH on As-Dep Au | 2927 | 2855 |

Table 3.2. $\nu_{as}(\text{CH}_2)$ and $\nu_s(\text{CH}_2)$ peak positions of (C₆C₂)₂DTPA, (C₅C₁)₂DTPA and C₆C₂SH on TS and As-Dep gold.

| | TS Gold | | | AsDep Gold | | |
|------------|--|----------------------------------|--|--|----------------------------------|--|
| | (C ₆ C ₂) ₂ DTPA | C ₆ C ₂ SH | (C ₅ C ₁) ₂ DTPA | (C ₆ C ₂) ₂ DTPA | C ₆ C ₂ SH | (C ₅ C ₁) ₂ DTPA |
| WATER | | | | | | |
| Stationary | 78° ± 3° | 84° ± 2° | 81° ± 1° | 81° ± 1° | 83° ± 2° | 83° ± 3° |
| Advancing | 80° ± 5° | 88° ± 1° | 83° ± 2° | 83° ± 2° | 82° ± 1° | 87° ± 4° |
| HEXADECANE | | | | | | |
| | <15° | <15° | <15° | <15° | <15° | <15° |

Table 3.3. Contact angles of water and hexadecane for (C₅C₁)₂DTPA, (C₆C₂)₂DTPA and C₆C₂SH SAMs on TS and As-Dep gold.

Hexadecane is more sensitive to small changes in the interfacial free energy due to its low surface tension, and the angles are all $<15^\circ$ with hexadecane. Hexadecane wets all these short-chain DTPA and thiol SAMs, which may result from that the hexadecane drop can penetrate the SAM and interact with the underlying gold.¹⁹ The water contact angles of the $(C_6C_2)_2DTPA$, $(C_5C_1)_2DTPA$ and C_6C_2SH SAMs (Table 3.3) have no big difference on both types of gold, θ_a (H_2O) is at the range of $80^\circ - 87^\circ$. θ_a (H_2O) of $(C_6C_2)_2DTPA$ SAM on TS gold is 80° , whereas the value is 87° on As-Dep gold, which is similar to that of C_6C_2SH on gold. This difference can be explained by the structure difference between $(C_6C_2)_2DTPA$ on TS and As-Dep gold from RAIRS. However, all the adsorbates have short alkyl chains, the water can penetrate the SAM, like hexadecane, and result the hydrophilic SAMs.

3.4. Conclusions

We have shown that the synthetic flexibility of DTPA molecules permits synthesis of new DTPA adsorbates **1** $(C_6C_2)_2DTPA$ and **2** $(C_5C_1)_2DTPA$. The branched $(C_6C_2)_2DTPA$ SAMs bind exclusively in bidentate fashion on TS gold and exhibit mixed bidentate and monodentate binding modes on As-Dep gold. SAMs formed from adsorbate **1** on TS gold exhibit an ordered and crystalline alkyl layer, in contrast, it is liquid-like on As-Dep gold. The contact angles of the short branched DTPA SAMs on gold are very close, but can still prove the DTPA SAM structure difference between As-Dep and TS gold.

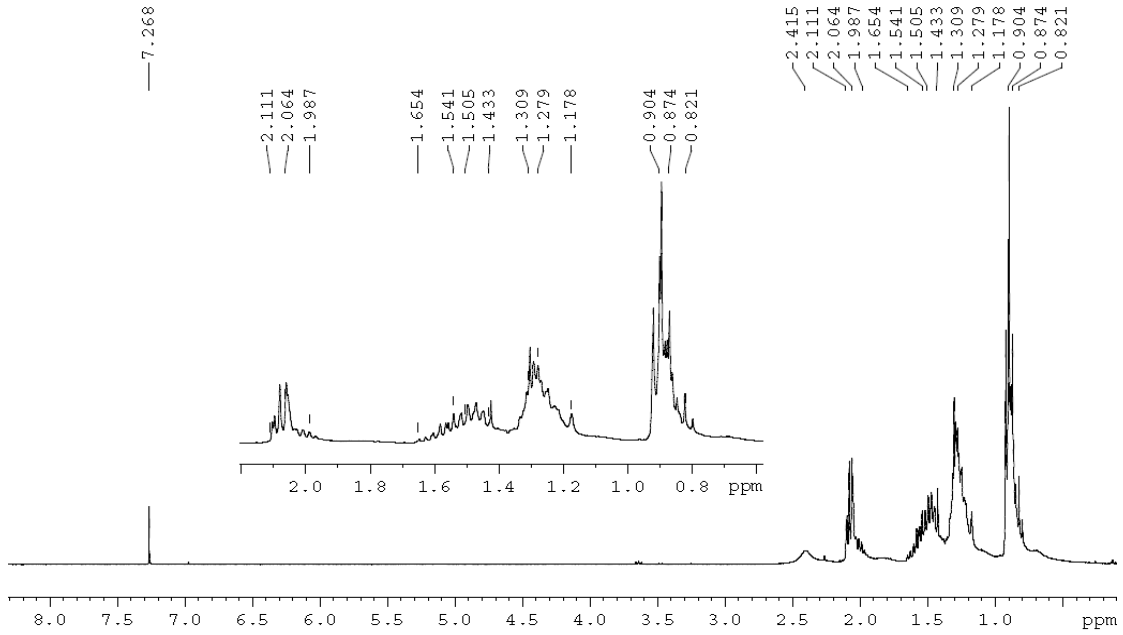
3.6. References

1. Srisombat, L.; Zhang, S.; Lee, T. R.; Thermal Stability of Mono-, Bis-, and Tris-Chelating Alkanethiol Films Assembled on Gold Nanoparticles and Evaporated “Flat” Gold. *Langmuir* **2010**, 26, 41-46.
2. Love, J. C.; Estroff, L. A.; Kriebel, J. K.; Nuzzo, R. G.; Whitesides, G. M. Self-Assembled Monolayers of Thiolates on Metals as a Form of Nanotechnology. *Chem. Rev.* **2005**, 105, 1103-1169.
3. Weiss, E. A.; Kaufman, G. K.; Kriebel, J. K.; Li, Z.; Schalek, R.; Whitesides, G. M. *Langmuir* **2007**, 23, 9686-9694.
4. Naumann, R.; Schiller, S. M.; Giess, F.; Grohe, B.; Hartman, K. B.; Karcher, I.; Koper, I.; Lubben, J.; Vasilev, K.; Knoll, W. Tethered Lipid Bilayers on Ultraflat Gold Surfaces. *Langmuir* **2003**, 19, 5435–5443.
5. Hegner, M.; Wagner, P.; Semenza, G. Ultralarge Atomically Flat Template-stripped Au Surface for Scanning Probe Microscopy. *Surf. Sci.* **1993**, 291, 39–46.
6. Wagner, P.; Zaugg, F.; Kernen, P.; Hegner, M.; Semenza, G. J. ω -Functionalized Self-Assembled Monolayers Chemisorbed on Ultraflat Au (111) Surfaces for Biological Scanning Probe Microscopy in Aqueous Buffers. *Vac. Sci. Technol. B* **1996**, 14, 1466–1471.
7. San Juan, R. R.; Carmichael, T. B.; Formation of Self-Assembled Monolayers with Homogeneously Mixed, Loosely Packed Alkyl Groups Using Unsymmetrical Dialkyldithiophosphinic Acids. *Langmuir* **2012**, 28, 17701-17708.
8. San Juan, R. R.; Allan, C. J.; Iqbal, M.; Eichhorn, S. H.; Macdonald, C. L. B.; Carmichael, T. B. New Dihexadecyldithiophosphate SAMs on Gold Provide Insight

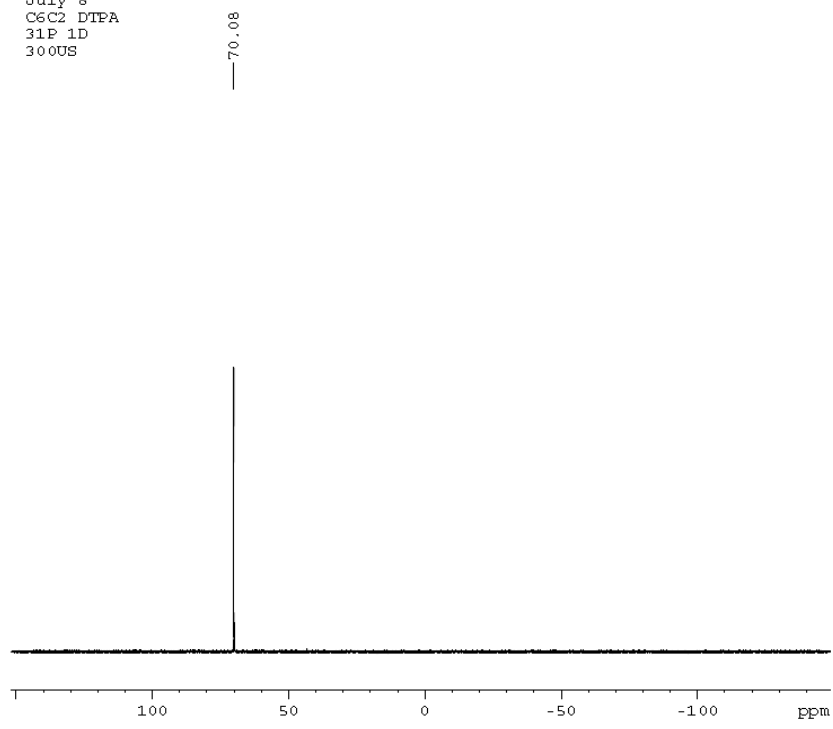
- into the Unusual Dependence of Adsorbate Chelation on Substrate Morphology in SAMs of Dialkyldithiophosphinic Acids. *J. Am. Chem. Soc.* **2013**, 42, 15784-15793.
9. San Juan, R. R.; Miller, M. S.; Ferrato, M. -A.; Carmichael, T. B.; Influence of Alkyl Chain Length on the Structure of Dialkyldithiophosphinic Acid Self-Assembled Monolayers on Gold. *Langmuir* **2012**, 28, 13253-13260.
 10. Miller, M. S.; San Juan, R. R.; Ferrato, M. -A.; Carmichael, T. B. New Dialkyldithiophosphinic Acid Self-Assembled Monolayers (SAMs): Influence of Gold Substrate Morphology on Adsorbate Binding and SAM Structure. *Langmuir* **2011**, 27, 10019-10026.
 11. Müller, J.; Brunnbauer, M.; Schmidt, M.; Zimmerman, A.; Terfort, A. *Synthesis* **2005**, 6, 998–1004.
 12. Guoxin, T.; Yongjun, Z.; Jingming, X. Extraction of Am(III) and Ln(III) by Dialkyldithiophosphinic Acid with Different Alkyl Groups. *Solvent Extract. Ion Exch.* **2001**, 19, 993-1005.
 13. Klaehn, J.R.; Peterman, D.R.; Harrup, M.K.; Tillotson, R.D.; Luther, T.A.; Law, J.D.; Daniels, L.M. Synthesis of Symmetric Dithiophosphinic Acids for “Minor Actinide” Extraction. *Inorg. Chim. Acta* **2008**, 361, 2522–2532.
 14. Castner, D.G.; Grainger, D.W. X-ray Photoelectron Spectroscopy Sulfur 2p Study of Organic Thiol and Disulfide Binding Interactions with Gold Surfaces. *Langmuir* **1996**, 12, 5083-5086.
 15. Ishida, T.; Choi, N.; Mizutani, W.; Tokumoto, H.; Kojima, L.; Azebare, H.; Hokari, H.; Akiba, U.; Fujihira, M. High-Resolution X-ray Photoelectron Spectra of

- Organosulfur Monolayers on Au(111): S(2p) Spectral Dependence on Molecular Species. *Langmuir* **1999**, 15, 6799-6806.
16. Moulder, J.F.; Stickle, W.F.; Sobol, P.E.; Bomben, K.D. *Handbook of X-Ray Photoelectron Spectroscopy*; Perkin-Elmer Corp.; Eden Prairie, MN, **1995**.
 17. Miller, M.S.; San Juan, R.R.; Ferrato, M.-A.; Carmichael, T.B. The Unusual Self-Organization of Dialkyldithiophosphinic Acid Self-Assembled Monolayers on Ultrasooth Gold. *J. Am. Chem. Soc.* **2014**, 136, 4212-4222.
 18. Porter, M.D.; Bright, T.B.; Allara, D.L.; Chidsey, C.E.D. Spontaneously Organized Molecular Assemblies. 4. Structural Characterization of n-Alkyl Thiol Monolayers on Gold by Optical Ellipsometry, Infrared Spectroscopy, and Electrochemistry. *J. Am. Chem. Soc.* **1987**, 109, 3559-3568.
 19. Bain, C. D.; Troughton, E. B.; Tao, Y. T.; Evall, J.; Whitesides, G. M.; Nuzzo, R. G. Formation of Monolayer Films by the Spontaneous Assembly of Organic Thiols from Solution onto Gold. *J. Am. Chem. Soc.* **1989**, 111, 321-335.

3.7. Supporting Information



July 8
 C6C2 DTFA
 31P 1D
 300US



```

NAME          20150uly8
EXPNO         1
PROCNO        1
Date_         20150708
Time          16.38
INSTRUM       spect
PROBHD        5 mm PABBO BB-
PULPROG       zgpg30
TD            32768
SOLVENT       CDCl3
NS            128
DS            0
SMH           36496.352 Hz
FIDRES        1.113780 Hz
AQ            0.4489716 sec
RG            26008
DW            13.700 usec
DE            6.00 usec
TE            296.1 K
D1            1.00000000 sec
D11           0.03000000 sec
TDO           1

===== CHANNEL f1 =====
NUC1           31P
P1            10.85 usec
PL1            0.00 dB
SFO1          121.4949575 MHz

===== CHANNEL f2 =====
CPDPRG2       waltz16
NUC2           1H
PCPD2         80.00 usec
PL2            0.00 dB
PL12          17.16 dB
PL13          24.00 dB
SFO2          300.1312005 MHz
SI            32768
SF            121.4947739 MHz
WDW            EM
SSB            0
LE            1.00 Hz
GB            0
PC            1.40
  
```

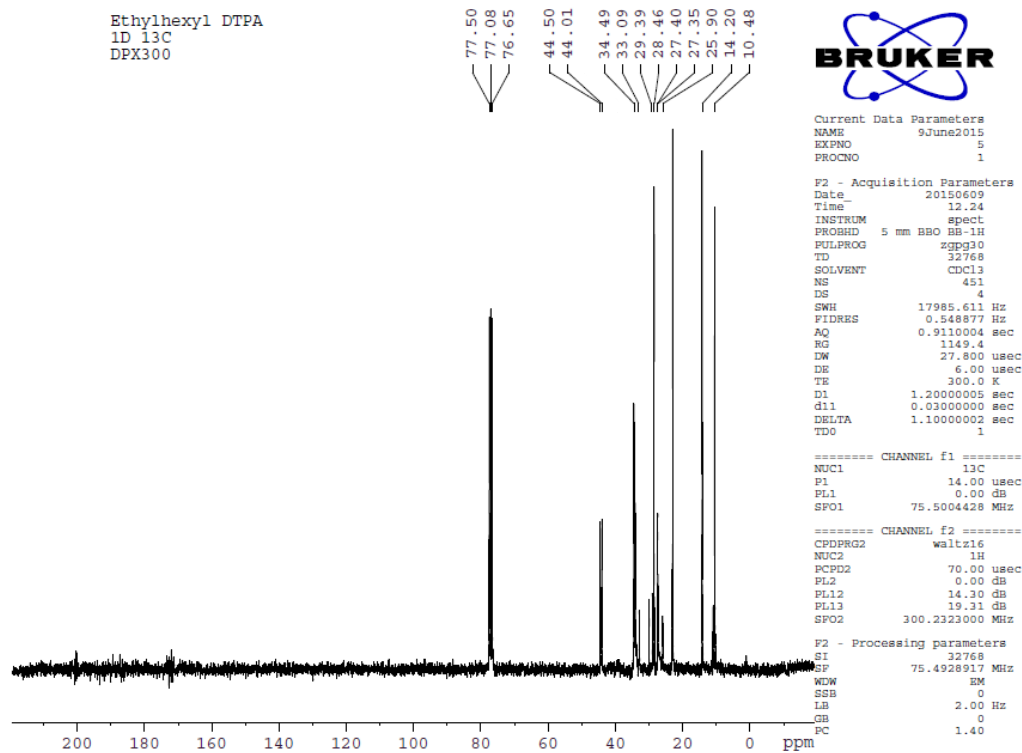
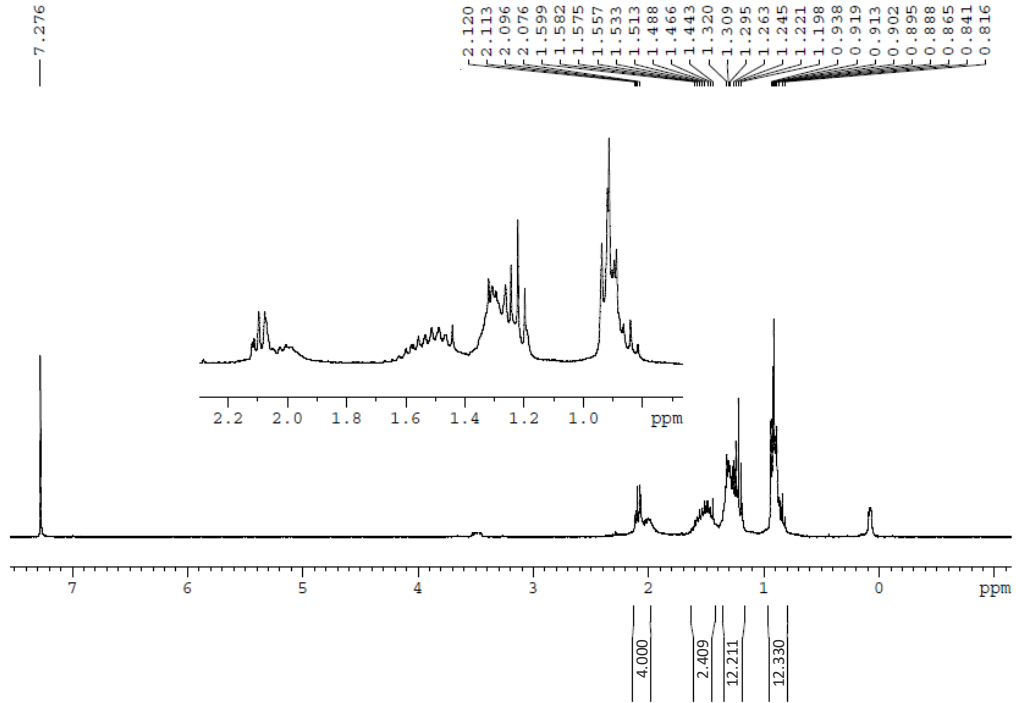
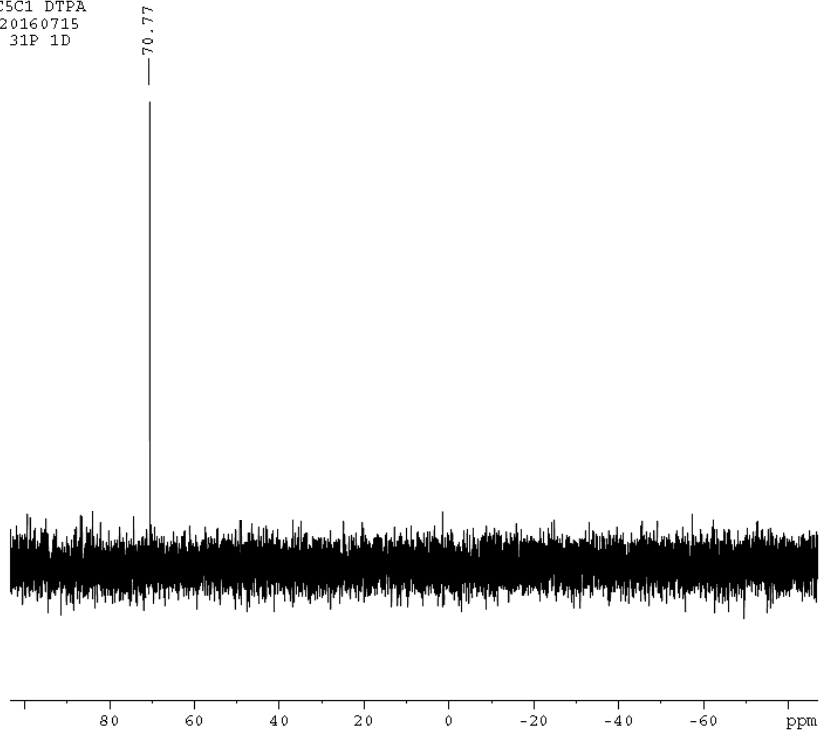


Figure S 3.1. ^{31}P , ^1H and ^{13}C NMR of $(\text{C}_6\text{C}_2)_2\text{DTPAs}$.

C5C1 DTPA
20160715
1H 1D



C5C1 DTPA
20160715
31P 1D



```

NAME      20160715
EXPNO     1
PROCNO    1
Date_     20160715
Time      15.26
INSTRUM   spect
PROBHD    5 mm PABBO BB-
PULPROG   zgpg30
TD         32768
SOLVENT   CDCl3
NS         256
DS         0
SWH        36496.352 Hz
FIDRES     1.113780 Hz
AQ         0.4488716 sec
RG         41235.1
DW         13.700 usec
DE         6.00 usec
TE         294.3 K
D1         1.0000000 sec
D11        0.0300000 sec
TDO        1

```

```

===== CHANNEL f1 =====
NUC1      31P
P1        10.85 usec
PL1       0.00 dB
SFO1      121.4949575 MHz

```

```

===== CHANNEL f2 =====
CPDPRG2   waltz16
NUC2      1H
PCPD2     80.00 usec
PL2       0.00 dB
PL12      17.16 dB
PL13      24.00 dB
SFO2      300.1312005 MHz
SI        32768
SF        121.4947696 MHz
WDW       EM
SGB       0
LB        1.00 Hz
GB        0
PC        1.40

```

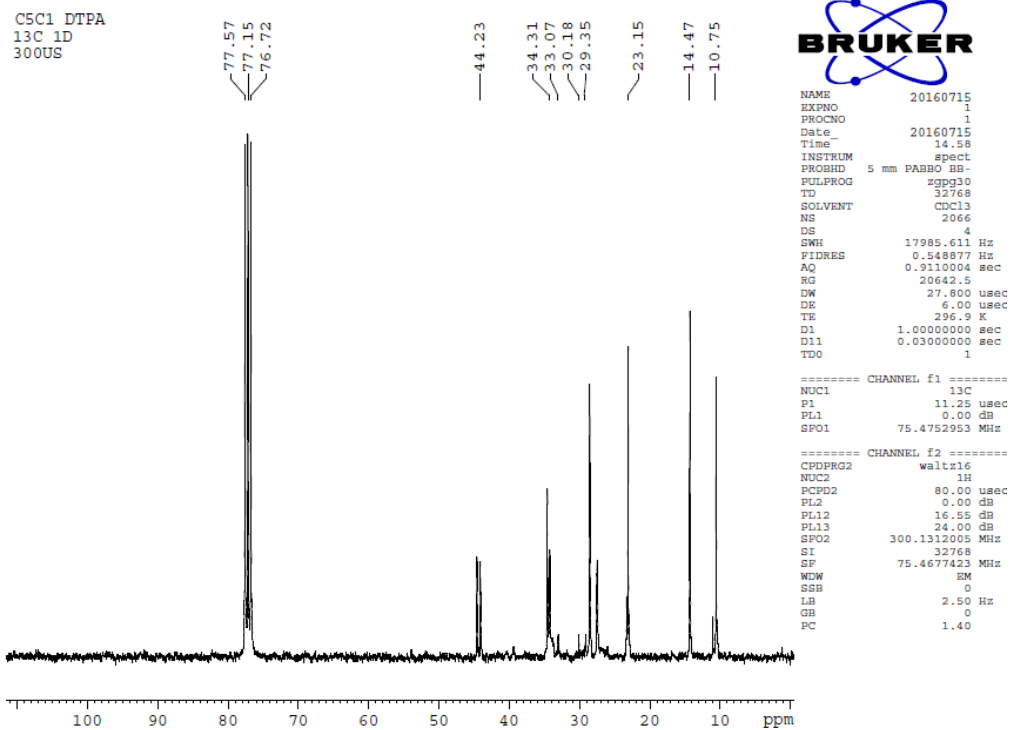


Figure S 3.2. ^{31}P , ^1H and ^{13}C NMR of $(\text{C}_5\text{C}_1)_2\text{DTPAs}$.

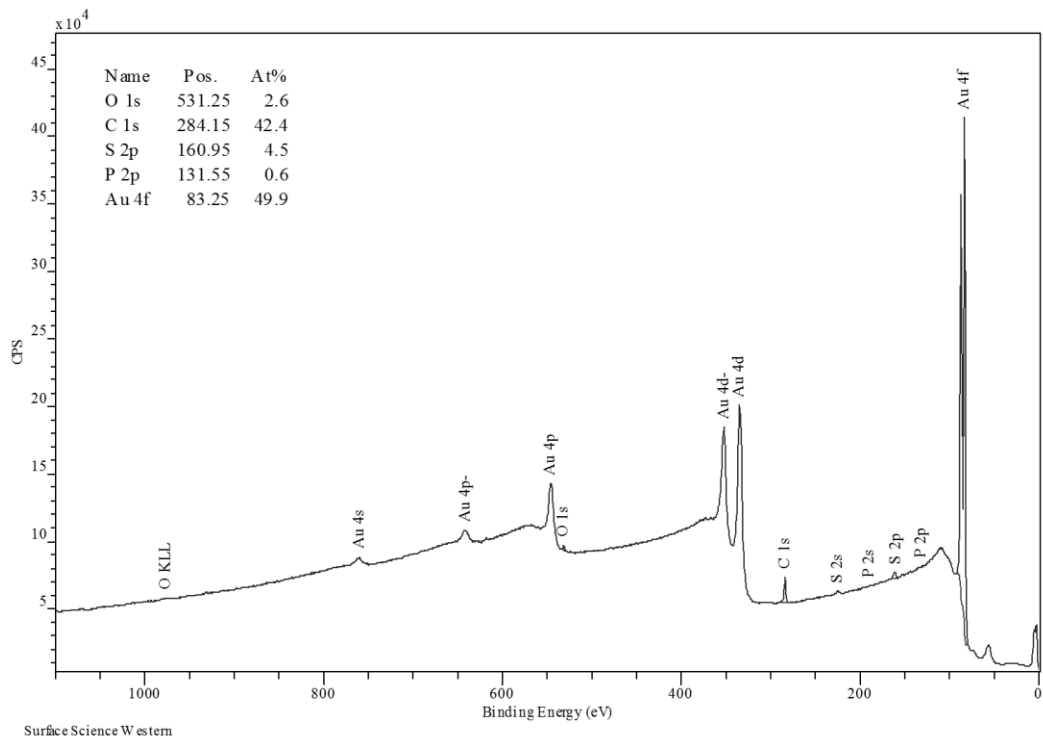
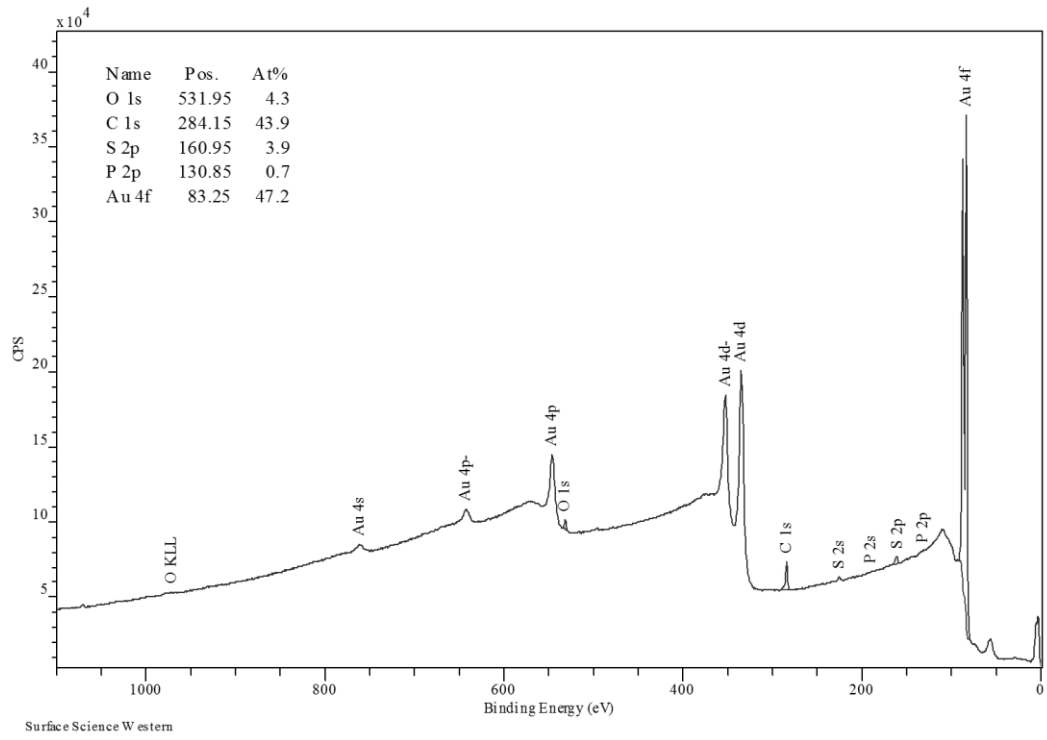


Figure S 3.3. XPS survey spectra of $(C_6C_2)_2DTPAs$ on TS (top) and As-Dep (bottom)

gold.

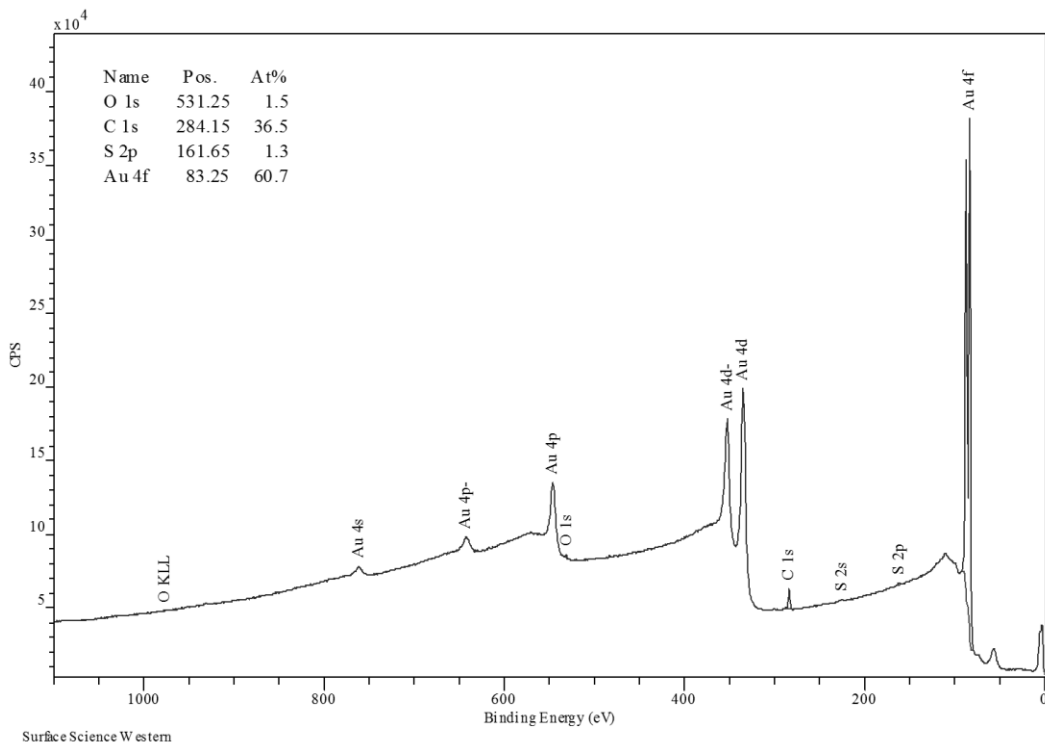
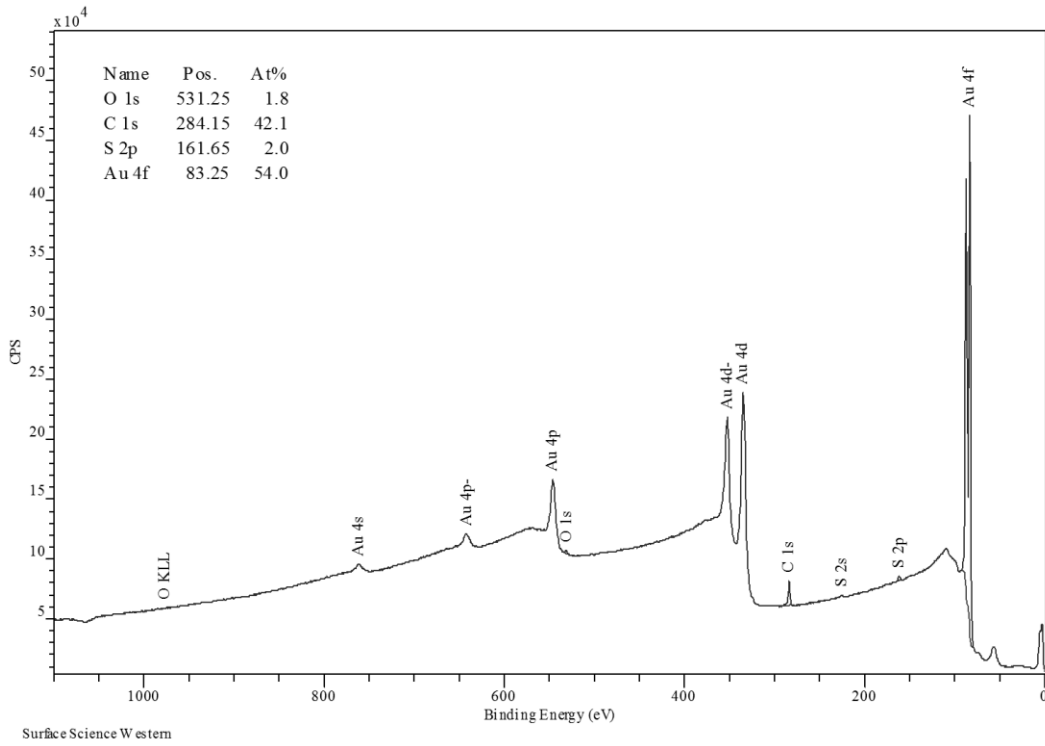


Figure S 3.4. XPS survey spectra of C_6C_2SH on TS (top) and As-Dep (bottom) gold.

Chapter 4

Stretchable Gold Film on Modified Silica Nanoparticles

4.1. Introduction

The development of stretchable electronics is very promising for the application in ultrathin electronic skin sensor, soft robotics¹⁻⁴ and human-machine interfaces,^{5,6,7} which can withstand high elongation without significant changes to their electrical performance. One remarkable application is using the smart artificial skin with integrated stretchable sensors to cover a prosthetic hand, allowing the wearer to feel pressure between a soft touch and a firm handshake.^{8,9}

The high conductivity of gold makes it ideal to be used as a conductor in comparison to the other frequently used materials, such as carbon nanotubes and graphene. Besides, gold is desirable in the soft electronics field since it is inert and will not be oxidized, which allows the devices to last longer. A free-standing metal film is inherently non-stretchable, electrically failing at 1-2% elongation. Deposit gold film on soft elastomeric substrates, such as polydimethylsiloxane (PDMS), can suppress the strain localization, which makes it possible to induce stretchability on the conductor. The challenge is that as the stretchability is increasing, the conductivity of the metal is decreasing rapidly, due to the cracks that propagate across the metal film as it is elongated and interrupt the conductive pathway. The distinction between methodologies to increase the stretchability of the elastomeric PDMS substrate is whether cracking is avoided or not. The first method, which is where cracking is avoided, can convert tensile strain applied to the film to bending strains of buckles on patterned serpentines. Pre-strained (stretch substrate at a certain strain before metal deposition and then release), buckled surface and serpentine routings¹⁰⁻¹³ remain at low resistance up to a critical strain point, by accommodating the strain by flattening buckles or straightening the serpentines.¹⁴ The resistance increases

dramatically beyond the critical strain point, due to the propagation of long cracks that interrupt the conductive pathway, which is a challenge for large-scale elongation. Mogul-patterned surface¹⁵ can be reached by soft lithography to generate a maximum density of peak-valley hexagonal structure. The applied strain on the substrate can be efficiently absorbed by straitening the mogul-patterned structure, resulting in minimal interference with motion-induced stress. The second method is where cracking is permitted, Lacour *et al.* have identified stretchable metal with microcracks, where the metal network twists and deflects out of plane but remains bonded to substrate, and conductive up to 32% strain.¹⁶ Several other methods that have been reported by changing the surface topography to affect the strain localization and create a favorable cracking pattern. Even when cracks form after stretching, the sample can still remain conductive. Sand-blasting and surface-etching can also reach a rough surface to preserve the conduction up to large strain.¹⁷ Metal films on micropillar array PDMS substrate exhibit high electrical conductivity and can stretch reversibly to 20% without failing electrically. In which the cracks seem to start or stop at the closest pillar base at site of local strain maxima, the cracks widen but do not propagate at higher strain, and additional narrower cracks appear in between the pillars.¹⁸ When metal films are deposited on pyramidal nanopatterned surfaces, the nanopatterned localize the microcracks that are formed during stretching, resistance increase by only 60% at 25% strain.¹⁹ But these surface topography methods involve photolithography or chemical etching, which makes the fabrication process complicated.

Our group demonstrated the cracking permitted approach by creating topographical features on the surface of PDMS that provided numerous sites for strain localization in a

gold film deposited on the surface. Our method used spin-coating to deposit an aqueous emulsion of poly(vinyl acetate) (PVAc) – common, commercially available white glue diluted in water – onto an oxidized PDMS surface. The density of the PVAc globules depends on the concentration of the glue in the emulsion. From the three different dilutions (1:1, 3:1, and 5:1 v/v water:glue) that we tested, the diameter of the PVAc cluster range from $\sim 40 \mu\text{m}$ to $< 1 \mu\text{m}$, and a film thickness from $3.5 \mu\text{m}$ to $\sim 2 \mu\text{m}$ in height. When coated with gold, the least diluted structure (PDMS/glue_{1:1}) remains remarkably conductive up to 65% elongation, with an increase in resistance to only 23x the initial resistance of the film.²⁰

Instead of the micro-structured PVAc glue, this paper uses MPTMS modified silica nanoparticles embedded in PDMS as an interlayer between gold film and the PDMS elastomeric substrate. After the gold deposition, these silica-based structures show an increase in resistance of 32x the initial resistance at 80% elongation. We further demonstrated that by altering the weight ratio of MPTMS modified silica:PDMS interlayer, the resistance change can be tuned, which leads to different functional samples.

4.2. Experimental Methods

Poly(dimethylsiloxane) (PDMS) (Sylgard 184) was obtained from Dow Corning, Midland, MI. Fumed silica (Aerosil 200) was obtained from Evonik Industries, Parsippany, NJ. All other chemicals were obtained from Sigma-Aldrich and were used as received.

Preparation of PDMS Substrates PDMS (Dow Corning Sylgard 184) was prepared by mixing a 10:1 w/w ratio of prepolymer : curing agent, followed by degassing under vacuum to remove the bubbles. A smooth PDMS surface was obtained by casting 15 g of the mixture against a 9 cm diameter polystyrene Petri dishes and curing at 60 °C for at least 1 h.

Oxidation of Substrates PDMS substrates were exposed to an air plasma at medium discharge setting for 30 seconds at an air pressure of 10 psig (flow rate of 32 mL/min). (Harrick Plasma PDC32-G coupled to a PlasmaFlo gas flow mixer).

Preparation of Nano-interlayer Fumed silica was modified by mixing a 1 : 1 w/w ratio of fumed silica : 3-mercaptopropyl-trimethoxysilane in toluene at 70 °C overnight. The solution was centrifuged at 3300 rpm for 15 mins to isolate the modified silica nanoparticles, which were dried in a vacuum oven at 100 °C for 6 h. Solutions of MPTMS-modified silica and PDMS were prepared by suspending the desired amount of MPTMS-modified silica (0.17 g, 0.26 g, 0.38 g, 0.50 g and 0.82g for 10%, 15%, 20%, 25% and 30%, respectively) in 10 mL n-hexane, and 1.50 g of a 10:1 w/w ratio of prepolymer : curing agent PDMS was then added into the modified silica suspension. Oxidized PDMS substrates were then spin coated with the MPTMS modified silica/PDMS mixture in hexane at 2000 rpm for 1 minute (Laurell Technologies WS-400A-6NPP). The resulting PDMS_{Si} substrates were cured in the oven at 60 °C for at least 1 h.

Deposition of Metal Layer An e-beam evaporator was used to deposit 30 Å titanium, followed by 250 Å gold, onto oxidized MPTMS/silica/PDMS samples at a rate of 0.3 Å/s and 1 Å/s respectively under high vacuum (10^{-6} mbar).

Characterization Optical characterization was performed using an Olympus BX51 microscope and stereo microscope (Leica MZ6) both equipped with an Olympus Q-Color3 digital camera. A micro-vice stretcher (S.T. Japan, USA, Inc.) was mounted to the microscope stage and samples were clamped in the stretcher to obtain microscope images of stretched samples. AFM images were obtained using a Digital Instruments Multimode atomic force microscope in tapping mode. A silicon cantilever was used with a nominal tip radius of 10 nm, resonance frequency of 300 kHz and a nominal spring constant of 40 N/m. The AFM images were collected from three spots on each sample in an area of $10\ \mu\text{m} \times 10\ \mu\text{m}$ using a scan rate of 1.0 Hz with a scanning resolution of 512 samples per line. Images were collected using Nanoscope 6 software and processed using WSxM 5.0 Develop 8.2 software.²¹ Electrical characterization was performed using a Keithley 2601A source meter. Gallium-Indium (EGaIn) (~0.01mL) was first deposited by syringe to the corners (for sheet resistance) or ends (for resistance measurements) of the gold surface to facilitate electrical contact. Data sets consisted of a minimum of three samples, and the average was reported. For electrical measurements under strain, samples were clamped in a micro-vice stretcher (S.T. Japan, USA, Inc.) and the resistance was measured at 5% strain intervals increments.

4.3. Results and Discussion

Pyrogenic (fumed) silica is a nanoparticle (particle size: 12 nm) which is produced by the hydrolysis of alkylchlorosilane in an O₂/H₂ flame between 1200 and 1600°C and has a high surface area covered by silanol groups. This hydrophilic surface does not mix well with the hydrophobic PDMS polymer matrix.²² The surface modification of silica with an organosilane, such as 3-aminopropyl-trimethoxysilane, 3-methacryloxypropyl-trimethoxysilane, ethyl triethoxysilane, octyl triethoxysilane and 3-mercaptopropyl-trimethoxysilane,^{23,24,25} reduces the number of the superficial silanol groups, by grafting molecules with an organic nature. In this way, these silane coupling agents increase the surface hydrophobicity, therefore improving the Van der Waals interactions between the modified silica particles and PDMS polymer to achieve better dispersion. 3-methacryloxypropyl-trimethoxysilane (MAPTMS) and 3-mercaptopropyl-trimethoxysilane (MPTMS) have less hydrophilic terminal groups than the other silane agents and MPTMS appears to be the most reactive by TGA analyses.²⁶

The fumed silica was modified by stirring with the MPTMS coupling agent in toluene at 70 °C. Solution of different weight of modified silica (0.17 g, 0.26 g, 0.38 g, 0.50g and 0.82 g) and 1.5 g uncured 10:1 w/w ratio of prepolymer : curing agent PDMS were prepared in n-hexane. We then spin-coated these solutions onto cured PDMS substrates that were oxidized to enable wetting, and cured in the oven to get PDMS_{xSi} samples (PDMS_{xSi}, where x = 10%, 15%, 20%, 25% and 30%, for different weight ratio of modified silica : PDMS). The dark-field optical micrographs of PDMS_{xSi} samples show that the modified silica nanoparticles appear to form micron-scale clusters within the

PDMS/modified silica layer, coated on the PDMS surface (Figure 4.1). The density of the clusters depends on the concentration of silica nanoparticle in the PDMS mixture.

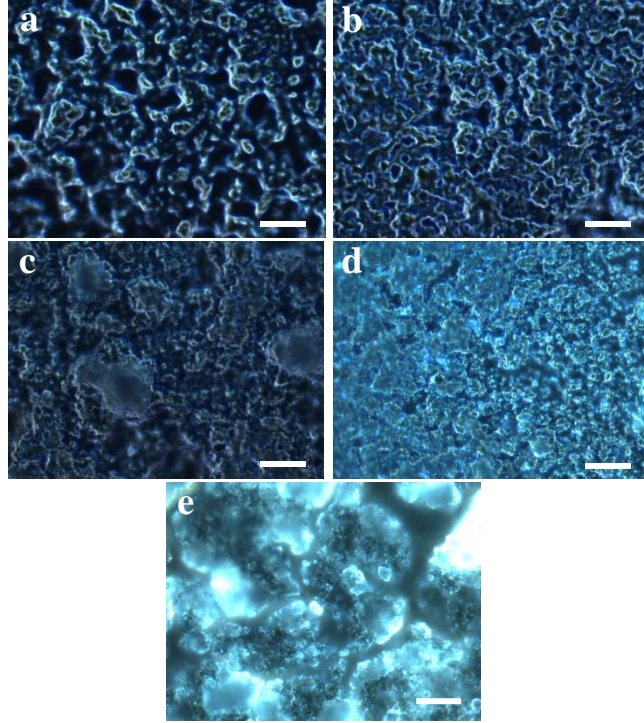


Figure 4.1. Dark-field optical micrographs of PDMS_{10Si} (a), PDMS_{15Si} (b), PDMS_{20Si} (c), PDMS_{25Si} (d) and PDMS_{30Si} (e) samples before Au deposition. Scale bar –20 μm .

We used AFM to characterize the surface morphology. Figure 4.2 shows the images of PDMS_{xSi} samples with cross sections. At the lowest concentrations of silica (PDMS_{10Si}), the surface consists of micron-scale clusters of modified silica which are separated by voids (bare regions with no topography) (Figure 4.2 a). Increasing the weight percentage of modified silica to 15% and 20% does not appreciably increase the cluster sizes, but the clusters on the surface increases as the weight percentage of modified silica increases

(overlapping clusters) (Figure 4.2 b, c). The optical and AFM images of these two samples (PDMS_{15Si} and PDMS_{20Si}) both show a more agglomerated micron-scale clusters of modified silica covered onto the surface. For the PDMS_{25Si} sample, it seems that the modified silica just covers the whole surface but with little cluster overlapped on top gives a rougher surface (Figure 4.2 d). At the highest concentration of silica, PDMS_{30Si} sample (Figure 4.2 e), the surface of the substrate is covered with too much modified silica, which aggregates together to form big clusters over the homogenously bottom modified silica layer throughout the sample.

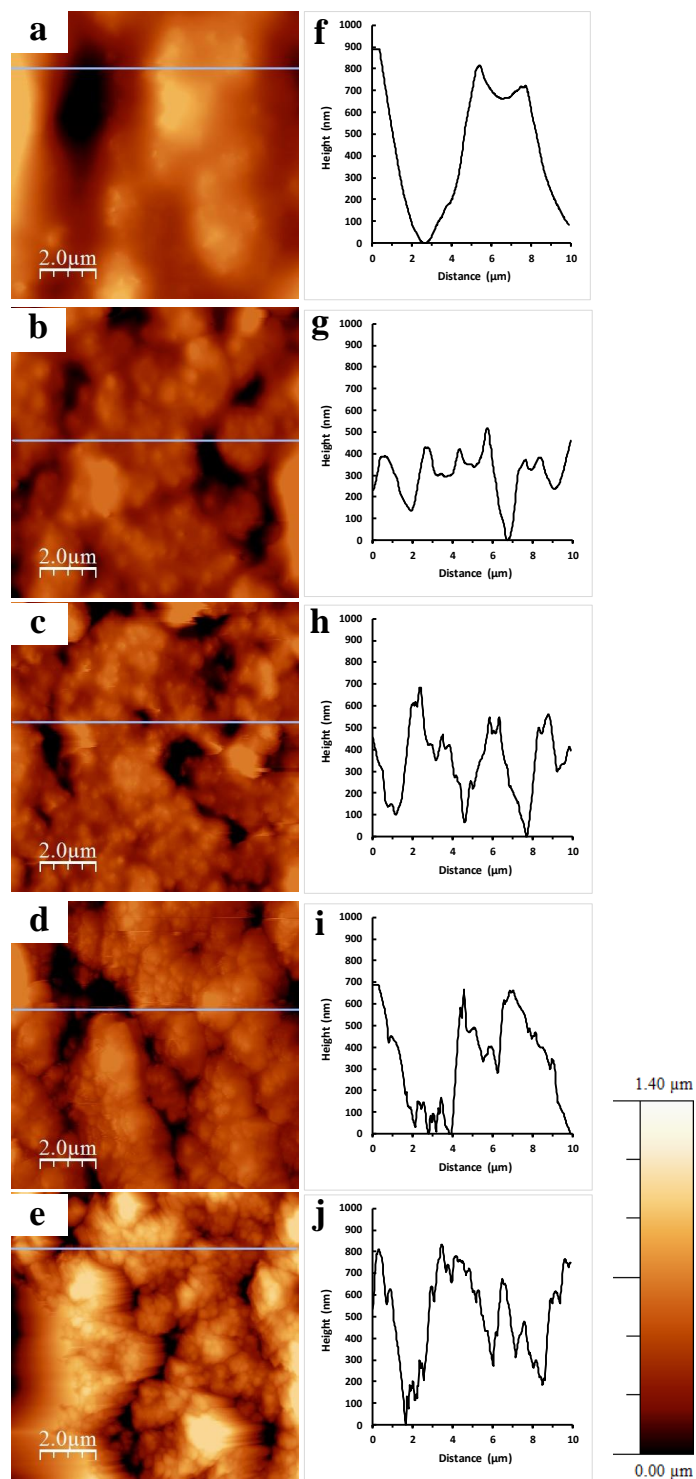


Figure 4.2. AFM images (a-e) and cross section (f-j) of PDMS_{10Si} (a, f), PDMS_{15Si} (b, g), PDMS_{20Si} (c, h), PDMS_{25Si} (d, i) and PDMS_{30Si} (e, j) samples before Au deposition.

The AFM image that we took has a geometrical area of $10\ \mu\text{m} \times 10\ \mu\text{m}$, but the actual topographical surface area is larger than the geometrical area. The developed interfacial area ratio (S_{dr}) is the percent increase in topographical surface area compared to the geometrical area. It expresses the roughness and density of topographical features on the surface. As more modified silica particles are added to the PDMS surface by increasing the modified silica weight percentage in the surface layer, the larger value it will be for the S_{dr} .

| Sample | RMS Roughness (nm) | | S_{dr} (%) | |
|----------------------|--------------------|------------------|---------------------|------------------|
| | Without Au | With 250 Å Au | Without Au | With 250 Å Au |
| PDMS _{10Si} | 105.8 ± 21.1 | 106.7 ± 6.8 | $8.2 \pm 2.4\%$ | $6.2 \pm 1.1\%$ |
| PDMS _{15Si} | 177.7 ± 31.5 | 169.1 ± 39.1 | $13.3 \pm 1.8\%$ | $14.3 \pm 0.9\%$ |
| PDMS _{20Si} | 180.4 ± 39.1 | 230.6 ± 62.9 | $26.5 \pm 6.3\%$ | $27.5 \pm 5.5\%$ |
| PDMS _{25Si} | 212.7 ± 42.3 | 268.3 ± 40.7 | $36.7 \pm 11.8\%$ | $39.6 \pm 2.0\%$ |
| PDMS _{30Si} | 328.4 ± 50.5 | 275.5 ± 30.6 | $52.1 \pm 6.1\%$ | $49.7 \pm 5.9\%$ |

Table 4.1. RMS roughness S_{dr} value of PDMS_{xSi} samples with and without Au deposition.

The PDMS_{10Si} sample has root-mean-square roughness of 105.8 ± 21.1 nm, S_{dr} value of $8.2 \pm 2.4\%$ and peak-valley distance of 900 nm, with agglomerates as large as ~ 24 μ m in diameter (Figure 4.1 a and 4.2 a, f).

As weight percentage of modified silica increases (15–30%), the topography becomes more detailed and complex, with layered micron-scale clusters. The entire surface of these samples is coated with modified silica micron-scale clusters. Peak-valley distances of the samples decrease to < 550 nm. All the clusters are < 16 μ m in diameter on PDMS_{15Si} sample; on PDMS_{20Si} sample, the clusters are < 24 μ m in diameter (Figure 4.1 b, c and Figure 4.2 b, g and c, h). These two samples (PDMS_{15Si} and PDMS_{20Si}) have very similar RMS roughness and surface topography referring to Table 1, although more modified silica is coated for the PDMS_{20Si} sample (larger S_{dr} value, $26.5 \pm 6.3\%$ for PDMS_{20Si} and $13.3 \pm 1.8\%$ for PDMS_{15Si}). The size of the clusters is < 40 μ m for PDMS_{25Si} (Figure 4.1 d), with the peak-valley distance ~ 690 nm (Figure 4.2 d, i) and a root-mean-square roughness of 212.7 ± 42.3 nm (Table 4.1). At the highest concentration of PDMS_{30Si} sample, the size of the cluster ranges in diameter from ~ 60 to < 16 μ m (Figure 4.1 e), with a peak-valley distance of ~ 850 nm (Figure 4.2 e, j) and a root-mean-square roughness of 328.4 ± 50.5 nm, S_{dr} % value of $52.1 \pm 6.1\%$ (Table 4.1). In this paper, the S_{dr} value presents the progress of the sample features as the concentration of modified silica increases (Table 4.1). As the modified silica concentration goes from 10% to 30%, the S_{dr} values increase from $\sim 8\%$ to $\sim 52\%$, which means the actual surface area is increasing due to the greater percentage of particles at the surfaces. So as the concentration of modified silica increases, the RMS roughness and S_{dr} values increase.

We used an e-beam evaporator to coat PDMS_{xSi} surfaces with a 30-Å-thick layer of titanium as an adhesion promoter followed by a 250-Å-thick layer of gold. AFM images show that the metal coats the surfaces with topographical features that are indistinguishable from those of unmetallized PDMS_{xSi} surfaces (Figure S4.1). The RMS roughness and S_{dr} % value for each PDMS_{xSi} sample before and after gold deposition are also similar (Table 4.1). However, optical images of the PDMS_{xSi}/Au samples (Figure 4.3) show that there are cracks formed during the deposition of gold onto the PDMS_{30Si} sample. The high concentration of modified silica nanoparticles can produce an extremely rough and brittle surface, which may crack due to the expansion of PDMS from heating during the gold evaporation process. In addition, the PDMS_{25Si}/Au sample has some cracks (smaller than PDMS_{30Si}/Au) which might be why the sheet resistance value (R_s) is higher than the lower weight percentage sample (PDMS_{20Si}/Au) (Table 4.2). Photographs of the resulting gold films are shown in Figure 4.4. Increasing the percentage of silica increases the roughness and texturing of PDMS_{xSi}/Au samples, which changes the reflective and scattering properties of the surface.

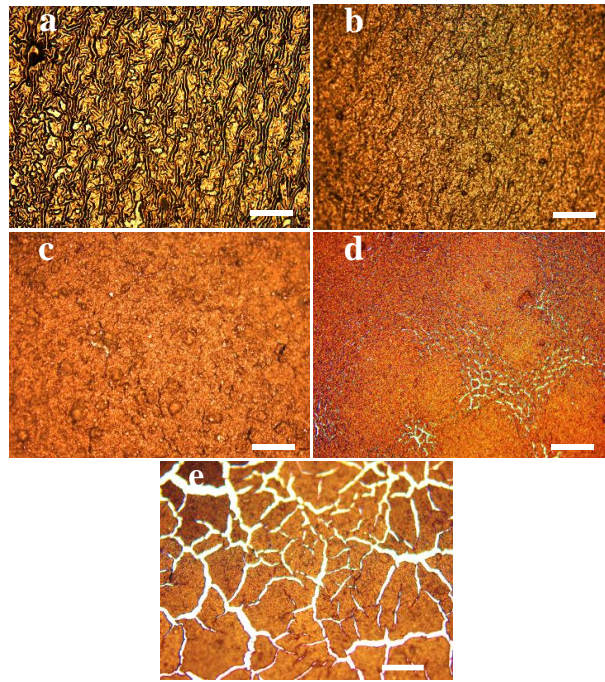


Figure 4.3. Optical images of PDMS_{xSi}/Au samples captured without stretch PDMS_{10Si}/Au (a), PDMS_{15Si}/Au (b), PDMS_{20Si}/Au (c), PDMS_{25Si}/Au (d) and PDMS_{30Si}/Au (e). Scale bar – 200 μ m.

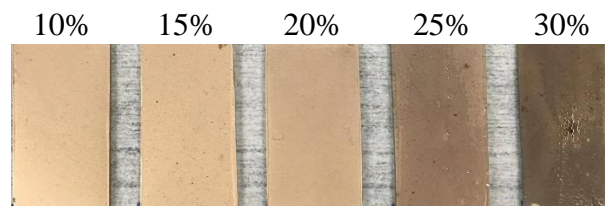


Figure 4.4. PDMS_{xSi}/Au sample images.

Sheet resistance (R_s) is not measurably affected by the topography difference for PDMS_{10-20Si}/Au samples. While the rougher sample (PDMS_{30Si}/Au) has a slightly larger R_s value, the PDMS_{30Si}/Au sample is not conductive at all (Table 4.2). From the results of the sheet resistance measurement and optical images, we chose PDMS_{25Si} as the upper concentration limit.

| Substrate | R_s (Ω/\square) |
|--------------------------|----------------------------|
| PDMS _{10Si} /Au | 1.2±0.5 |
| PDMS _{15Si} /Au | 0.6±0.2 |
| PDMS _{20Si} /Au | 0.8±0.03 |
| PDMS _{25Si} /Au | 1.8±0.2 |
| PDMS _{30Si} /Au | G Ω |

Table 4.2. Sheet resistance (R_s) of 250-Å-thick-gold PDMS_{xSi} samples.

We stretched all the PDMS_{xSi}/Au samples under microscope, it showed that the topography of the nano-interlayer on PDMS substrates changes how the cracks initiate and propagate. Optical microscope images of PDMS_{10-25Si}/Au samples taken at 5%, 50% and 70% strain (Figure 4.5) show a trend that the rougher the topography is, the more sites are for strain localization and new crack nucleation.

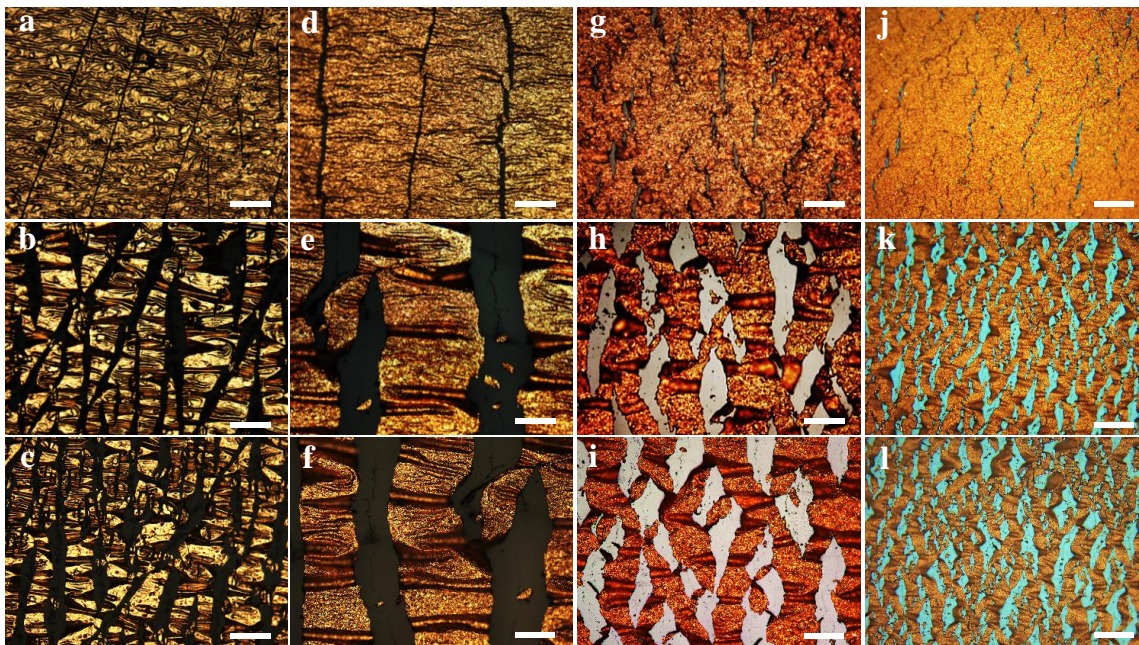


Figure 4.5. Evolution of cracks on $\text{PDMS}_{x\text{Si}}/\text{Au}$ samples with stretching. Optical images captured at 5% (top), 50 % (middle) and 70% (bottom) strain for $\text{PDMS}_{10\text{Si}}/\text{Au}$ (a-c), $\text{PDMS}_{15\text{Si}}/\text{Au}$ (d-f), $\text{PDMS}_{20\text{Si}}/\text{Au}$ (g-i) and $\text{PDMS}_{25\text{Si}}/\text{Au}$ (j-l) samples. In all images, the samples were stretched in the horizontal direction. Scale bar – 200 μm .

From the stretching images of $\text{PDMS}_{10\text{Si}}/\text{Au}$ and $\text{PDMS}_{15\text{Si}}/\text{Au}$ samples (Figure 4.5), there are narrow and long cracks propagated through half the field of a 10x microscope objective, which is $\sim 700 \mu\text{m}$ in length, at low strain of 5%. For $\text{PDMS}_{10\text{Si}}/\text{Au}$ sample, the number and width of cracks increases with further elongation to 70%, but the long cracks fail to propagate at a certain site in the metal film, resulting in more individual cracks rather than fewer long cracks. The cracks in $\text{PDMS}_{15\text{Si}}/\text{Au}$ are observed to be transitioning from those appearing in $\text{PDMS}_{10\text{Si}}/\text{Au}$ to those in $\text{PDMS}_{20\text{Si}}/\text{Au}$. This may

be a result of the intermediate distribution of strain-relieving locations in the surface of the film creating a unique intermediate morphology.

The cracks that formed by PDMS_{20Si}/Au and PDMS_{25Si}/Au samples are totally different than that of PDMS_{15Si}/Au sample (Figure S4.2). At 5% strain, the cracks are much shorter (~ 333 μm). As for the stretching micrograph of PDMS_{20Si}/Au and PDMS_{25Si}/Au samples, it is clear that the crack density is increasing as the strain is increasing, but the width (< 30 μm) and the length (< 333 μm) of the cracks remain small. These narrow, short cracks have a “zigzag” appearance that retains gold bridges between the cracks. In contrast, PDMS_{10Si}/Au and PDMS_{15Si}/Au samples have long (~ 700 μm) cracks with no visible bridges in the region that we focused by the time we get to 70% strain, but must be few bridges since both samples are still conductive *vide infra*.

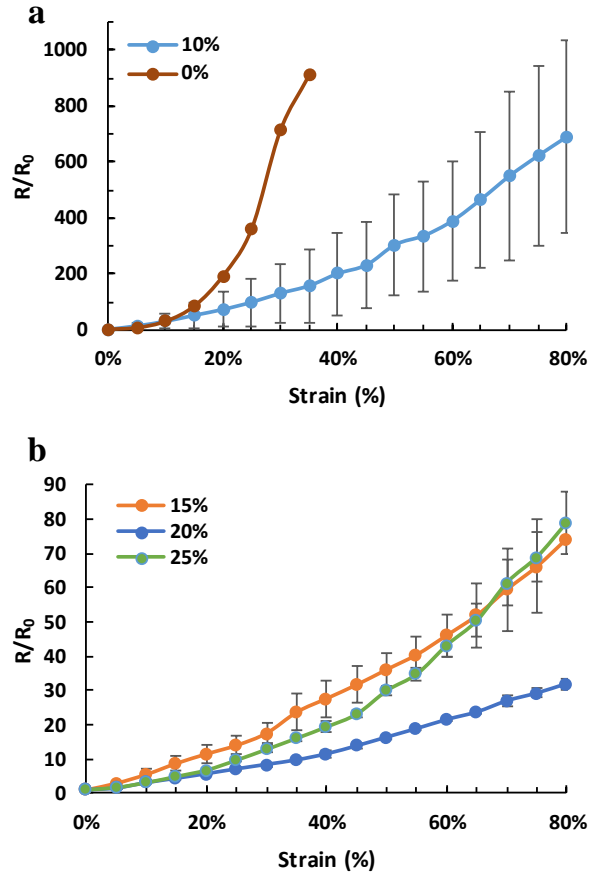


Figure 4.6. Plot of normalized resistance as a linear strain for 0% (Au/PDMS sample) and PDMS_{10Si}/Au (a) and PDMS_{15Si}/Au, PDMS_{20Si}/Au, and PDMS_{25Si}/Au (b) samples.

A comparison of the plots of the change in resistance of gold on flat PDMS and PDMS_{xSi}/Au samples (Figure 4.6) reveal that the resistance changes of gold film with stretching can be modified by varying the modified silica : PDMS weight ratio in the interlayer. Without an interlayer, the resistance of gold on flat PDMS rises rapidly to 909 times the initial value at small strain (35%), the cracks propagate to form lots of long and straight cracks at this strain, which causes the electrical failure (Figure S4.3). The sample

is not conductive after further stretching. At the lowest concentration of silica (PDMS_{10Si}/Au) sample, the modified silica in the interlayer has an effect on the gold conductivity with stretching. PDMS_{10Si} gold sample remains conductive to higher elongation than gold on flat PDMS without silica (80% vs. 35%). The R/R₀ value for PDMS_{10Si}/Au is lower (R/R₀ = 157) than that of gold on flat PDMS at 35% strain (Figure 4.6 a). While of PDMS_{10Si}/Au sample, the nanoparticle sites prevent the formation of long cracks (compared to PDMS_{0Si}/Au sample, but the crack are still long) that break the conductive pathway, it remains conductive up to 80% elongation, and the R/R₀ value is 690 (Figure 4.6 a).

For PDMS_{15-25Si}/Au samples, the R/R₀ all remain under 100 up to 80% elongation (Figure 4.6 b). The PDMS_{20Si}/Au sample shows the best electrical stretching behavior among all the concentrations. At 5% elongation, the R/R₀ value are similar (~2) for all the three modified silica gold samples (Figure 4.6 b). At 50% elongation, the PDMS_{20Si}/Au sample is slightly different than the PDMS_{15Si}/Au and PDMS_{25Si}/Au samples. The R/R₀ value is 16 ± 0.6 for PDMS_{20Si}/Au sample, but the R/R₀ value for 15% and 25% gold samples are 36 ± 4.7 and 30 ± 1.5 , which are ~ 2x higher than that of the PDMS_{20Si}/Au. As the elongation goes up to 70% strain, the R/R₀ value for the PDMS_{20Si}/Au sample continues to increase at a slower rate, which is just 27 ± 1.7 . While at 70% elongation, the R/R₀ values are 59 ± 11.8 and 61 ± 6.6 for the PDMS_{15Si}/Au and PDMS_{25Si}/Au samples, respectively.

The cracks showed in optical images (Figure 4.5) appear very different after PDMS_{15Si}/Au, which does not reveal the cause of similarities or differences in R/R₀. We used stereomicroscope images, which provide a larger field of view (5.6 mm).

We stretched the PDMS_{15Si}/Au, PDMS_{20Si}/Au and PDMS_{25Si}/Au samples under stereomicroscope (Figure 4.7), the modified silica nanoparticles were aggregated in the interlayer which initiate and terminate the crack propagation at the edge of the isolated modified silica. It is interesting that PDMS_{15Si}/Au and PDMS_{25Si}/Au samples are indistinguishable in terms of R/R_0 vs. strain, but are completely different in cracking. The width of the crack of PDMS_{15Si}/Au sample increases from ~114 to ~570 μm as the sample is stretching up to 70% strain and some of the cracks get interrupted and new cracks formed (Figure 4.7 a-c). For PDMS_{25Si}/Au sample, the cracks are much smaller than the big long cracks that PDMS_{15Si}/Au sample has. At low strain (5% elongation), the PDMS_{25Si} gold sample has some short cracks ($< 110 \mu\text{m}$) formed and gold film delaminated in some regions (Figure 4.7 g). At higher strain (70%) elongation, the short cracks are getting wider ($< 460 \mu\text{m}$), however, the gold film in some regions seemed to be out of plane, i.e. the gold film is peeling off while stretching the brittle modified silica surface (Figure 4.7 i and Figure S4.2 c). This can explain why PDMS_{25Si}/Au sample has a higher R/R_0 value (61) than that of PDMS_{20Si}/Au sample (27) at 70% elongation, and also explain why it is comparable to PDMS_{15Si}/Au at this elongation.

For the PDMS_{20Si}/Au sample, although the crack density is increasing as the strain is increasing just like PDMS_{25Si}/Au sample, the size of the short cracks remains small ($< 229 \mu\text{m}$), even at 70% elongation. From Figure 4.7 f, the gold film is still connected to continue the conductive pathway. The concentration of modified silica is lower in PDMS_{20Si}/Au sample than that of the PDMS_{25Si}/Au sample, so the surface is less brittle, which can withstand the high strain without peeling off the gold film. This support the view that the PDMS_{20Si}/Au sample has the best stretchable electrical performance.

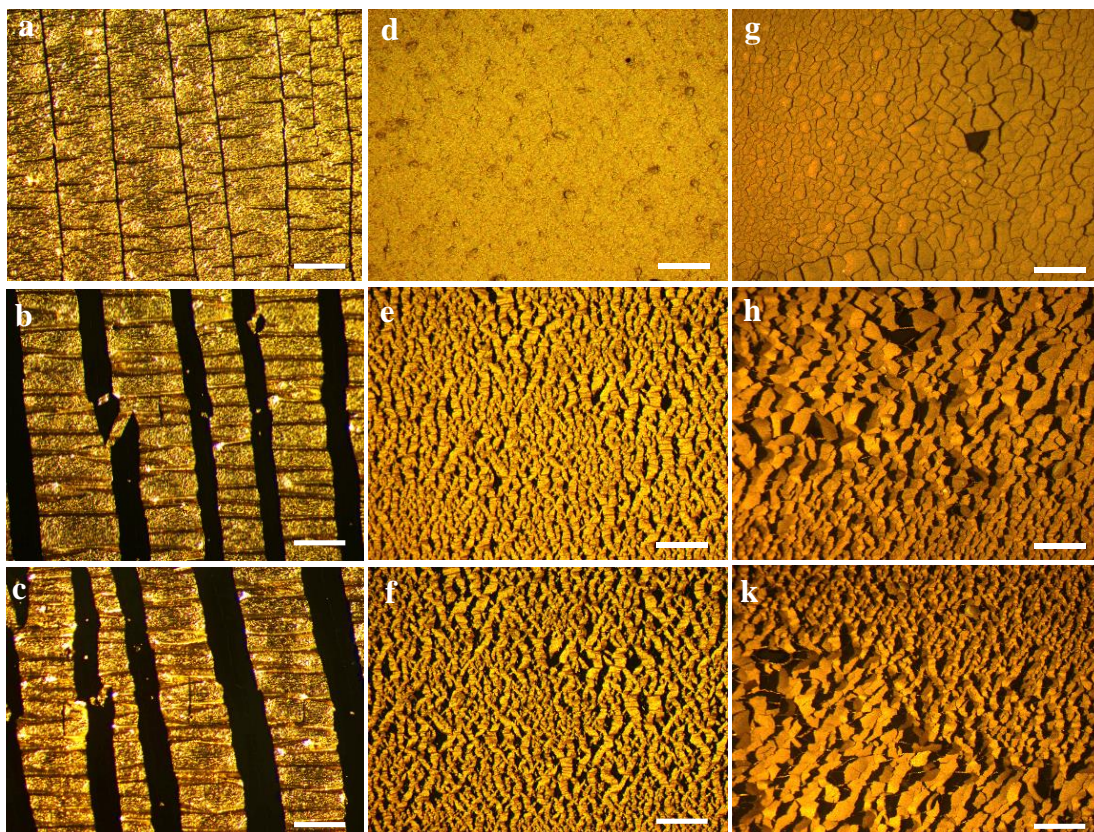


Figure 4.7. Evolution of cracks on PDMS_{xSi}/Au films with stretching. Optical images captured at 5% (top), 50% (middle) and 70% (bottom) strain for PDMS_{15Si}/Au (a-c), PDMS_{20Si}/Au (d-f) and PDMS_{25Si}/Au (g-i) samples. In all images, the samples were stretched in the horizontal direction. Scale bar – 800 μ m.

4.4. Conclusion

All the PDMS_{xSi}/Au samples that we have tested (10, 15, 20 and 25%) can prove the success of achieving high conductivity of thin gold film on elastomer substrates by simply varying the weight ratio of modified silica:PDMS interlayer between metal and substrate. The PDMS_{20Si}/Au sample has the best stretchable electrical behavior and highest stability.

We can reach highly stretchable and conductive gold film on PDMS with less rough surface (the peak-valley distance < 550 nm for the PDMS_{20Si}/Au sample), comparing to PDMS/glue paper by Filiatrault *et al.* in our group (the peak-valley distance < 3.5 μm for PDMS/glue_{1:1}), by using a nanoparticle as an interlayer. The PDMS_{20Si}/Au sample can persist high conductivity at 80% elongation, which is 32× the initial resistance with negligible standard deviation ($R/R_0 = 32 \pm 1.6$).

4.5. References

1. Kim, S. Y.; Park, S.; Park, H. W.; Park, D. H.; Jeong, Y.; Kim, D. H. High Sensitive and Multimodal All-Carbon Skin Sensors Capable of Simultaneously Detecting Tactile and Biological Stimuli. *Adv. Mater.* **2015**, 28, 4178-4185.
2. Meital, S. –B.; Avigail, L.; Maayan, N. –S.; Gregory, S.; Hossam, H. Tunable Touch Sensor and Combined Sensing Platform: Toward Nanoparticle-based Electronic Skin. *ACS Appl. Mater. Inter.* **2013**, 5, 5531-5541.
3. Levering, V.; Wang, Q.; Shivapooja, P.; Zhao, X.; López, G. P. Soft Robotic

- Concepts in Catheter Design: An On-Demand Fouling-Release Urinary Catheter. *Adv. Healthcare Mater.* **2014**, 3, 1588-1596.
4. Bauer, S.; Bauer-Gogonea, S.; Graz, I.; Kaltenbrunner, M.; Keplinger, C.; Schwödiauer, R. 25th Anniversary Article: A Soft Future: From Robots and Sensor Skin to Energy Harvesters. *Adv. Mater.* **2014**, 26, 149-162.
 5. Roh, E.; Hwang, B. -U.; Kim D.; Kim, B. -Y.; Lee, N. -E. Stretchable, Transparent, Ultra sensitive, and Patchable Strain Sensor for Human-Machine Interfaces Comprising a Nanohybrid of Carbon Nanotubes and Conductive Elastomers. *ACS Nano*, **2015**, 9, 6252-6261.
 6. Park, M.; Do, K.; Kim, J.; Son, D.; Koo, J. H.; Park, J.; Song, J. -K., Kim, J. H., Lee, M., Hyeon, T.; Kim, D. -H. Oxide Nanomembrane Hybrids with Enhanced Mechano-and Thermo-Sensitivity for Semitransparent Epidermal Electronics. *Adv. Healthcare Mater.* **2015**, 4, 992-997.
 7. Lim, S.; Son, D.; Kim, J.; Lee, Y. B.; Song, J. -K.; Choi, S.; Lee, D. J.; Kim, J. H.; Lee, M.; Hyeon, T.; Kim, D. -H. Transparent and stretchable interactive human machine interface based on patterned graphene heterostructures. *Adv. Funct. Mater.* **2015**, 25, 375-383.
 8. Park, Y. L.; Chen, B. -R.; Wood, R. J. Design and Fabrication of Soft Artificial Skin Using Embedded Microchannels and Liquid Conductors. *IEEE Sensors Journal*. **2012**, 12, 2711-2718.
 9. Kim, J.; Lee, M; Shim, H. J.; Ghaffari, R.; Cho, H. R.; et al. Stretchable Silicon Nanoribbon Electronics for Skin Prosthesis. *Nat. Commun.* **2014**, 5, 5747.
 10. Drack, M.; Graz, I.; Sekitani, T.; Someya, T.; Kaltenbrunner, M.; Bauer, S. An

- Imperceptible Plastic Electronic Wrap. *Adv. Mater.* **2015**, 27, 34-40.
11. Kim, J.; Park, S. -J.; Nguyen, T.; Chu, M.; Pegan, J. D.; Khine, M. Highly Stretchable Wrinkled Gold Thin Film Wires. *Appl. Phys. Lett.* **2016**, 108, 061901-1.
 12. Tang, J.; Guo, H.; Zhao, M.; Yang, J.; Tsoukalas, D.; Zhang, B.; Liu, J.; Xue, C.; Zhang, W. Highly Stretchable Electrodes on Wrinkled Polydimethylsiloxane Substrates. *Sci. Rep.* **2015**, 5, 16527.
 13. Gutruf, P.; Walia, S.; Ali, M. N.; Sriram, S.; Bhaskaran, M. Strain Response of Stretchable Micro-electrodes: Controlling Sensitivity with Serpentine Designs and Encapsulation. *Appl. Phys. Lett.* **2014**, 104, 021908.
 14. Yao, S.; Zhu, Y. Nanomaterial-Enabled Stretchable Conductor: Strategies, Material and Devices. *Adv. Mater.* **2015**, 27, 1480-1511.
 15. Lee, H. -B.; Bae, C. -W.; Duy, L. T.; Sohn, I.; Kim, D. -I.; Song, Y. -J.; Kim, Y. -J.; Lee, N. -E. Mogul-Patterned Elastomeric Substrates for Stretchable Electronics. *Adv. Mater.* **2016**, 28, 3069-3077.
 16. Lacour, S. P.; Chan, D.; Wagner, S.; Li, T.; Suo, Z. Mechanisms of Reversible Stretchability of Thin Metal Films on Elastomeric Substrates. *Appl. Phys. Lett.* **2006**, 88, 204103.
 17. Lambricht, N.; Pardoen, T.; Yunus, S. Giant Stretchability of Thin Gold Films on Rough Elastomeric Substrates. *Acta Materialia* **2013**, 61, 540-547.
 18. Robinson, A. P.; Mineev, I.; Graz, I. M.; Lacour, S. P. Microstructured Silicone Substrate for Printable and Stretchable Metallic Films. *Langmuir* **2011**, 27, 4279-4284.
 19. Mandlik, P.; Lacour, S. P.; Li, J. W.; Chou, S. Y.; Wagner, S. Fully Elastic

- Interconnects on Nanopatterned Elastomeric Substrates. *IEEE Electron Device Lett.* **2006**, *27*, 650-652.
20. Filiatrault, H. L.; Carmichael, R. S.; Boutette, R. A.; Carmichael, T. B. A Self-Assembled, Low-Cost, Microstructured Layer for Extremely Stretchable Gold Films. *ACS Appl. Mater. Interfaces* **2015**, *7*, 20745-20752.
 21. Horcas, L.; Fernandez, R.; Gomez-Rodriguez, J.M.; Colchero, J.; Gomez-Herrero, J.; Barp, A M. WSXM: a software for scanning probe microscopy and a tool for nanotechnology. *Rev. Sci. Instrum.* **2007**, *78*, 13705-13708.
 22. Kim, H.; Kim, H. -G.; Kim, S.; Kim, S. S. PDMS-Silica Composite Membranes with Silane Coupling for Propylene Separation. *Journal of Membrane Science.* **2009**, *344*(1):211-8.
 23. Jesionowski, T.; Krysztafkiewicz, A. Influence of Silane Coupling Agents on Surface Properties of Precipitated Silicas. *Appl. Surf. Sci.* **2001**, *172*, 18-32.
 24. Gevers, L. E. M.; Vankelecom, I. F. J.; Jacobs, P. A.; Solvent-Resistant Nanofiltration with Filled Polydimethylsiloxane (PDMS) Membranes. *J. Membr. Sci.* **2006**, *278*, 199-204.
 25. Su, X.; Shi, B. Effect of Silane Coupling Agents with Different Non-Hydrolytic groups on Tensile Modulus of Composite PDMS Crosslinked Membranes. *Reactive and Functional Polymers* **2016**, *98*, 1-8.
 26. Khayet, M.; Villaluenga, J. P. G.; Valentin, J. L.; Lopez-Manchado, M. A.; Mengual, J. I.; Seoane, B. Filled Poly (2,6-Dimethyl-1,4-Phenylene Oxide) Dense Membranes by Silica and Silane Modified Silica Nanoparticles: Characterization and Application in Pervaporation. *Polymer* **2005**, *46*, 9881-9891.

4.6. Supporting Information

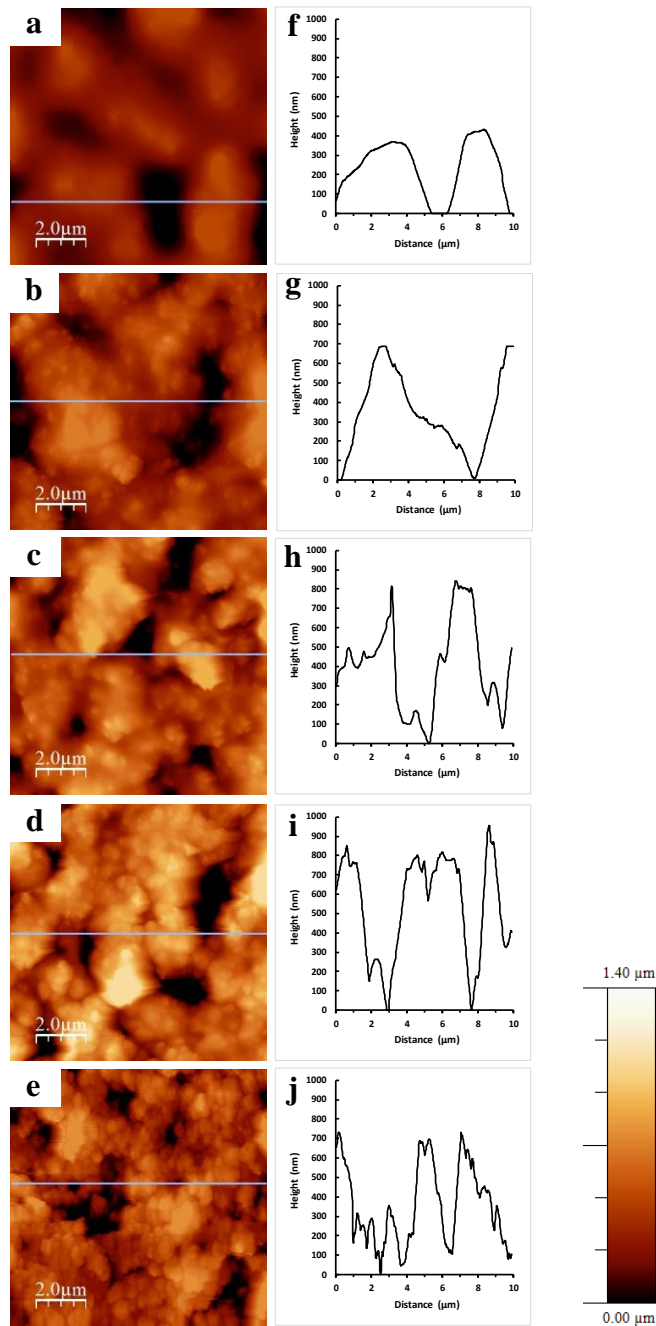


Figure S 4.1. AFM images (a-e) and cross section (f-j) of 10% (a, f), 15% (b, g), 20% (c, h), 25% (d, i) and 30% (e, j) PDMS_xSi samples after 250 Å Au deposition.

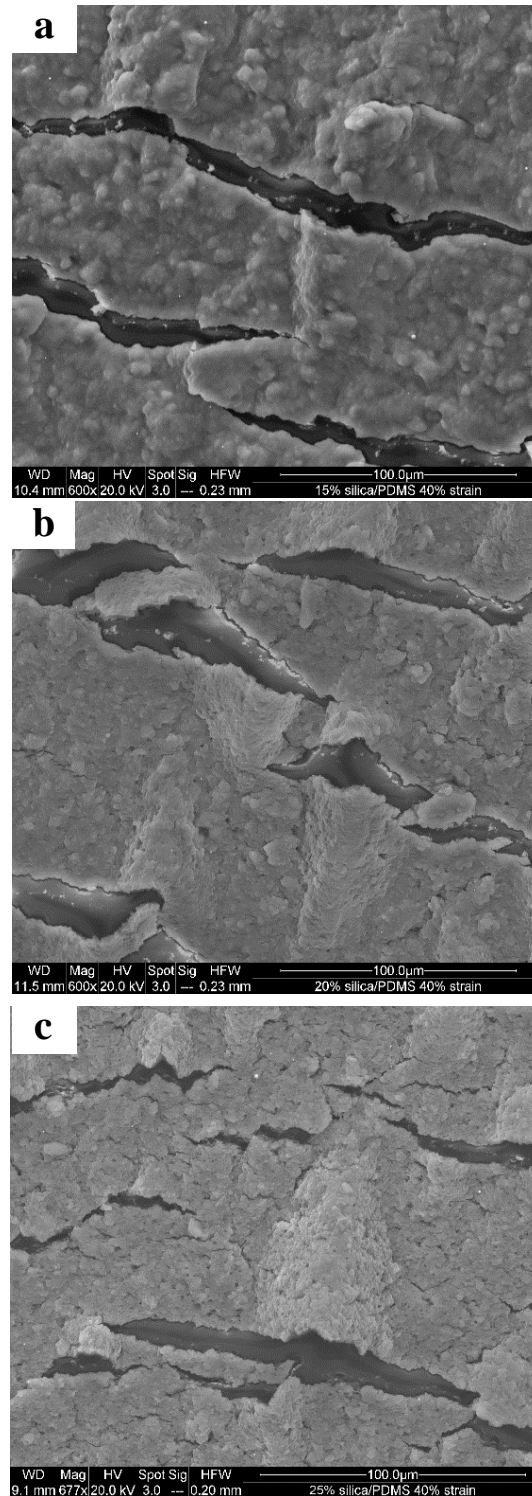


Figure S 4.2. SEM images of 15% (a), 20% (b) and 25% (c) PDMS_xSi/Au samples under 40% strain. In all images, the samples were stretched in vertical direction.

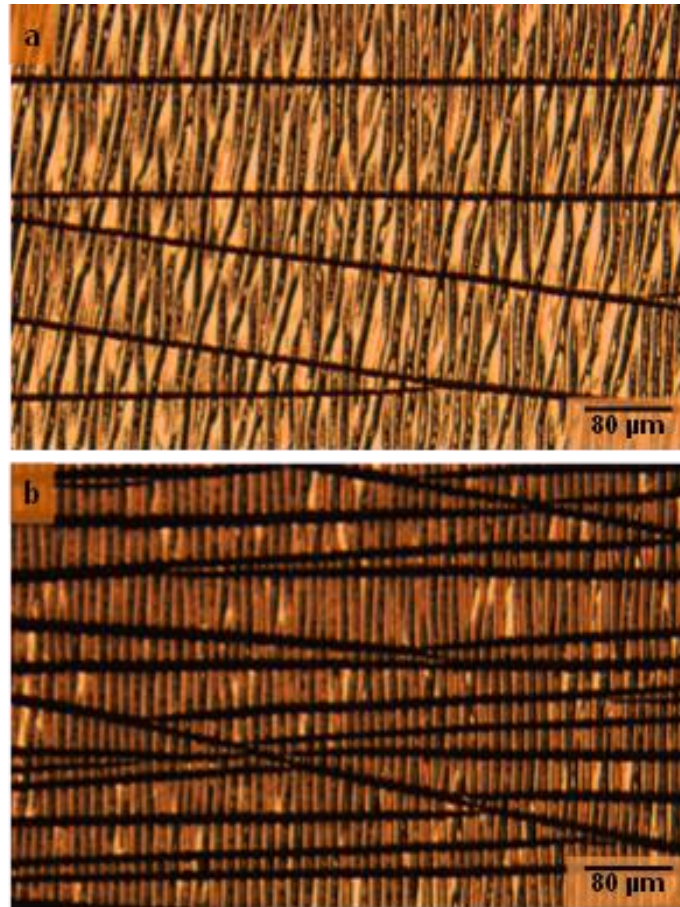


Figure S 4.3. Evolution of cracks on PDMS/gold structures with stretching. Optical images captured at (a) 5% strain and (b) 25% strain. In all images, the samples were stretched in vertical direction.

Chapter 5

Outlook

5.1. Branched DTPAs with Other Terminal Groups or Chain Length

It is reported that fluorocarbon-terminated molecular layers offer lower surface energy and interfacial friction compared to CH_3 – terminated analogues.¹ As the packing densities of molecules with identical chain lengths but different terminations (i.e., CF_3 vs. CH_3) were found to be indistinguishable by atomic force microscopy (AFM), the increased of friction in the case of CF_3 – terminated SAMs has been related to an increase in the interaction between adjacent CF_3 – terminal groups.^{2,3,4} SAMs formed from fluoroalkyl thiols have been shown to be more hydrophobic than the analogous alkane thiols, thus higher contact angles are expected.⁵ It would be interesting to demonstrate the formation of branched DTPA SAM on TS gold by fluorinating the terminal methyl group or part of the methylene groups in the SAM molecular chains to reach high crystalline DTPA SAMs with similar surface coverage and more hydrophobicity than the non-fluorinated branched DTPA SAMs.

If we can successfully synthesize longer branched chain DTPA molecules, we can form SAMs that have larger contact angles. The tradeoff would be the increased steric demand of long alkyl chains on TS gold resulting in liquid-like and disorder chain organization SAMs. It is interesting to alternate the length of main chain and investigate how much space could we fill with branched chain before we perturb the chelation of the molecules on TS gold. If we can find the effective chains that can fill the space and allow the crystalline organization, we might expect the contact angles to change, because the gold would be shielded by the crystalline but short alkyl chains.

5.2. Ways to Increase Stretchability of PDMS_{xSi}/Au Samples

Even though we used nanoparticles as the interlayer to increase the stretchability and conductivity of the metal film, the roughness for the sample is still too high for these films to be used as electrodes in stretchable devices. However, we can probably reduce the size of silica clusters that form on the surface by changing the organosilane coupling agents used to study the relationship between roughness and gold cracking (and R/R_0). It would also be interesting to see how the sample will behave without the Ti adhesive layer before gold evaporation, since the silica layer could act as the adhesive layer as well. Future work will involve embedding the silica nanoparticles in a shallow layer of PDMS at the surface, which we hypothesize will generate a smooth surface while simultaneously retaining the strain-relieving effects of silica suspensions in PDMS.

The stretchability of the PDMS_{xSi}/Au sample is also limited by PDMS substrate. Besides PDMS, Ecoflex is researched in our group as a substrate for constructing devices and thin films. This elastomer can stretch up to 900% tensile strain without breaking, so it seems very promising that by using Ecoflex as the elastic substrate would remove substrate stretchability as a limitation on the performance of the conducting layer.

5.3. References

1. Kim, H. I.; Graupe, M.; Oloba, O.; Koini, T.; Imaduddin, S.; Lee, T.R.; Perry, S.S.; Molecularly Specific Studies of the Frictional Properties of Monolayer Films: A Systematic Comparison of CF₃-, (CH₃)₂CH-, and CH₃-Terminated Films. *Langmuir* **1999**, *15*, 3179-3185.
2. Burnhan, N. A.; Dominguez, D. D.; Monery, R. L.; Colton, R. J. Probing the Surface Forces of Monolayer Films with an Atomic-Force Microscopy. *Phys. Rev. Lett.* **1990**, *64*, 1931-1934.
3. Kim, H. I.; Koini, T.; Lee, T. R.; Perry, S. S. Systematic Studies of the Frictional Properties of Fluorinated Monolayers with Atomic Force Microscopy: Comparison of CF₃- and CH₃-Terminated Films. *Langmuir* **1997**, *13*, 7192-7196.
4. Pflaum, J. Bracco, G.; Schreiber, F.; Colorado Jr. R.; Shmakova, O. E.; Lee, T. R.; Scoles, G.; Kahn, A. Structure and Electronic Properties of CH₃- and CF₃-Terminated Alkanethiol Monolayers on Au (111): A Scanning Tunneling Microscopy, Surface X-Ray and Helium Scattering Study. *Surface Science* **2002**, *498*, 89-104.
5. Tsao, M.-W.; Rabolt, J.F.; Schönherr, H.; Castner, D.G. Semifluorinated/Hydrogenated Alkylthiol Thin Films: A Comparison between Disulfides and Thiol Binary Mixtures. *Langmuir* **2000**, *16*, 1734-1743.

Appendices

Copyright Permission



RightsLink®

[Home](#)[Account Info](#)[Help](#)ACS Publications
Most Trusted. Most Cited. Most Read.**Title:** Self-Assembled Monolayers of Thioliates on Metals as a Form of Nanotechnology**Author:** J. Christopher Love, Lara A. Estroff, Jennah K. Kriebel, et al**Publication:** Chemical Reviews**Publisher:** American Chemical Society**Date:** Apr 1, 2005

Copyright © 2005, American Chemical Society

Logged in as:

Jincheng Xu

[Logout](#)**PERMISSION/LICENSE IS GRANTED FOR YOUR ORDER AT NO CHARGE**

This type of permission/license, instead of the standard Terms & Conditions, is sent to you because no fee is being charged for your order. Please note the following:

- Permission is granted for your request in both print and electronic formats, and translations.
- If figures and/or tables were requested, they may be adapted or used in part.
- Please print this page for your records and send a copy of it to your publisher/graduate school.
- Appropriate credit for the requested material should be given as follows: "Reprinted (adapted) with permission from (COMPLETE REFERENCE CITATION). Copyright (YEAR) American Chemical Society." Insert appropriate information in place of the capitalized words.
- One-time permission is granted only for the use specified in your request. No additional uses are granted (such as derivative works or other editions). For any other uses, please submit a new request.

If credit is given to another source for the material you requested, permission must be obtained from that source.

[BACK](#)[CLOSE WINDOW](#)

Copyright © 2016 Copyright Clearance Center, Inc. All Rights Reserved. [Privacy statement](#). [Terms and Conditions](#). Comments? We would like to hear from you. E-mail us at customerscare@copyright.com



RightsLink®

[Home](#)[Account Info](#)[Help](#)ACS Publications
Most Trusted. Most Cited. Most Read.**Title:** Multidentate Adsorbates for Self-Assembled Monolayer Films**Author:** Pawilai Chinwangso, Andrew C. Jamison, T. Randall Lee**Publication:** Accounts of Chemical Research**Publisher:** American Chemical Society**Date:** Jul 1, 2011

Copyright © 2011, American Chemical Society

Logged in as:

Jincheng Xu

[Logout](#)**PERMISSION/LICENSE IS GRANTED FOR YOUR ORDER AT NO CHARGE**

This type of permission/license, instead of the standard Terms & Conditions, is sent to you because no fee is being charged for your order. Please note the following:

- Permission is granted for your request in both print and electronic formats, and translations.
- If figures and/or tables were requested, they may be adapted or used in part.
- Please print this page for your records and send a copy of it to your publisher/graduate school.
- Appropriate credit for the requested material should be given as follows: "Reprinted (adapted) with permission from (COMPLETE REFERENCE CITATION). Copyright (YEAR) American Chemical Society." Insert appropriate information in place of the capitalized words.
- One-time permission is granted only for the use specified in your request. No additional uses are granted (such as derivative works or other editions). For any other uses, please submit a new request.

If credit is given to another source for the material you requested, permission must be obtained from that source.

[BACK](#)[CLOSE WINDOW](#)

Copyright © 2016 Copyright Clearance Center, Inc. All Rights Reserved. [Privacy statement](#). [Terms and Conditions](#).
Comments? We would like to hear from you. E-mail us at customerscare@copyright.com



RightsLink®

[Home](#)[Account Info](#)[Help](#)ACS Publications
Most Trusted. Most Cited. Most Read.

Title:

New Dialkyldithiophosphinic Acid Self-Assembled Monolayers (SAMs): Influence of Gold Substrate Morphology on Adsorbate Binding and SAM Structure

Logged in as:

Jincheng Xu

[Logout](#)

Author:

Michael S. Miller, Ronan R. San Juan, Michael-Anthony Ferrato, et al

Publication: Langmuir

Publisher: American Chemical Society

Date: Aug 1, 2011

Copyright © 2011, American Chemical Society

PERMISSION/LICENSE IS GRANTED FOR YOUR ORDER AT NO CHARGE

This type of permission/license, instead of the standard Terms & Conditions, is sent to you because no fee is being charged for your order. Please note the following:

- Permission is granted for your request in both print and electronic formats, and translations.
- If figures and/or tables were requested, they may be adapted or used in part.
- Please print this page for your records and send a copy of it to your publisher/graduate school.
- Appropriate credit for the requested material should be given as follows: "Reprinted (adapted) with permission from (COMPLETE REFERENCE CITATION). Copyright (YEAR) American Chemical Society." Insert appropriate information in place of the capitalized words.
- One-time permission is granted only for the use specified in your request. No additional uses are granted (such as derivative works or other editions). For any other uses, please submit a new request.

If credit is given to another source for the material you requested, permission must be obtained from that source.

[BACK](#)[CLOSE WINDOW](#)

Copyright © 2016 Copyright Clearance Center, Inc. All Rights Reserved. [Privacy statement](#). [Terms and Conditions](#). Comments? We would like to hear from you. E-mail us at customercare@copyright.com



RightsLink®

Home

Account
Info

Help



Title: A Highly Sensitive Capacitive Touch Sensor Integrated on a Thin-Film-Encapsulated Active-Matrix OLED for Ultrathin Displays

Author: Sunkook Kim

Publication: Electron Devices, IEEE Transactions on

Publisher: IEEE

Date: 0 Oct. 2011

Copyright © 2011, IEEE

Logged in as:
Jincheng Xu

Logout

Thesis / Dissertation Reuse

The IEEE does not require individuals working on a thesis to obtain a formal reuse license, however, you may print out this statement to be used as a permission grant:

Requirements to be followed when using any portion (e.g., figure, graph, table, or textual material) of an IEEE copyrighted paper in a thesis:

- 1) In the case of textual material (e.g., using short quotes or referring to the work within these papers) users must give full credit to the original source (author, paper, publication) followed by the IEEE copyright line © 2011 IEEE.
- 2) In the case of illustrations or tabular material, we require that the copyright line © [Year of original publication] IEEE appear prominently with each reprinted figure and/or table.
- 3) If a substantial portion of the original paper is to be used, and if you are not the senior author, also obtain the senior author's approval.

Requirements to be followed when using an entire IEEE copyrighted paper in a thesis:

- 1) The following IEEE copyright/ credit notice should be placed prominently in the references: © [year of original publication] IEEE. Reprinted, with permission, from [author names, paper title, IEEE publication title, and month/year of publication]
- 2) Only the accepted version of an IEEE copyrighted paper can be used when posting the paper or your thesis on-line.
- 3) In placing the thesis on the author's university website, please display the following message in a prominent place on the website: In reference to IEEE copyrighted material which is used with permission in this thesis, the IEEE does not endorse any of [university/educational entity's name goes here]'s products or services. Internal or personal use of this material is permitted. If interested in reprinting/republishing IEEE copyrighted material for advertising or promotional purposes or for creating new collective works for resale or redistribution, please go to http://www.ieee.org/publications_standards/publications/rights/rights_link.html to learn how to obtain a License from RightsLink.

If applicable, University Microfilms and/or ProQuest Library, or the Archives of Canada may supply single copies of the dissertation.

BACK

CLOSE WINDOW

Copyright © 2016 Copyright Clearance Center, Inc. All Rights Reserved. [Privacy statement](#). [Terms and Conditions](#).
Comments? We would like to hear from you. E-mail us at customerservice@copyright.com



RightsLink®

Home

Account
Info

Help



Title: Stretchable Interconnects for Elastic Electronic Surfaces

Author: S.R Lacour

Publication: Proceedings of the IEEE

Publisher: IEEE

Date: 0 Aug. 2005

Copyright © 2005, IEEE

Logged in as:

Jincheng Xu

Account #:

3001069030

LOGOUT

Thesis / Dissertation Reuse

The IEEE does not require individuals working on a thesis to obtain a formal reuse license, however, you may print out this statement to be used as a permission grant:

Requirements to be followed when using any portion (e.g., figure, graph, table, or textual material) of an IEEE copyrighted paper in a thesis:

- 1) In the case of textual material (e.g., using short quotes or referring to the work within these papers) users must give full credit to the original source (author, paper, publication) followed by the IEEE copyright line © 2011 IEEE.
- 2) In the case of illustrations or tabular material, we require that the copyright line © [Year of original publication] IEEE appear prominently with each reprinted figure and/or table.
- 3) If a substantial portion of the original paper is to be used, and if you are not the senior author, also obtain the senior author's approval.

Requirements to be followed when using an entire IEEE copyrighted paper in a thesis:

- 1) The following IEEE copyright/ credit notice should be placed prominently in the references: © [year of original publication] IEEE. Reprinted, with permission, from [author names, paper title, IEEE publication title, and month/year of publication]
- 2) Only the accepted version of an IEEE copyrighted paper can be used when posting the paper or your thesis on-line.
- 3) In placing the thesis on the author's university website, please display the following message in a prominent place on the website: In reference to IEEE copyrighted material which is used with permission in this thesis, the IEEE does not endorse any of [university/educational entity's name goes here]'s products or services. Internal or personal use of this material is permitted. If interested in reprinting/republishing IEEE copyrighted material for advertising or promotional purposes or for creating new collective works for resale or redistribution, please go to http://www.ieee.org/publications_standards/publications/rights/rights_link.html to learn how to obtain a License from RightsLink.

If applicable, University Microfilms and/or ProQuest Library, or the Archives of Canada may supply single copies of the dissertation.

BACK

CLOSE WINDOW

Copyright © 2016 Copyright Clearance Center, Inc. All Rights Reserved. [Privacy statement](#). [Terms and Conditions](#).
Comments? We would like to hear from you. E-mail us at customercare@copyright.com



RightsLink®

[Home](#)
[Account Info](#)
[Help](#)


Title: Materials and Mechanics for Stretchable Electronics
Author: John A. Rogers, Takao Someya, Yonggang Huang
Publication: Science
Publisher: The American Association for the Advancement of Science
Date: Mar 26, 2010
 Copyright © 2010, Copyright © 2010, American Association for the Advancement of Science

Logged in as:
 Jincheng Xu
 Account #:
 3001069030

[Logout](#)

Order Completed

Thank you for your order.

This Agreement between Jincheng Xu ("You") and The American Association for the Advancement of Science ("The American Association for the Advancement of Science") consists of your license details and the terms and conditions provided by The American Association for the Advancement of Science and Copyright Clearance Center.

Your confirmation email will contain your order number for future reference.

[Get the printable license.](#)

| | |
|-------------------------------------|---|
| License Number | 3967830126035 |
| License date | Oct 14, 2016 |
| Licensed Content Publisher | The American Association for the Advancement of Science |
| Licensed Content Publication | Science |
| Licensed Content Title | Materials and Mechanics for Stretchable Electronics |
| Licensed Content Author | John A. Rogers, Takao Someya, Yonggang Huang |
| Licensed Content Date | Mar 26, 2010 |
| Licensed Content Volume | 327 |
| Licensed Content Issue | 5973 |
| Volume number | 327 |
| Issue number | 5973 |
| Type of Use | Thesis / Dissertation |
| Requestor type | Scientist/Individual at a research institution |
| Format | Print and electronic |
| Portion | Figure |
| Number of figures/tables | 1 |
| Order reference number | |
| Title of your thesis / dissertation | Studies of Branched Dialkyldithiophosphinic Acids on Gold and Stretchable Gold Films Using Silica Nanoparticles |
| Expected completion date | Oct 2016 |
| Estimated size(pages) | 105 |
| Requestor Location | |
| Billing Type | Invoice |
| Billing address | |

**NATURE PUBLISHING GROUP LICENSE
TERMS AND CONDITIONS**

Oct 03, 2016

This Agreement between Jincheng Xu ("You") and Nature Publishing Group ("Nature Publishing Group") consists of your license details and the terms and conditions provided by Nature Publishing Group and Copyright Clearance Center.

| | |
|--|---|
| License Number | 3961430966976 |
| License date | Oct 03, 2016 |
| Licensed Content Publisher | Nature Publishing Group |
| Licensed Content Publication | Nature Communications |
| Licensed Content Title | Stretchable silicon nanoribbon electronics for skin prosthesis |
| Licensed Content Author | Jaemin Kim, Mincheol Lee, Hyung Joon Shim, Roozbeh Ghaffari, Hye Rim Cho, Donghee Son |
| Licensed Content Date | Dec 9, 2014 |
| Licensed Content Volume Number | 5 |
| Type of Use | reuse in a dissertation / thesis |
| Requestor type | non-commercial (non-profit) |
| Format | print and electronic |
| Portion | figures/tables/illustrations |
| Number of figures/tables/illustrations | 1 |
| High-res required | no |
| Figures | smart artificial skin covering a prosthetic hand |
| Author of this NPG article | no |
| Your reference number | |
| Title of your thesis / dissertation | Studies of Branched Dialkyldithiophosphinic Acids on Gold and Stretchable Gold Films Using Silica Nanoparticles |
| Expected completion date | Oct 2016 |
| Estimated size (number of pages) | 105 |
| Requestor Location | |

Billing Type

Billing Address

Total 0.00 USD

[Terms and Conditions](#)

Terms and Conditions for Permissions

Nature Publishing Group hereby grants you a non-exclusive license to reproduce this material for this purpose, and for no other use, subject to the conditions below:

1. NPG warrants that it has, to the best of its knowledge, the rights to license reuse of this material. However, you should ensure that the material you are requesting is original to Nature Publishing Group and does not carry the copyright of another entity (as credited in the published version). If the credit line on any part of the material you have requested indicates that it was reprinted or adapted by NPG with permission from another source, then you should also seek permission from that source to reuse the material.
2. Permission granted free of charge for material in print is also usually granted for any electronic version of that work, provided that the material is incidental to the work as a whole and that the electronic version is essentially equivalent to, or substitutes for, the print version. Where print permission has been granted for a fee, separate permission must be obtained for any additional, electronic re-use (unless, as in the case of a full paper, this has already been accounted for during your initial request in the calculation of a print run). NB: In all cases, web-based use of full-text articles must be authorized separately through the 'Use on a Web Site' option when requesting permission.
3. Permission granted for a first edition does not apply to second and subsequent editions and for editions in other languages (except for signatories to the STM Permissions Guidelines, or where the first edition permission was granted for free).
4. Nature Publishing Group's permission must be acknowledged next to the figure, table or abstract in print. In electronic form, this acknowledgement must be visible at the same time as the figure/table/abstract, and must be hyperlinked to the journal's homepage.

5. The credit line should read:

Reprinted by permission from Macmillan Publishers Ltd: [JOURNAL NAME] (reference citation), copyright (year of publication)

For AOP papers, the credit line should read:

Reprinted by permission from Macmillan Publishers Ltd: [JOURNAL NAME], advance online publication, day month year (doi: 10.1038/sj.[JOURNAL ACRONYM].XXXXX)

Note: For republication from the *British Journal of Cancer*, the following credit lines apply.

Reprinted by permission from Macmillan Publishers Ltd on behalf of Cancer Research UK: [JOURNAL NAME] (reference citation), copyright (year of publication) For AOP papers, the credit line should read:

Reprinted by permission from Macmillan Publishers Ltd on behalf of Cancer Research UK: [JOURNAL NAME], advance online publication, day month year (doi: 10.1038/sj.[JOURNAL ACRONYM].XXXXX)

6. Adaptations of single figures do not require NPG approval. However, the adaptation should be credited as follows:

Adapted by permission from Macmillan Publishers Ltd: [JOURNAL NAME] (reference citation), copyright (year of publication)

Note: For adaptation from the *British Journal of Cancer*, the following credit line applies.

Adapted by permission from Macmillan Publishers Ltd on behalf of Cancer Research UK: [JOURNAL NAME] (reference citation), copyright (year of publication)

7. Translations of 401 words up to a whole article require NPG approval. Please visit <http://www.macmillanmedicalcommunications.com> for more information. Translations of up

to a 400 words do not require NPG approval. The translation should be credited as follows:

Translated by permission from Macmillan Publishers Ltd: [JOURNAL NAME] (reference citation), copyright (year of publication).

Note: For translation from the *British Journal of Cancer*, the following credit line applies.

Translated by permission from Macmillan Publishers Ltd on behalf of Cancer Research UK: [JOURNAL NAME] (reference citation), copyright (year of publication)

We are certain that all parties will benefit from this agreement and wish you the best in the use of this material. Thank you.

Special Terms:

v1.1

Questions? customercare@copyright.com or +1-855-239-3415 (toll free in the US) or +1-978-646-2777.

**NATURE PUBLISHING GROUP LICENSE
TERMS AND CONDITIONS**

Oct 03, 2016

This Agreement between Jincheng Xu ("You") and Nature Publishing Group ("Nature Publishing Group") consists of your license details and the terms and conditions provided by Nature Publishing Group and Copyright Clearance Center.

| | |
|--|--|
| License Number | 3961460518748 |
| License date | Oct 03, 2016 |
| Licensed Content Publisher | Nature Publishing Group |
| Licensed Content Publication | Nature Materials |
| Licensed Content Title | Materials for multifunctional balloon catheters with capabilities in cardiac electrophysiological mapping and ablation therapy |
| Licensed Content Author | Dae-Hyeong Kim, Nanshu Lu, Roozbeh Ghaffari, Yun-Soung Kim, Stephen P. Lee, Lizhi Xu |
| Licensed Content Date | Mar 6, 2011 |
| Licensed Content Volume Number | 10 |
| Licensed Content Issue Number | 4 |
| Type of Use | reuse in a dissertation / thesis |
| Requestor type | non-commercial (non-profit) |
| Format | print and electronic |
| Portion | figures/tables/illustrations |
| Number of figures/tables/illustrations | 1 |
| High-res required | no |
| Figures | an intrinsically stretchable polymer light-emitting device |
| Author of this NPG article | no |
| Your reference number | |
| Title of your thesis / dissertation | Studies of Branched Dialkylidithiophosphinic Acids on Gold and Stretchable Gold Films Using Silica Nanoparticles |
| Expected completion date | Oct 2016 |
| Estimated size (number of pages) | 105 |
| Requestor Location | |

Billing Type

Billing Address

Total 0.00 USD

[Terms and Conditions](#)

Terms and Conditions for Permissions

Nature Publishing Group hereby grants you a non-exclusive license to reproduce this material for this purpose, and for no other use, subject to the conditions below:

1. NPG warrants that it has, to the best of its knowledge, the rights to license reuse of this material. However, you should ensure that the material you are requesting is original to Nature Publishing Group and does not carry the copyright of another entity (as credited in the published version). If the credit line on any part of the material you have requested indicates that it was reprinted or adapted by NPG with permission from another source, then you should also seek permission from that source to reuse the material.
2. Permission granted free of charge for material in print is also usually granted for any electronic version of that work, provided that the material is incidental to the work as a whole and that the electronic version is essentially equivalent to, or substitutes for, the print version. Where print permission has been granted for a fee, separate permission must be obtained for any additional, electronic re-use (unless, as in the case of a full paper, this has already been accounted for during your initial request in the calculation of a print run). NB: In all cases, web-based use of full-text articles must be authorized separately through the 'Use on a Web Site' option when requesting permission.
3. Permission granted for a first edition does not apply to second and subsequent editions and for editions in other languages (except for signatories to the STM Permissions Guidelines, or where the first edition permission was granted for free).
4. Nature Publishing Group's permission must be acknowledged next to the figure, table or abstract in print. In electronic form, this acknowledgement must be visible at the same time as the figure/table/abstract, and must be hyperlinked to the journal's homepage.

5. The credit line should read:

Reprinted by permission from Macmillan Publishers Ltd: [JOURNAL NAME] (reference citation), copyright (year of publication)

For AOP papers, the credit line should read:

Reprinted by permission from Macmillan Publishers Ltd: [JOURNAL NAME], advance online publication, day month year (doi: 10.1038/sj.[JOURNAL ACRONYM].XXXXX)

Note: For republication from the *British Journal of Cancer*, the following credit lines apply.

Reprinted by permission from Macmillan Publishers Ltd on behalf of Cancer Research UK: [JOURNAL NAME] (reference citation), copyright (year of publication) For AOP papers, the credit line should read:

Reprinted by permission from Macmillan Publishers Ltd on behalf of Cancer Research UK: [JOURNAL NAME], advance online publication, day month year (doi: 10.1038/sj.[JOURNAL ACRONYM].XXXXX)

6. Adaptations of single figures do not require NPG approval. However, the adaptation should be credited as follows:

Adapted by permission from Macmillan Publishers Ltd: [JOURNAL NAME] (reference citation), copyright (year of publication)

Note: For adaptation from the *British Journal of Cancer*, the following credit line applies.

Adapted by permission from Macmillan Publishers Ltd on behalf of Cancer Research UK: [JOURNAL NAME] (reference citation), copyright (year of publication)

7. Translations of 401 words up to a whole article require NPG approval. Please visit <http://www.macmillanmedicalcommunications.com> for more information. Translations of up to a 400 words do not require NPG approval. The translation should be credited as follows:

Translated by permission from Macmillan Publishers Ltd: [JOURNAL NAME] (reference citation), copyright (year of publication).

Note: For translation from the *British Journal of Cancer*, the following credit line applies.

Translated by permission from Macmillan Publishers Ltd on behalf of Cancer Research UK: [JOURNAL NAME] (reference citation), copyright (year of publication)

We are certain that all parties will benefit from this agreement and wish you the best in the use of this material. Thank you.

Special Terms:

v1.1

Questions? customercare@copyright.com or +1-855-239-3415 (toll free in the US) or +1-978-646-2777.



RightsLink®

[Home](#)[Account Info](#)[Help](#)ACS Publications
Most Trusted. Most Cited. Most Read.**Title:** A Self-Assembled, Low-Cost, Microstructured Layer for Extremely Stretchable Gold Films**Author:** Heather L. Filiatrault, R. Stephen Carmichael, Rachel A. Boutette, et al**Publication:** Applied Materials**Publisher:** American Chemical Society**Date:** Sep 1, 2015

Copyright © 2015, American Chemical Society

Logged in as:

Jincheng Xu

Account #:

3001069030

[LOGOUT](#)**PERMISSION/LICENSE IS GRANTED FOR YOUR ORDER AT NO CHARGE**

This type of permission/license, instead of the standard Terms & Conditions, is sent to you because no fee is being charged for your order. Please note the following:

- Permission is granted for your request in both print and electronic formats, and translations.
- If figures and/or tables were requested, they may be adapted or used in part.
- Please print this page for your records and send a copy of it to your publisher/graduate school.
- Appropriate credit for the requested material should be given as follows: "Reprinted (adapted) with permission from (COMPLETE REFERENCE CITATION). Copyright (YEAR) American Chemical Society." Insert appropriate information in place of the capitalized words.
- One-time permission is granted only for the use specified in your request. No additional uses are granted (such as derivative works or other editions). For any other uses, please submit a new request.

If credit is given to another source for the material you requested, permission must be obtained from that source.

[BACK](#)[CLOSE WINDOW](#)

Copyright © 2016 Copyright Clearance Center, Inc. All Rights Reserved. [Privacy statement](#). [Terms and Conditions](#). Comments? We would like to hear from you. E-mail us at customercare@copyright.com

Vita Auctoris

Name: Jincheng Xu

Place of Birth: Hai'an, Nantong, Jiangsu, China

Education:

University of Windsor, **M.Sc. in Chemistry**, Windsor, ON, 2016

St. Francis Xavier University, **B.Sc. in Chemistry**, Antigonish, NS, 2014

Lifa High School, Nantong, Jiangsu, China, 2009

Work Experience:

Research Assistant

Department of Chemistry and Biochemistry, University of Windsor,
Windsor, Ontario, Canada, June 2016 – September 2014.

Graduate Assistant

Department of Chemistry and Biochemistry, University of Windsor,
Windsor, Ontario, Canada, June 2016 – September 2014.